2012-06-15

Determination of Phase Equilibria and the Critical Point Using Two-Phase Molecular Dynamics Simulations with Monte Carlo Sampling

Sonal Patel
Brigham Young University - Provo

Determination of Phase Equilibria and the Critical Point Using Two-Phase Molecular Dynamics Simulations with Monte Carlo Sampling

Sonal Patel

A dissertation submitted to the faculty of
Brigham Young University
in partial fulfillment of the requirements for the degree of

Doctor of Philosophy

W. Vincent Wilding, Chair
Richard L. Rowley
Thomas A. Knotts
Kenneth A. Solen
Larry L. Baxter

Department of Chemical Engineering

Brigham Young University

June 2012

ABSTRACT

Determination of Phase Equilibria and the Critical Point Using Two-Phase Molecular Dynamics Simulations with Monte Carlo Sampling

Sonal Patel
Department of Chemical Engineering, BYU
Doctor of Philosophy

The two-phase MD technique employed in this work determines the liquid and vapor phase densities from a histogram of molecular densities within phase clusters in the simulation cell using a new Monte Carlo (MC) sampling method. These equilibrium densities are then fitted in conjunction with known critical-point scaling laws to obtain the critical temperature, and the critical density. This MC post-processing method was found to be more easily implemented in code, and it is efficient and easily applied to complex, structured molecules. This method has been successfully applied and benchmarked for a simple Lennard-Jones (LJ) fluid and a structured molecule, propane. Various degrees of internal flexibility in the propane models showed little effect on the coexisting densities far from critical point, but internal flexibility (angle bending and bond vibrations) seemed to affect the saturated liquid densities in the near-critical region, changing the critical temperature by approximately 20 K. Shorter cutoffs were also found to affect the phase dome and the location of the critical point.

The developed MD+MC method was then used to test the efficacy of two all-atom, site-site pair potential models (with and without point charges) developed solely from the energy landscape obtained from high-level *ab initio* pair interactions for the first time. Both models produced equivalent phase domes and critical loci. The model's critical temperature for methanol is 77 K too high while that for 1-propanol is 80 K too low, but the critical densities are in good agreement. These differences are likely attributable to the lack of multi-body interactions in the true pair potential models used here. Lastly, the transferability of the *ab initio* potential model was evaluated by applying it to 1-pentanol. An attempt has been made to separate the errors due to transferability of the potential model from errors due to the use of a true-pair potential. The results suggested a good level of transferability for the site-site model. The lack of multi-body effects appears to be dominant weakness in using the generalized *ab initio* potential model for determination of the phase dome and critical properties of larger alcohols.

Keywords: Sonal Patel, molecular dynamics simulations, monte carlo sampling method, vapor-liquid equilibrium, critical point, coexistence curve, vapor pressure, phase equilibrium, ab-initio potential model, TraPPE model

ACKNOWLEDGMENTS

First of all I would like to thank my husband Ketan whose constant support and patient love throughout this process enabled me to complete this work. I wish to acknowledge my advisors, Dr. Vincent W. Wilding and Dr. Richard L. Rowley whose continued advice, encouragement, and guidance helped me in my research and writing of this dissertation. I also wish to thank my other committee members Dr. Oscarson, Dr. Knotts, Dr. Solen, and Dr. Baxter for their inputs and assistance during this research project. I am thankful to DIPPR® 801 for funding my research. I am also grateful for the faculty and staff in the Chemical Engineering Department at Brigham Young University for the many things that they have taught me. I would like to extend my sincere thanks to Abhishek Asthana for all his moral support and help to overcome the difficulties I faced during this project completion. I would like to thank all my friends specially Katie Poole, Yin Zhang, Shrinivas Lokare, Chelise Van De Graaff who helped me directly or indirectly in completion of this project work. Last but not the least; I sincerely acknowledge the warm blessings and unfailing support of my loving family who have been there in every step before and during the completion of my dissertation.

TABLE OF CONTENTS

LIST OF TABLES

LIST OF FIGURES

1 INTRODUCTION

As the terminus of the vapor pressure curve where the liquid and vapor densities become identical, the critical point of a fluid provides important information about the molecular interactions and thermodynamic properties specific to the fluid. For example, the principle of corresponding states has proven to be very valuable in predicting properties of fluids from the properties of other reference fluids. Such predictions are based on equivalency of reduced properties for conformal fluids when compared at the same reduced temperature and pressure; i.e., temperatures and pressures scaled by the fluid's critical temperature (T_c) and pressure (P_c), respectively. Additionally, many empirical property estimation methods have been developed based on the strong correlation between the property and values of T_c, P_c, and the critical volume (V_c).

Critical properties of larger molecular weight compounds are difficult to measure due to thermal instability as compounds approach the critical temperature. Within a homologous series, the first few members are usually stable at their critical point but the heavier ones are unstable. Nevertheless, many thermodynamic and transport property calculations require knowledge of critical constants of such substances. The critical constants are needed for prediction of fluid thermodynamic and transport properties using corresponding-state methods, construction of equations of state, determination of properties by many empirical property estimation methods, and for reliable extrapolation of low-temperature vapor pressures to higher temperatures[1].

Methods developed to obtain critical properties fall into the following categories:

- Experimental methods
- Analytical prediction methods
- Simulation methods.

Although the experimental measurements[2] that are available for critical properties determination are extremely precise as mentioned above there are many compounds for which the critical properties cannot be determined. Due to the scarcity of experimental data for such compounds, it is desirable to have methods to predict the locus of the critical point and values of the critical properties. Several such methods exist, most of which are based on group contributions. These empirical and group contribution methods[3] can estimate the critical properties of systems where experimental data are not available. These methods involve quick calculations, but are often only applicable to certain types or families of compounds, and they may lead to large errors in the predicted properties. For example, empirical correlations can only be used for families or compounds similar to the ones for which the correlation has been developed. Group contribution methods are also limited in the types of molecules and families that can be considered. The accuracy of these prediction methods when applied to larger molecules, however, is in question because the group contributions are based primarily on experimental data for smaller molecules.[4]

Molecular simulation methods provide an alternative route for obtaining critical constants for fluids that decompose below their critical point. One relatively new molecular simulation technique uses two-phase (2φ) simulations (simulations in the two-phase region so that both liquid and vapor domains are present in the simulation cell) to obtain the densities of the coexisting liquid and vapor phases at various temperatures. The resultant simulated equilibrium bimodal data are then used in a guided extrapolation to obtain T_c and ρ_c, the critical density.

Simulation methods can be used at conditions where experiments are not (yet) feasible, and are sometimes less expensive and less time consuming than conducting experiments. Simulation will never replace experiments in providing primary data for process development and design, but it can play an important role in extending the range and "filling in the gaps" of experimental measurements.

The most commonly employed simulation method for obtaining equilibrium densities is the Gibbs-ensemble Monte Carlo method (GEMC).[5,6] A GEMC study was successfully used to help establish the infinite-carbon-limit of the critical density for long-chain *n*-alkanes by simulating C_{48}.[7] Standard GEMC simulations develop efficiency problems near the critical temperature owing to frequent swapping of the two simulation boxes as the densities of the two equilibrium phases approach one another. The use of indirect simulation techniques like Histogram Reweighting or Gibbs-Duhem Integration[6] can be used to avoid this difficulty. Alternatively one can make the vapor box much larger than the liquid box to ameliorate the identity-switch problem.[8]

Though GEMC methods are the most common approach, other techniques including NPT simulations with test particles,[9] Grand Ensemble techniques,[10,11] and two-phase molecular dynamics simulations (2φMD) have also been used to study liquid-vapor equilibrium and the location of the critical point. In 2φMD the liquid and the vapor phases are simulated in the same box, usually separated by an interface. An advantage of the MD method is that it is easy to implement even for complex molecules. However, determination of liquid and vapor phase properties can be a challenge in 2φMD simulations because of complications caused by the presence of the interface and the difficulty in determining to which phase molecules collectively belong. Techniques have been proposed to identify the densities of coexisting phases in the same

simulation box by fitting a hyperbolic tangent function to the interface[12,13,14] and by using spatial and inverse histograms of local densities.[15,16] These methods fail as the critical point is approached and the densities of the coexisting phases approach one another. Adjustable parameters in these methods can also require re-parameterization at each temperature.

Recently, a 2φMD method[17,18] was reported that can be used to determine the equilibrium vapor and liquid densities accurately even very near the critical point because complete bulk phase segregation is not required. This is a convenient aspect of this method because mass transfer rates are particularly slow in the near-critical region. In the reported 2φMD method, only equilibrated large clusters of phases produced by equilibration at a 2φ temperature and density or by a temperature quench into the 2φ region were required. Voronoi tessellations were used to determine the molecular volume of each molecule in its local environment.

In the 2φMD method, a time-averaged histogram of the molecular volumes computed from the Voronoi tessellations yields a bimodal distribution when the simulation is performed in the two-phase region. This allows for a preliminary identification of average bulk and liquid densities. Two quick, individual, single-phase, bulk liquid and vapor simulations are then performed at the same temperature and average densities to compare the liquid and vapor distributions from the one-phase (1φ) and 2φ simulations. The variance of the Voronoi volume of the single-phase simulation is calculated and compared to that from the two-phase simulation. If they match, one has the correct density. If they do not match, the process is iterated with a new estimate of the density until the normalized variance of the liquid and vapor distributions from the 1φ simulations match within an acceptable tolerance those in the 2φ simulation. While the iterative process can involve several fast 1φ simulations, the 2φ simulation is not repeated in this

process. Larger molecules can be handled easily using this method since the system evolves under the influence of continuous potentials without the need for molecular insertions.

In this work, a similar algorithm for determining the phase densities has been employed, but a Monte Carlo (MC) sampling method has been developed and used in place of Voronoi tessellations to determine the volume associated with each molecule in the simulation cell. We have found this MC post-processing method to be more easily implemented in code than Voronoi tessellations, and it is efficient and easily applied to complex, structured molecules. This new 2φMD + MC method is very versatile and can be efficiently and easily scaled to any molecular size or structural complexity without requiring many modifications. The aim of this research is to test the ability of 2φMD simulations along with MC sampling method in obtaining accurate equilibrium phase densities and obtaining relatively accurate values for the critical properties of fluids. Though not within the scope of the present dissertation, the expectation is that the methods and techniques developed herein can then be used to obtain the critical properties of higher-molecular-weight molecules.

This project will be very significant to the DIPPR® 801 Pure Chemical Database[19] project at Brigham Young University, which maintains arguably the best database of pure component thermophysical property data. Because of its importance in fixing the end point of the vapor pressure curve of a substance and its importance in property prediction, the critical point has a primary role in this pure-chemical database. Accurate values of T_c, P_c, and V_c are vital in such databases for obtaining a complete set of self-consistent properties. Here, prediction methods are used when no experimental data are found for a particular compound in the database. For higher molecular weight compounds, experimental data are scarce and often contradictory. Furthermore, present prediction methods are often inaccurate and not generalize, i.e., they do not

apply to all families of compounds as discussed in the following chapter. Therefore, a more general and efficient simulation technique to determine the critical properties will be very significant to the DIPPR 801 project and to thermodynamic data generally. The first objective of this work is to develop such a method.

Another objective of this project is to use the developed 2φMD + MC method and test the efficacy of the *ab-initio* based potential model developed by Rowley et al.[20, 21] for the first time to determine the vapor-liquid equilibrium properties of alcohols. The potential model is based entirely on the interactions between two isolated molecules and is therefore a true pair potential model and has no adjustable parameters. Here, the intent is also to investigate the effect on the coexistence curve of multi-body interactions and polarization. The transferability of the *ab initio* potential model has also been evaluated. The next section describes the summary of the work performed in this project.

1.1 Summary of work performed

In Chapter 2, an overview of current simulation techniques for determining critical properties, with their advantages and limitations, is presented. The capabilities and limitations of the methods currently available are discussed to provide comparison basis for the method developed in this work. Chapter 3 provides a brief description of the 2φMD simulation method and the Monte Carlo sampling method used in this work. The procedure for determining the bulk vapor and liquid densities, and the critical points are described.

In Chapter 4, the MC sampling method in conjunction with the 2φ method is validated by reproducing the results presented by Fern et al.[17] for a simple Lennard-Jones fluid. The method is then extended for a structured molecule (propane) and the coexisting densities and critical properties for propane are determined using flexible (bond vibrations and angle bending) and

rigid models. The results for the flexible model phase-dome results are also compared with the GEMC results of Martin and Siepmann[8] and the results from rigid models are compared to that of flexible models. This study evaluates the importance of the details of the molecular model used to describe the fluid. The models used in this chapter to describe the intermolecular interactions are parameterized for VLE simulations, but the effects of internal degrees of freedom on the coexistence curve are evaluated.

In Chapter 5, the *ab-initio* based potential model developed by Rowley et al.[20, 21] is tested by determining the vapor-liquid equilibrium properties for methanol and 1-propanol. This will also help in evaluating how well a true pair potential, with no adjustable parameter and with no multi-body interactions implemented, is able to represent the coexistence curve for alcohols, i.e. the effect on the coexistence curve of multi-body interactions and polarization. The intent is also to test the efficacy of a new *ab initio* model that does not require point charges. The coexistence phase diagram and critical properties for methanol and 1-propanol are determined using the *ab-initio* based potential model for two cases; one model includes the fixed point charges, while the other includes no electrostatic interactions. The results are compared with the literature values.

In Chapter 6, the generalized set of Morse parameters for the *ab-initio* based potential model obtained by Rowley et al. [20, 21] (from a composite regression using the energy landscape data of all small alcohols containing up to four carbon atoms) is used to determine coexisting liquid and vapor densities of 1-pentanol as a function of temperature. This test of the transferability of the site parameters will help in examining the extent to which the model parameters can be taken as independent of the alcohol dimers from which they were regressed. Errors due to transferability of the potential model are separated from errors due to the use of a true-pair potential by calculating energy landscapes for dimers of 1-pentanol using counterpoise

(CP) corrected energies at the MP2/6-311 + G(2df,2pd) level and comparing these to the transferred potential models. In Chapter 7, a synopsis of the conclusions drawn from this study and several recommendations for further study are provided.

2 MOLECULAR SIMULATION TECHNIQUES FOR PHASE EQUILIBRIUM

Simulation techniques offer a method for predicting critical properties that can be used to supplement experimental data. The determination of phase coexistence by computer simulations originally was a very difficult task requiring many simulations, thermodynamic integration of many states along a temperature path, or iterations to match the chemical potential of individually simulated phases. Development of the Gibbs ensemble method[22] was a major step forward in this field. With the help of this method, binary coexisting densities could be obtained in one single simulation at each desired temperature. Additional methods have been developed since the introduction of the Gibbs ensemble method including Grand ensemble methods and two-phase (2φ) methods, an example of which will be used in this work.

With any molecular simulation method, whether it's Gibbs ensemble method or two-phase molecular dynamics method, it is important to keep in mind that successful modeling of any fluid property has two requirements:

1. A reliable theoretical framework given by statistical mechanics, and
2. A realistic and efficient potential model to describe intermolecular and intramolecular interactions in complex fluids.

Much work has been dedicated to improving either one or both of these. Increased accuracy and success of the simulation method depends critically on the development of improved intermolecular and intramolecular potential functions for describing the interactions between the

components in the system. The reliability of the model used to represent the intermolecular potential primarily determines the effectiveness and accuracy of properties obtained using any molecular simulation methods. It is often found to be the limiting factor for prediction accuracy. A simulation method can be perfectly correct but the shortcomings in the force field used are the main limitations that prevent molecular simulations from making reliable, quantitative prediction of different thermophysical properties over a wide range of physical conditions.

2.1 Various molecular simulation methods

Today, several computational methods are available for the study of vapor-liquid equilibrium (VLE). They fall into one of the two categories:

- Monte Carlo (MC) simulation: In this method configurations are generated by sampling phase space directly using a random walk based on the Metropolis algorithm, and the properties are calculated from ensemble averages over those configurations. Only equilibrium properties can be obtained from MC simulations.
- Molecular Dynamic (MD) simulation: This method is based on solving the time-evolution equations for the dynamics (positions and velocities) of all the molecules within the system and then using time averages of the instantaneous properties calculated from the mechanical variables of the system to obtain property values. MD simulations can be used to calculate transport properties and equilibrium properties.

In each category, there are different ways to simulate VLE. For example, using molecular dynamic simulations, one can simulate a slab of liquid and a slab of vapor in contact with and at equilibrium with each other to find the surface tension and equilibrium densities.[23,12] Another method of direct simulation of vapor-liquid equilibrium is to conduct MD simulations in an isothermal-isobaric ensemble (NPT) coupled with Widom's particle insertion method in which

simulations are performed on both the vapor and liquid phases independently to obtain the chemical potential of the system and the results are used to calculate equilibrium points on the two-phase envelope.[9] The most common MC method to study phase equilibrium is the Gibbs Ensemble Monte Carlo (GEMC) method.[22,24] In GEMC, bulk liquid and bulk vapor are simulated in two different boxes and the molecules are allowed to exchange between the two boxes until the boxes are in thermal, mechanical, and chemical equilibrium. Much effort has been devoted in the study of phase equilibrium by using the MD and the GEMC methods. Though my work is based on molecular dynamics simulation, it is helpful to have an understanding of the prior work done on both these techniques to study phase equilibrium.

The next sections will cover the work done on improving the theoretical framework; i.e., MC and MD simulations. A summary of the main points (e.g., the method used and the potential model) of the methods used by various researchers who have worked to improve the theoretical framework is given in Table 2-1.

2.1.1 Monte carlo simulations

The most common MC simulation method to study VLE is the Gibbs Ensemble Monte Carlo (GEMC). In this method, the simulations are performed in two distinct simulation boxes which are not connected physically. Monte Carlo rules that allow for particle exchanges between the two boxes and the volume changes of the two boxes, such that the total volume remains constant, ensure that the two boxes (liquid and vapor) are in chemical and mechanical equilibrium, respectively, with each other. Since the two boxes are not in physical contact, there is no interface, and the bulk properties of the two coexisting phases can be obtained directly with a relatively small number of particles. Sometimes, additional algorithms are used to improve the sampling of the phase space, or to increase the acceptance probability of insertion of particles.

Table 2-1: Summary of main points of work done by various researchers on improving the theoretical framework

Reference	*Issues addressed*	*Molecule, method, & potential used*	*Conclusions*
Laso et al.[25]	- Phase equilibrium simulation of longer alkane chains - Comparison of the results with conventional GEMC and with experiments	Molecules Pentane through Decane, & Pentadecane Method Continuum-Configurational-Bias-Gibbs-ensemble method (CCBG) Potential model LJ potential with internal rotation about C-C bond hindered by a torsional potential- energy function	- Compared with conventional methods: higher success rate for transfer, efficiency did not decrease rapidly with chain length - Compared with experiments: liquid phase and vapor phase densities were lower - Disagreement with experiment became pronounced as chain length increases
Siepmann et al.[26]	- Reported VLE	Molecules *n*-Pentane (C_5), *n*-Octane (C_8) Method CBMC + GE method Potential model OPLS model	- Compared with VLE experimental data: good prediction for C_5, reasonable for C_8 - Compared with experimental critical properties: for C_5: 2% deviation (T_c) & 4% deviation (ρ_c), for C_8: 9% deviation (T_c) & 2% deviation (ρ_c)
Siepmann et al.[7]	- Phase diagram up to vicinity of vapor-liquid critical points	Molecules Alkanes up to C_{48} Method CBMC + GE method Potential model United-atom model, bond bending by harmonic potential & torsional angle controlled by Jorgenson potential[27]	- Simulation value agreed with experimental critical temperature vs. carbon number very well - Critical density vs. carbon number was maximum at C_8 & then decreased monotonically as found by experimental data of Anselme et al.[28]
Alejandre et al.[29]	- Use of direct MD methods to predict accurate fluid phase equilibria - Bulk densities, vapor pressure, & surface tension as a function of temperature	Molecules *n*-Hexane Method direct MD Potential model Laso et al.[25] (model I) Siepmann et al.[7] UA model (model II)	- Calculated properties were in better agreement with experiment for model I - Good agreement with GEMC results for coexisting densities

Table 2-1 continued

Reference	*Issues addressed*	*Molecule, method, & potential used*	*Conclusions*
Cui et al.[30]	- Effect of branching on vapor-liquid coexistence and critical properties - Accuracy of the Siepmann potential model[31] for short-branched alkanes	Molecules Short-branched alkanes with long backbone & several short side branches (from C_9 to C_{30}) & their corresponding linear isomers Method CBMC + GEMC Potential model Siepmann et al.[31] UA model for branched alkanes	- The model accurately predicted the critical density of short-branched alkanes - The predicted T_c for branched short chain alkanes were slightly lower than the experimental values - The effect of branching was to lower the critical temperature & increase the critical density for short branched alkanes
Vlugt et al.[32]	- More efficient algorithms for trial orientations and calculation of Rosenbluth weights in CBMC simulation	Molecules *n*-Octane, *3*-Methylheptane, 3,4-Dimethylhexane Method CBMC algorithms tested for NPT and NVT simulations Potential model TraPPE model	- For a system of 144 molecules these algorithms: sped up calculations by 3 times for n-octane, sped up calculations by 4 times for 3,4-dimethylhexane, for larger system the speedup factor was even greater - Simulation of branched alkanes remained computationally more expensive but the difference in CPU time per accepted move was reduced
Trokhymch-uk et al.[33]	- Effect of intermolecular interaction truncation on coexisting densities - Differences between the spherically truncated (ST) & spherically truncated & shifted (STS) LJ potential models in MC & MD simulations of liquid/vapor coexistence	Molecules Lennard-Jones fluid (LJ) fluid Method MD and MC simulations under the same setup conditions (e.g., number of particles, box size, initial configurations, temperature region, etc.) Potential model LJ potential model	- An additional force due to the discontinuity of the truncated potential at cut-off distance had to be included into the virial calculations in MC and MD, & into the trajectories computations in the MD simulations of two-phase systems - The ST and STS model became indistinguishable with respect to coexisting densities beyond a cutoff of 4.44σ (σ is the LJ diameter) & beyond 5.5σ the two model did not differ significantly from the full LJ potential model

Table 2-1 continued

Reference	*Issues addressed*	*Molecule, method, & potential used*	*Conclusions*
Gelb & Müller[15]	- Presented a method to locate phase coexistence points using MD simulations and a post-simulation analysis method	Molecules Lennard-Jones (LJ) fluid Method Temperature quench molecular dynamics (TQMD) NVT conditions Potential model LJ potential model	- Gave correct results for pure & multi-component vapor-liquid equilibria - Method could be used to locate vapor-liquid, liquid-liquid, or solid-liquid equilibria. Could be used to determine phase equilibria for systems about which little is known
Pamies et al.[16]	- Vapor-liquid orthobaric densities - Effect of interaction truncation on the accuracy of orthobaric liquid densities	Molecules Methane and Propane Method MD and GEMC with CBMC simulations Potential model TraPPE-UA force field	- A cut-off of at least 5.5σ was needed to obtain saturated liquid densities with an accuracy of about 2% when compared to experimental values & GEMC simulations (with finite range cut-off with long-range correction)
Wescott et al.[4]	- Estimated the critical points of two branched alkane series	Molecules 2,2-Dimethylalkanes (up to 16 carbon atoms), 2-Methylalkanes Method GEMC method Potential model NERD model	- Vapor-liquid coexistence curves were constructed with very good correspondence to experimental data (where possible) - Addition of small branches decreased T_c and increased ρ_c when compared to less branched isomers - ρ_c vs. carbon number showed maximum at C_7 for both linear & branched molecules
Martínez - Veracoechea et al.[34]	- Presented detailed analysis of the equilibration process in the TQMD method	Molecules Pure LJ fluid, Eicosane Method TQMD method Potential model LJ potential for pure LJ fluid, for Eicosane intra & intermolecular potential given by Supple & Quirke[35]	- By quenching local equilibration of densities and compositions occurred quickly and the results were representative of the bulk equilibrium values - Results obtained were comparable to that obtained by GEMC and volume expansion molecular dynamics (VEMD) method

Table 2-1 continued

Reference	*Issues addressed*	*Molecule, method, & potential used*	*Conclusions*
Fern et al.[17]	- Determined critical properties using MD + Voronoi tessellations (VT) method	Molecules Pure LJ fluid Method MD method with Voronoi tessellations Potential model LJ potential	- Allowed simulations very close to the critical point - Excellent agreement of critical properties with experimental and GEMC method results
Fern et al.[18]	- Extended the MD + VT method for polyatomic fluid	Molecules Ethanol Method MD + VT method Potential model OPLS-AA	- Coexisting densities agree well with values reported in the literature from GEMC at low temperatures where available

The advantages of the GEMC method are its simplicity, efficiency, and accuracy in predicting the equilibrium properties of both phases in a single simulation. Early studies of phase equilibrium were generally based on fluids of spherical particles.[24] De Pablo et al.[36] employed phase equilibrium simulations for small alkanes and their mixtures using conventional GEMC method. For longer chain molecules, successful particle insertions become extremely unlikely, and additional method might be needed to improve the efficiency of insertions. But for moderately long molecules, i.e. linear alkanes up to six carbon atoms, by using a large enough number of exchanges trails a good statistics for successful exchange could be achieved without any need for such methods. Due to this inherent limitation of their method, the longest alkane for which coexistence properties could be obtained was up to six carbon atoms.

As mentioned above, establishing and maintaining chemical equilibrium in the GEMC method involves exchange of particles between the two boxes. For a dense fluid or solid phase,

the insertion of the particle from the low-density phase into the high-density phase becomes difficult due to the low probability for finding an energetically favorable location for insertion (a spot that is not within the repulsive field of the surrounding molecules). For chain molecules, the successful particle interchanges become so rare that it is impractical to use this simulation method. Therefore, new methods have been proposed for simulating the equilibrium properties of chain molecules. The Configuration-Bias Monte Carlo (CBMC) technique[26] has been developed to insert chain molecules in moderately dense systems.

De Pablo et al.[37] proposed a method for simulation of the chemical potential of chain molecules. It is based on "growing" the chains in a dense fluid in a manner that "looks" for available space thereby increasing the probability of finding low-energy configurations. The bias thus introduced is later corrected by adjusting the MC acceptance rules. In this method, the chain molecule is inserted into a phase in one step, often leading to steric overlaps.

Laso et al.[25] proposed a different method based on the same ideas used by De Pablo et al.[37] In their work, instead of inserting a chain molecule into a phase in one step, the chain was inserted in a segmental manner, thereby avoiding the steric overlap and increasing the likelihood of accepting the move. One observation made in their work was that a single set of LJ parameters did not yield good agreement between experimental and simulated phase diagrams for both short and long alkanes.

Siepmann et al.[7] used a combination of the GEMC technique and the CBMC method for unbranched alkanes as long as C_{48} to determine coexistence curves at temperatures up to the vicinity of the liquid-vapor critical point. In their work, the chain was 'grown' atom by atom finding regions of favorable energies as the simulation progressed. The bias was then removed by adjusting the acceptance rules. This increased the number of successful exchanges by an order

of magnitude for the smaller chains and up to 15 orders of magnitude for octatetracontane (C_{48}). Each cycle of their Gibbs ensemble simulation consisted of the following Monte Carlo moves: translational displacement of a molecule within its current box, rotation of the molecule, volume exchange of the two boxes, re-growing parts of a molecule, and exchanging molecules between the two boxes. For the latter two moves, CBMC was used. The probability of acceptance of an exchange move ranged from 2-10% for C_5 down to 0.5-3% for C_{48}, depending on the temperature. The coexistence curve and critical properties showed satisfactory agreement between their simulation results and the experimental data. They reported that the critical density reaches a maximum at C_8 and then decreases monotonically with carbon number, a trend that agrees with the experimental findings of Anselme et al.[28]

Cui et al.[30] carried out a study of the effect of branching on the vapor-liquid coexistence curve and the critical properties of alkanes. For linear alkanes, the chain growth method was similar to that developed by Siepmann et al.[7] For branched chain alkanes, the backbone was grown first and the side groups were then appended to the backbone. The simulation result did not depend on this choice of sequence in growing the molecule. Though Cui et al.[30] simulated the behavior of branched alkanes (octane isomers) beyond the experimentally known range there has not been a systemic study to understand the influence of branching on the coexistence and critical properties of branched alkanes. Wescott et al.[4] systematically predicted the pure-component, vapor-liquid phase equilibrium of two branched alkane series. Critical temperature and critical density values were also estimated from these data and compared with predictions from empirical correlations and group contribution methods. Unlike their observations where the critical temperature plateaus towards a limiting value as the molecular weight increases, group contribution estimate of critical temperature continually increases with increasing molecular

weight. For intermediate size molecules, the critical temperature from group contribution theories are in agreement with simulated results. However, for molecules with more than 20 carbon atoms their results suggested that group contribution calculations will overestimate critical temperature value with increasing severity. Their simulated critical densities initially increase with increasing number of carbon atoms, reaching a maximum at C_7, and decrease thereafter. The group contribution methods predicted critical densities continue to increase with the molecular weight, suggesting the disagreement with simulation results for critical density is severe for number of carbon atoms greater than 7 atoms. Comparison of simulation and experimental data with results from available group contribution methods shows that group contribution methods are inadequate for accurate estimation of critical temperature and densities for long-chain molecules, as evidenced by the fact that they predict that both critical temperature and critical density increase continuously with an increase in carbon number.

Though the most popular method for locating the phase coexistence in molecular simulation is still the GEMC method, it has three known deficiencies as mentioned by Gelb and Müller.[15] When simulating dense phases, equilibration is difficult to achieve because of the poor statistics associated with the insertion/deletion steps. The GEMC method can be difficult to apply to systems containing very complex molecules without substantial system-specific modifications (such as Configurational-Bias Monte Carlo). Investigation of very large systems can be problematic using this method because of the difficulty in performing calculations on parallel computers. Standard GEMC simulations develop efficiency problems near the critical temperature owing to frequent swapping of the two simulation boxes as the densities of the two equilibrium phases approach one another. Once this swap occurs, one utilizes an indirect simulation technique such as Histogram Reweighting[38] or Gibbs-Duhem Integration[6] to

determine the remainder of the phase envelope. These indirect methods use an established state point or phase coexistence point and then use statistical methods to obtain the rest of the two-phase region close to the critical point. However, this will be problematic for investigating unknown systems. To ameliorate the identity-switch problem[8] alternatively one can make the vapor box much larger than the liquid box. Another method to study phase equilibria is the "NPT + test particle" method[39]. Because it also includes the particle insertion step, it suffers from the same limitations as the GEMC method for dense fluid.

In contrast, molecular dynamics simulations have advantages that they can be easily applied to both dilute and dense phases, easily parallelized, and routinely applied to complex fluids. The increase in available computing power and the development of parallel algorithms make the use of direct molecular dynamics simulations even more attractive as an efficient method for studying phase equilibrium.

2.1.2 Molecular dynamics simulations

In 2φMD the liquid and the vapor phases are simulated in the same box, usually separated by an interface. In addition to the study of vapor-liquid equilibria and the location of the critical point, MD simulations also allow study of different interfacial properties like molecular orientation, diffusion of molecules through the interface, and interfacial thickness. Related but different approaches to the study of vapor-liquid equilibria with MD have been developed. [14, 15, 16]

Holcomb et al.[14] placed previously equilibrated fractions of a bulk liquid and vapor phase in the form of a slab of liquid surrounded by a vapor phase. The system was then allowed to evolve under NVT conditions through diffusive mass transport. This method, though viable for studying interfacial properties, was not very efficient in obtaining vapor-liquid coexistence data

because of the long equilibration time required for complete phase separation. Harris et al.[40] studied Decane (10 carbon atoms) and Eicosane (20 carbon atoms) using the direct molecular dynamics method. Using the OPLS-UA intermolecular potential model of Jorgensen[27], they obtained good agreement for the coexisting densities, although the surface tensions were overestimated by 20%. The simultaneous simulation of two bulk phases and the two corresponding interfaces, along with slow diffusion made these direct MD methods costly from a computational point of view.

Currently two different ways are preferred to establish the interfaces in MD simulations are the Temperature Quench Molecular Dynamics (TQMD) and the Volume Expansion Molecular Dynamics (VEMD). In the TQMD method[15], the interface is established by equilibrating a homogeneous fluid at temperatures above the critical point and then lowering the temperature into the two-phase region where a phase separation is observed. The VEMD method[16] starts as an equilibrated liquid then the size of the simulation cell can be suddenly extended in one of the coordinate directions to give density in the unstable region along the line of rectilinear diameters. The system then separates into the liquid and vapor phases separated by an interface.

Gelb and Müller[15] in their TQMD method determined the phase coexistence data from the locally equilibrated system, thus it did not require the simulation to continue until global equilibration was reached. This dramatically reduced the computational time. Martínez-Veracoechea et al.[34] showed that results obtained using the TQMD method to be of the same precision as that obtained by the GEMC or VEMD methods.

Fern et al.[17] in 2007 presented a new algorithm to determine the bulk liquid and vapor densities from a 2φMD simulation. This new method uses Voronoi tessellations (VT) to

determine the volume of every molecule in the simulation cell. The densities of the two-phase envelope were determined from the generated molecular volumes using simple statistical parameters such as mean and variance. The critical properties obtained using this method are T_c = 1.293 and ρ_c = 0.313. One advantage of this method is that it allows simulations to run very close to the critical point. Direct simulation of two-phase system was performed up to a temperature of 1.292. When compared to experimental values and the GEMC method, the results showed excellent agreement. Fern et al.[18] further extended the MD + VT method for a polyatomic fluid (Ethanol) using the OPLS-AA potential. Properties like critical temperature, critical density, critical pressure, phase diagram, surface tension, vapor pressure, hydrogen bonding along the two phase envelope, and molecule orientation at the interface were determined. The resultant coexisting densities agree well with the values reported in the literature from GEMC at low temperatures where they are available. The VT method allowed determining coexisting densities much closer to the critical point. Details of all these studies and additional work are summarized in Table 2-1.

2.2 Various potential models

A main limitation of molecular simulation is the lack of intermolecular potentials that can adequately describe complex interactions. Various potential models have been proposed for a wide range of components. There has been continual development of more accurate force fields to describe the intermolecular and intramolecular potentials describing the interactions between the molecules in the system. To describe intermolecular interactions, two common approaches for dividing molecules into interaction sites are usually used in building the molecular force field: the united-atom (UA) model or the all-atom (AA) model (the latter sometimes also called explicit-hydrogen models). The comparison between the two models is shown in Table 2-2.

Table 2-2: Comparison between the UA and AA model

United-atom (UA) model	*All-atom model*
Unites each carbon and its bonded hydrogen atoms into a single interaction site	Treats each hydrogen and carbon atom as separate interaction sites
Treats methyl and methylene segments as single pseudoatoms with their interaction sites commonly located at the position of the carbon atoms	Treats all hydrogen atoms explicitly
Reduces the number of interaction sites by a factor of roughly 3 and thus the computational burden by an order of magnitude.	Considered to be more appropriate for solid or high-density (low-temperature) liquid phases.
Does not allow distribution of partial charges so may not be suitable for polar molecules.	Allows distribution of partial charges to the individual hydrogen and carbon atoms, which may be important in representing the interactions of alkanes with more polar molecules.
e.g.: OPLS, SKS, NERD, TraPPE etc.	e.g.: OPLS-AA, TraPPE-EH, MMFF94 etc.

2.2.1 United-atom models

Several force fields have been developed for the united atom model. The most prominent ones are:

- The OPLS model: The Optimized Potentials for Liquid Simulations[27] model was parameterized using isobaric-isothermal Monte Carlo simulations to give accurate liquid densities and heats of vaporization for short alkanes at atmospheric pressure
    - This force field contained different LJ (Lennard-Jones) parameters for the CH_3 group (methyl group) in ethane, for CH_3 groups in all other *n*-alkanes, and for CH_2 groups (methylene groups).
    - $\sigma_{CH_3}^{ethane} \neq \sigma_{CH_3} = \sigma_{CH_2}$ (i.e. the LJ size parameter for the CH_3 group in all other *n*-alkanes except for ethane is equal to the size parameter for the CH_2 group); $\varepsilon_{CH_3}^{ethane} \neq \varepsilon_{CH_3} \neq \varepsilon_{CH_2}$ (i.e. the LJ well depth parameter is

different for the CH_3 group in ethane, the CH_3 group in all other *n*-alkane and for the CH_2 group in all *n*-alkanes); a total of five LJ parameters

- The SKS model: The Siepmann-Karaborni-Smit model[7, 41] was developed especially for vapor-liquid phase equilibrium, and the parameters were fitted to coexistence liquid densities and the critical point.
    - This force field used the same LJ diameter for methyl and methylene groups, but different well depths, to account for variations in interactions between various sites.
    - $\sigma_{CH_3} = \sigma_{CH_2}$ (i.e. the LJ size parameter for the CH_3 group and that for the CH_2 group for all *n*-alkanes are equal); $\varepsilon_{CH_3} \neq \varepsilon_{CH_2}$ (i.e. the LJ well depth parameter for the CH_3 group is different than that for the CH_2 group for all *n*-alkanes); a total of three LJ parameters
- The TraPPE model: The Transferable Potentials for Phase Equilibria (TraPPE)[31, 8] model, like the SKS model, was based on calculations of the vapor-liquid coexistence curve (VLCC).
    - The methyl group was obtained first from the simulation of ethane and then retained for the longer alkanes. The methylene group parameters were fitted to the VLCC of *n*-octane.
    - $\sigma_{CH_3} \neq \sigma_{CH_2}$ (i.e. the LJ size parameter for the CH_3 group and that for the CH_2 group for all *n*-alkanes are different) ; $\varepsilon_{CH_3} \neq \varepsilon_{CH_2}$ (i.e. the LJ well depth parameter for the CH_3 group is different than that for the CH_2 group for all *n*-alkanes); a total of four LJ parameters

In general, the OPLS force field overestimated the critical temperature of *n*-alkanes. The SKS model was developed to overcome this shortcoming, but it overestimated the critical temperature of shorter alkanes. This was corrected in the TraPPE force field. However, the TraPPE force field model's performance deteriorated with increasing chain length.

2.2.2 All-atom models

There is growing evidence of the inadequacy of the UA model. For example, self-diffusion, viscosity, and local dynamics obtained using the UA model were too fast due to the smoother potential energy surface that results from the neglect of hydrogen atoms. Experimental crystal structures were poorly reproduced. These problems can be overcome by an all-atom model. The computational cost for the all-atom model became less of a burden with the fast evolution of computers. The OPLS-AA force field is one of the most successful and accurate all-atom force field models. In this model, the interatomic potentials were carefully calibrated to the liquid densities and enthalpies of vaporization of small organic compounds near their normal boiling temperatures, so they became less accurate when they were used away from the conditions for which the potential parameters are optimized. Several different all-atom force field models, like the TraPPE-EH, MMFF94 etc., have been reported in the literature. A detailed discussion of these force fields is outside the scope of this project.

There are also some intermediate approaches such as anisotropic (not spherically symmetric) potentials called anisotropic united atoms (AUA) centered at carbon atoms[42], or displacement of the position of the pseudoatom interaction sites away from the carbon atom position[43]. Additional satellite sites (not located at nuclear centers) can also be used to represent electron pairs, aromatic pi orbitals, or other electron density distributions within the molecule.

Using combinations of these approaches, intermolecular potentials can be modeled which have satisfactory efficiency and accuracy when the parameters are adjusted with experimental data.[44]

2.2.3 Background

A summary of the main issues and features of various models is shown in Table 2-3. Martin and Siepmann[8] determined the vapor-liquid coexistence curve for methane to dodecane using three united-atom force field models: OPLS[27], SKS[7], and TraPPE. They proposed a new set of united-atom Lennard-Jones interaction parameters for *n*-alkanes by fitting the parameters to critical temperatures and saturated liquid densities. The new parameters did not reproduce experimental second virial coefficients correctly. Saturated vapor pressures and densities showed small but systematic deviation from the experimental data.

Table 2-3: Summary of main points of work done by various researchers on improving the potential models

Reference	*Issues addressed*	*Molecule, method, & potential model used*	*Conclusions*
Jorgensen et al.[27]	- Optimized intermolecular potential functions for hydrocarbons - 12 constituent groups identified and corresponding LJ parameters optimized	Molecules 15 hydrocarbon liquids including alkanes & alkenes Method MC simulations (NPT ensemble) Potential model OPLS-UA model, with interaction sites centered on carbon for CH_n groups	- Energies & liquid densities showed average error of 2% when compared with experiments
Jorgensen et al.[45]	- Optimized intermolecular potential functions for liquid alcohols - Only four independent parameters were	Molecules Liquid methanol, ethanol, 1-propanol, 2-propanol, & 2-methyl-2-propanol Method MC simulations (NPT	- Average deviation for liquid densities from the experimental value was found to be 1.8% with reported values uniformly a little low

Table 2-3 continued

Reference	*Issues addressed*	*Molecule, method, & potential model used*	*Conclusions*
	added to the OPLS set to describe alcohols	ensemble) Potential model OPLS model one site on each atom except CH_n group represented as united atom centered on carbon	
Smit et al.[41]	- Determined vapor-liquid co-existence curve - Accurate modeling of phase behavior over a large temperature range and chain lengths - Critical properties as a function of carbon number	Molecules C_8 through C_{48} Method CBMC + GE method Potential model OPLS model de Pablo model Toxvaerd model A new model	- A simple UA model was sufficient to obtain good agreement with experiment over a large range of temperature & chain length (only a large difference between the energy parameter of CH_2 & CH_3 is required) - Good agreement between predicted & experimental values for T_c and ρ_c[28] -Simulations of an 8-bead Lennard-Jones polymer model by Mooji et al.[46] agreed with simulations by Laso et al.[25]
Van Leeuwen[47]	- Tested the transferability of the OPLS force field[45] parameter - Derived new parameters for higher alkanols	Molecules Methanol to Hexanol Method GEMC method Potential model OPLS-UA model	- The OPLS force field model was transferable to longer alcohols & to elevated temperatures - Force field proposed performed better but required fine-tuning the methyl group parameters for each alcohol
Jorgensen et al.[48]	- Parameterized and tested OPLS all-atom force field - Thermodynamics, & structural properties	Molecules 34 organic liquids Method MC simulation with BOSS program Potential model OPLS-AA potential model	- 2% average error for heats of vaporization and densities when compared to experimental data
Siepmann et al.[31]	- VLE data - New united atom model to predict phase behavior &	Molecules Three Heptane isomers: n-Heptane, 2-Methylhexan-e,3-Ethylpentane	- T_c & ρ_c of the three isomers were in satisfactory agreement with experimental values - A simple UA model,

Table 2-3 continued

Reference	*Issues addressed*	*Molecule, method, & potential model used*	*Conclusions*
	fluid properties of branched alkanes	Method CBMC + GE method Potential model A new UA model	distinguishing three types of methyl groups, was sufficient to obtain accurate fluid phase diagram of the three isomers
Martin & Siepmman[8]	- Determined vapor-liquid coexistence curve (VLCC) using three UA model force fields - Found optimized set of LJ methyl & methylene parameters for the *n*-alkanes using UA description	Molecules Methane to Dodecane Method CBMC + GE method Potential model OPLS model SKS model TraPPE model	- For OPLS model reasonable results for short alkanes but overpredicted T_c of longer alkanes - Improved results for medium to longer alkanes but over predicted T_c of shorter alkanes for SKS the model. Good prediction of VLCC & critical properties for the TraPPE model - Systematic deviation from experiments for vapor densities and pressures - None of the force fields were able to reproduce experimental second virial coefficients
Chen et al.[49]	- Performance of several all-atom force field, for alkanes were compared & evaluated	Molecules Methane, Ethane, *n*-Butane, *n*-Pentane, *n*-Octane Method CBMC + GE method Potential model OPLS-AA model Williams force field MMFF94	- MMFF94 did not describe thermodynamic properties well - T_c best reproduced by OPLS-AA, agreement improved for longer alkanes - The Williams force field yielded slightly better results for saturated liquid densities
Nath et al.[50]	- Assessed ability of recently proposed force fields to predict orthobaric densities, second virial coefficients & PVT data for long and short alkanes - Proposed a new force field (NERD)	Molecules C_2 through C_{16} (for orthobaric densities) lower alkanes (for experimental virial coefficients) C_8, C_{16}, C_{36}, C_{44}, C_{70} (for liquid densities) Method CBMC + GE method	- SKS was not good for predicting equilibrium properties for moderately long alkanes. TraPPE provided good agreement over SKS for small alkanes but its performance deteriorated as chain length increases. NERD provided good overall agreement with experiment for both short and long alkanes

Table 2-3 continued

Reference	*Issues addressed*	*Molecule, method, & potential model used*	*Conclusions*
	that gave good agreement with experimental phase equilibrium & second virial coefficient data over wide range of temperature & chain length	Potential model SKS model TraPPE model NERD model	The virial coefficients predicted by NERD for short alkanes were in better agreement with experiment than those predicted by TraPPE. The NERD & TraPPE model predictions for longer alkanes were comparable (i.e. deviations between experiments & theory became more pronounced as chain length increased) - NERD gave good agreement with available experimental phase equilibrium data for short and long alkanes - For medium to long alkanes TraPPE slightly overpredicted both T_c & ρ_c, and NERD slightly underestimated the ρ_c but within experimental uncertainty - For short alkanes, NERD slightly overpredicted T_c and for longer chains agreement with experiment gradually increased
Chen & Siepmann[51]	- TraPPE-EH (Transferable Potentials for Phase Equilibrium Explicit Hydrogen) was developed from fitting to one-component fluid properties	Molecules Methane to *n*-Dodecane Method CBMC in the Gibbs ensemble method Potential model TraPPE-EH (Transferable potentials for phase equilibrium-explicit hydrogen)	- Results were compared to TraPPE-UA, OPLS-UA, & OPLS-AA model - Better agreement with experimental were obtained compared to united atom description, but at higher computational cost
Errington & Panagiotop-oulos[52]	- A new united-atom model for the n-alkane homologous series was proposed	Molecules A range of chain lengths Method Histogram reweighting grand canonical MC method Potential model Buckingham exponential-6 potential model TraPPE model	- The new model overpredicted the P_c for longer chain - The critical parameters for the models were found to be in agreement with experiment - T_c was reproduced most accurately with all three models - ρ_c overestimated by TraPPE and slightly underpredicted by NERD

Table 2-3 continued

Reference	*Issues addressed*	*Molecule, method, & potential model used*	*Conclusions*
		NERD model	- P_c overpredicted by all three models, with the deviation from experiment increasing with chain length
Nath & de Pablo[53]	- Proposed a new united-atom force field for branched & linear alkanes	Molecules Different branched & linear alkanes Method CBMC + GE Potential model For simple *n*-alkanes NERD model For branched alkanes NERD model by slight different parameters	- Good agreement with experimental coexistence properties found for branched alkanes up to C_8 - A set of three different methyl units along with a single CH_2, and a single CH unit were sufficient to describe the phase behavior of C_6 & longer alkanes. For smaller alkanes slightly different parameters for the methyl group were required
Ungerer et al.[54]	- Further optimized parameters of AUA3 potential, resulting potential called AUA4	Molecules Various alkanes with chain lengths up to 20 atoms Method GE + CBMC method Thermodynamic integration MD simulation Potential model AUA4 potential	- The AUA4 potential predicted equilibrium properties of pure *n*-alkanes in a large range of temperature and carbon number
Kettler et al.[55]	- Vapor-liquid coexistence data	Molecules Pentane, Decane, & Pentadecane Method Gibbs ensemble (GE) & extended Gibbs ensemble (EGE) monte carlo simulations Potential model Kihara pair potential with elongated molecules	- EGE method performed better for dense, low temperature states - Comparison with second-order perturbation theory showed the theory performs better for large elongated molecule (Pentadecane) but not for Pentane

Table 2-3 continued

Reference	*Issues addressed*	*Molecule, method, & potential model used*	*Conclusions*
Chen et al.[56]	- Extended the TraPPE-UA force field to primary, secondary & tertiary alcohols	Molecules Methanol, Ethanol, Propan-1-ol, Propan-2-ol, Butan-2-ol, 2-Methylpropan-2-ol, Pentan-1-ol, Pentane-1,5-diol & Octan-1-ol Method CBMC + GE method Potential model TraPPE-UA force field with new O and H, α-CH_3, α-CH_2, α-CH pseudoatoms	- 1% error for the saturated liquid densities & normal boiling points, 1.5 & 3% for the critical temperatures & densities, respectively. Overpredicted the saturated vapor pressures.
Bourasseau et al.[57]	- The AUA4 potential was used to predict several equilibrium properties for long and branched alkanes - Transferability evaluated	Molecules N-alkanes (C_{20}, C_{25}, C_{30}), four Heptane isomers (*n*-Heptane, 2-Methylhexane, 2,4-Dimethylpentane, 2-Ethylpentane) Method CBMC + GE Potential model AUA4	- Equilibrium properties of long chain alkanes were accurately predicted - Small differences between Heptane isomers were represented with good accuracy - The AUA4 potential showed an interesting degree of transferability
Khare et al.[58]	- Extended the NERD force field for primary alcohols for study of vapor-liquid equilibria	Molecules Ethanol to 1-octanol Method GEMC method Potential model The NERD force field with new parameter for the hydroxyl group. The hydrogen atom in hydroxyl group was considered explicitly in their model	- The predicted coexistence curve & vapor pressure for the pure component vapor-liquid equilibria were in good agreement with experimental data - One set of parameter was sufficient for predicting phase equilibria of alcohols larger than methanol, but a separate set of parameter was required for methanol
Chang & Sandler[59]	- Developed accurate all-atom force field for linear and branched alkanes	Molecules For linear and branched alkanes Method GEMC method	- The vapor-liquid coexistence densities were reproduced well - The predicted phase envelope was in good agreement with experiment except near the critical point

Table 2-3 continued

Reference	*Issues addressed*	*Molecule, method, & potential model used*	*Conclusions*
	- Validity of potential parameter set tested with extensive GEMC simulations over a wide range of temperatures and chain structures	Potential model Interatomic LJ potential Intramolecular OPLS-AA potential	- The critical densities were well predicted by this model - P_c was predicted within 5.7% for linear alkanes. T_c values were predicted with error of 1.4% - The critical properties for singly branched alkanes were predicted as accurately as those of linear alkanes with an error of 1.3% - With more branches and with a closer proximity of the branches the accuracy of critical properties decreased somewhat
Ahunbay et al.[44]	- Used AUA potential to predict thermodynamic properties	Molecules Several isoalkanes, alkylbenzenes, alkyl-substituted cycloalkanes, polycyclic alkanes, naphtenoaromatics Method GEMC method (at high temperature) & NPT algorithm followed by thermodynamic integration (to predict near lower temp.) Potential model AUA potential	- Good agreement with experiment was found for equilibrium properties. - T_c & ρ_c were predicted with an accuracy of 1.1% and 1.4% respectively
Martin[60]	- Liquid densities and vapor-liquid coexistence curves	Molecules Ethane, Ethanol, Pentane 2-Methylbutane, Isobutane, Isopropanol Method NVT Gibbs ensemble with CBMC for vapor-liquid coexistence: isobaric-isothermal ensemble for liquid densities	- CHARMM and TraPPE force fields were recommended for fluid phase simulations. CHARMM predicted better vapor phase densities, whereas TraPPE predicted the liquid density better and was computationally less expensive

Table 2-3 continued

Reference	*Issues addressed*	*Molecule, method, & potential model used*	*Conclusions*
		Potential model AMBER-96, CHARMM22, COMPASS, OPLS-AA, GROMOS 43A1, TraPPE-UA, and UFF force fields	
Pérez-Pellitero et al.[61]	- AUA4 intermolecular potential were derived for family of alkanols by adjusting the LJ parameters for the OH group & optimizing a set of charges to reproduce the electrostatic distributions of methanol & ethanol	Molecules Methanol, Ethanol, Phenol Octanol, Propan-1-ol Method CBMC + GE method for phase equilibria. Grand Canonical Monte Carlo (GCMC) with histogram reweighting technique to explore critical region Potential model AUA4 intermolecular potential	- Predicted saturated liquid densities and vapor pressures agreed well with experimental values - Model had difficulties reproducing heats of vaporization -Higher deviations at lower temperatures below the critical region
Ferrando et al.[62]	- Extended the AUA4 potential model by proposing a new force field with one new pseudoatom for the OH group	Molecules Methanol, Ethanol, Propan-1-ol, Hexan-1-ol, Octan-1-ol, Propan-ol, 2-Methyl-propan-2-ol, Phenol and Diols Method GEMC method Potential model AUA4 intermolecular potential model	- Good agreement with experimental data for the critical points, thermodynamic properties along the liquid/vapor saturation curve, the normal boiling temperature, and the liquid structure at room temperature

Chen et al.[49] selected the Williams, OPLS-AA, and MMFF94 force field models to calculate the vapor-liquid phase equilibrium for normal alkanes. They selected the above mentioned force field models as representative of all atom models for the following reasons:

- They were fitted using three different strategies (Williams: crystal structure and heats of sublimation; OPLS-AA: liquid densities and heats of vaporization; MMFF94: rare

gas pair potential and quantum mechanics)

- They employed potentials with three different functional forms to describe nonbonded van der Waals interactions (Williams: Buckingham exp- r^{-6}; OPLS-AA: Lennard-Jones 12-6; MMFF94: buffered 14-7) and used different combining rules to determine van der Waals interactions for the interaction of unlike atoms.

They showed that seemingly small differences in the potential functions could account for very large changes in the fluid-phase behavior. Table 2-3 shows the evolution of work performed in improving intermolecular potentials for the study of phase equilibrium.

To explore the properties of long alkanes over a wide temperature range with some degree of confidence, a robust force field should be able to describe quantitatively a range of equilibrium thermodynamics properties for moderately long alkanes. Nath et al.[50] predicted a new, modified force field denoted as NERD which provided good agreement with experimental phase equilibrium data over a wide range of temperatures and chain length. For short alkanes, the NERD model slightly over predicted the critical temperatures. However, agreement with experiment gradually improved with longer chain lengths. For intermediate to long chains, the NERD model appeared to slightly underestimate the critical density.

The TraPPE and NERD models adequately reproduced the critical properties and saturated liquid densities of *n*-alkanes over a wide range of chain lengths; however, the agreement with experimental saturated vapor densities and vapor pressures was less satisfactory. Errington and Panagiotopoulos[52] proposed a new united-atom model for the *n*-alkane homologous series with these features:

- They used the Buckingham exponential-6 potential instead of the Lennard-Jones 12-6 potential to describe the nonbonded interaction energies.

- Histogram reweighting grand canonical Monte Carlo methods were used to determine the model parameters

Previously using Gibbs ensemble method to determine the coexisting densities and vapor pressures for a trial parameter set, the uncertainty in the vapor pressure and vapor density was found to be around 10%. In comparison the vapor pressure and vapor density were calculated to within less than 1 % of the experimental data using histogram reweighting allowing one to fine-tune the parameters such that both the liquid and vapor properties could be reproduced to a high level of accuracy. The drawback of the histogram reweighting technique was that it increases computation time because multiple runs are needed to cover the range of temperatures and densities relevant for determining a complete coexistence curve. The model has now been used to reproduce the saturated liquid and vapor densities, vapor pressures, and critical parameters of the *n*-alkanes series.

In the more classical UA potentials, each force center is located on the carbon, while in the Anisotropic United Atom (AUA) potential, the force center is shifted so that it is placed between the carbon and hydrogen atoms of the related group. In the AUA4 potential, the CH_2 and CH_3 Lennard-Jones parameters were optimized simultaneously to describe differently those two types of force centers. Ungerer et al.[54] used the AUA4 potential to predict the equilibrium properties of *n*-alkanes in a large range of temperature and carbon number using a unique set of parameters.

In the work of Ungerer et al.,[54] it appeared that long chain *n*-alkanes such as *n*-eicosane were not well described because the MC algorithm was not achieving a sufficient internal relaxation of the chain. To achieve internal relaxation of long chains with good efficiency, Bourasseau et al.[57] implemented a specific Monte Carlo move to relax the internalconfiguration

of chains containing more than ten carbon atoms by rotating a UA site (chosen at random) around its nearest neighbors. They also tested AUA4 transferability (i.e. application of the same potential to different molecules containing the same groups) by applying the potential to molecules other than those used to optimize the potential, without modifying any of its parameters. Their work also showed that small differences in properties between isomers could be predicted using the AUA4 potential model. These investigators concluded that a shift in the center of force used in AUA models allowed a significant improvement of potential transferability.

In the work of Ahunbay et al.[44], a variety of hydrocarbons with different molecular structures was used to demonstrate transferability of AUA potential parameters. They implemented configuration-bias, reservoir bias, and parallel tempering to increase the efficiency of the simulations. The critical temperature and critical density were determined by fitting vapor-liquid co-existence data to the critical scaling law and to the law of rectilinear diameters. The predicted properties were found to be in very good agreement with the available experimental data. These predictions also suggested the good transferability of the AUA intermolecular potential and that the off-center sites accounted for the influence of the hydrogen atoms even though a UA-type model was used.

2.3 Conclusions

Out of all the methods to study VLE each has its strength and weaknesses. Even the most common and widely popular method Gibbs Ensemble Monte Carlo (GEMC) to study VLE is not without limitations, particularly, in the context of the simulation of very dense phases and/or complex molecules. Problem also arises as the temperature approaches the critical temperature due to frequent swapping of the identities of the individual simulation cells thereby smearing out

all the data. To address the limitations of the GEMC method, other methods to investigate phase equilibrium by Molecular Dynamics (MD) simulations began to appear in the literature. Different MD methods differ by how the two-phase system within an MD simulations are created or ways to extract the bulk phase densities within the two-phase simulation volume. Fern et al.[17,18] developed a new method which uses the MD simulation along with Voronoi tessellations to deal with the deficiencies in the previous MD method. The new method allowed simulations very close to the critical point. Complex fluid can be handled very easily using this method. Phases were determined self consistently by matching the means and variance from the two-phase and one-phase simulations.

Improvements to predict critical properties using any method requires better method, more efficient way to predict properties and better accuracy. The simplicity and clarity of a method, easier code implementation and quicker simulation time for a given accuracy are also good characteristics for a particular method. The method used in our work is very similar to that developed by Fern et al.[17, 18] except that it uses an MC sampling technique instead of the VT with the MD simulations to determine the coexisting densities and the critical properties. This MD + MC method described in detail in the next chapter has all the good characteristics of VT but without the complications of requiring modifications for multisite molecules. The new method is very simple to program and implement and is very versatile in the sense that it can be easily extended from one system to another and can be used for different molecules without requiring much modifications.

3 SIMULATION METHODS

3.1 Molecular dynamics simulation method

In Molecular Dynamics simulations, the equations of motion for the interacting molecules in the system are solved to obtain a transient map of the system's trajectory in phase space. Comprehensive overviews of MD simulations have been written by Allen and Tildesley[63] and Frenkel and Smit[6]. In this work, MD simulations were performed to determine two-phase configurations of model molecules below the critical point and in the near-critical, two-phase region. A post-processor that uses a MC method for determination of volumes attributable to each molecule was used to obtain density histograms of the particles from which the bulk coexisting equilibrium vapor and liquid densities were determined. This method of analyzing coexisting densities in a two-phase simulation is straight forward and can be easily implemented for complex, multisite models.

An in-house Fortran code for standard NVT MD simulations with periodic boundary conditions and the minimum image convention was used to perform the simulations. Simulations started with particles on a body-centered cubic lattice at a uniform density in the 2φ region. Both positions and velocities were initialized in the starting configuration. Newton's equations of motion were then used to move the system forward in time from the initial conditions. The code employs a Gear predictor-corrector method to integrate the equations of motion. The initial dimensionless starting system density was fixed at a value chosen to be in the 2φ region to yield

substantial numbers of particles in both phases. The system was allowed to run long enough to equilibrate, thereby eliminating any dependence upon the initial configuration. Equilibration runs consisted of longer equilibration times at higher temperatures.

As pointed out by Pamies et al.,[16] finite size effects play an important role in the MD technique because of the high energy cost of forming the interfaces. Larger system sizes for MD 2φ simulations are therefore required than are commonly used in GEMC simulations of phase equilibrium. Although many properties are not impacted by potentials cut off at a distance beyond 3.5 – 4.0σ, previous studies[12, 14 , 64, 65] have found that the length of simulated tie lines, hence the width of the phase envelope, can depend significantly on cutoffs shorter than 4.0σ. Fern et al.[17] found that a cutoff of 6σ was sufficiently large to eliminate effects of the truncated pair potential on the phase dome loci, and we have used that value in all of our LJ simulations. No long-range corrections to energy or pressure were included in the calculations owing to the large cutoff distance employed.

A neighborhood list with a 2 Å buffer distance and automatic neighbor updates was used to improve simulation efficiency. Temperature re-scaling was used initially to set the dimensionless temperature, $T^* = kT/\varepsilon$ where k is Boltzmann's constant, to the desired simulation condition. A Gaussian thermostat was employed to maintain constant temperature conditions. After equilibration, molecular configurations were saved as particle Cartesian coordinates at desired time intervals. Only the resultant configurations were required to determine the 2φ densities. A post-processor code for MC sampling method was used to obtain the volume associated with each particle from the configurations output by the MD code.

3.2 Monte carlo sampling method

A Monte Carlo sampling method was used to determine the volume associated with every particle in the simulation cell. Once the equilibration and production run were completed, the positions at the last step were saved. The MC sampling method was then employed on this saved configuration. This was done by placing a very large number, N_{MC}, of equally-spaced grid points within the simulation cell. Figure 3-1 depicts an example of how the grid points were assigned to the nearest LJ sites (in 2D). It shows a magnified view of grid points (squares) around five molecules (circles). For convenience, the grid points shown in the figure were placed randomly rather than equally-spaced as done in the actual calculations. The distances between each particle and each of the grid points within the simulation cell was determined and each of the N_{MC} points was then assigned to the closest LJ site. As shown in the top figure, the distances from the grid point (square) to all the five

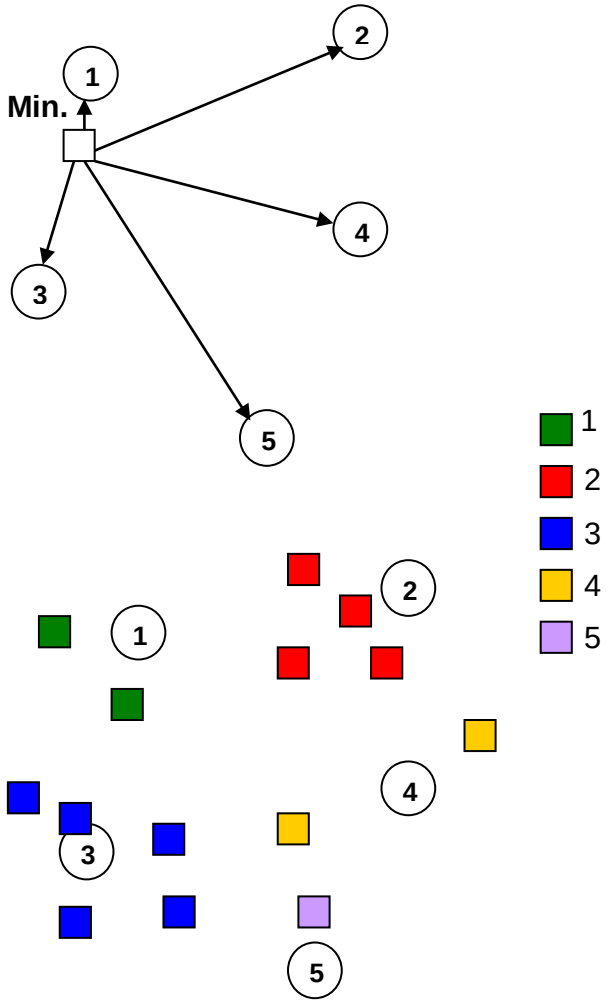

Figure 3-1: A magnified view of grid of points (in two dimensions) around a couple of molecules showing the assignment of grid points to its nearest molecule

molecules (circles) were calculated. Since the grid point is closest to molecule ‘1’, it was assigned to molecule ‘1’. The color code here indicates which molecule the grid points belonged to (bottom figure). A green color grid point means the point belongs to molecule ‘1’, an orange color indicates that the grid point belongs to molecule ‘2’ and so on. Using this procedure, all the grid points associated with each molecule were determined. In the example, molecule ‘1’ has two grid points (green squares) closest to it, molecule ‘2’ has four grid points (orange squares). Molecule ‘3’, ‘4’ and ‘5’ has five (blue squares), two (yellow squares) and one (lavender square) respectively.

Once we had the grid points associated with each particle, the volume of each LJ particle, V_i, was calculated as the fraction of the total box volume V given by the ratio of the grid points closest to particle i to the total number of grid points; i.e.,

$$\rho_i = V_i^{-1} = \left(\frac{N_i}{N_{MC}} V \right)^{-1}, \tag{3-1}$$

For structured molecules, the molecular volume is obtained by summing over all the individual site volumes for that molecule. A histogram of particle densities was prepared by assigning each particle to a discrete bin of finite width $\Delta\rho_{\text{bin}}$ that spans the particle’s density as calculated from Eq. (3-1). Once the particle density histograms were generated, the average bulk vapor and liquid densities were determined using similar iterative procedure proposed by Fern et al[17, 18]. This iterative process is describes in more detail in the next section. The algorithm used to determine the volume associated with each molecule is implemented in a C++ code called *volconfig.cpp*. The coded algorithm is given in Appendix A.

3.3 Phase determination

The 2φMD method reported by Fern et al [17, 18] has been shown to determine the equilibrium vapor and liquid densities accurately even near the critical point because complete phase separation is not required. This method utilizes Voronoi tessellations along with the MD simulations, rather than the MC sampling method mentioned above, to determine the molecular volume of each molecule in its local environment. In the 2φMD method, the Voronoi tessellations give a time-averaged histogram of the molecular volumes with a bimodal distribution when the simulation is performed in the two-phase region. The bulk vapor and liquid densities are then determined using an iterative process as described below by performing several one-phase MD (1φMD) simulations until the normalized mean and variance of the liquid and vapor distributions from the 1φ simulations match within an acceptable tolerance to those in the 2φ simulation.

In the 2φ region, the resultant density histogram exhibits a bimodal behavior with peaks that correspond to the densities of the two phases (like the blue curve in Figure 3-2). Following the procedure developed by Fern et al.,[17] we determine the densities of the coexisting phases by requiring that both the first and second moments of the two peaks generated by the 2φ simulation match, in a least squares sense, those obtained from 1φ simulations of the saturated liquid and vapor phases. This is done iteratively in a self-consistent manner (this iterative process is also illustrated as a flow chart in Figure 3-3). Initial values for the mean liquid and vapor densities are taken from the corresponding maxima of the two peaks as illustrated in Figure 3-2. The liquid peak distribution from the 2φMD simulations is then defined to include all densities above the mean and all densities less than the mean, down to a cutoff density that will reproduce the estimated liquid mean density from the truncated histogram distribution. Similarly one defines

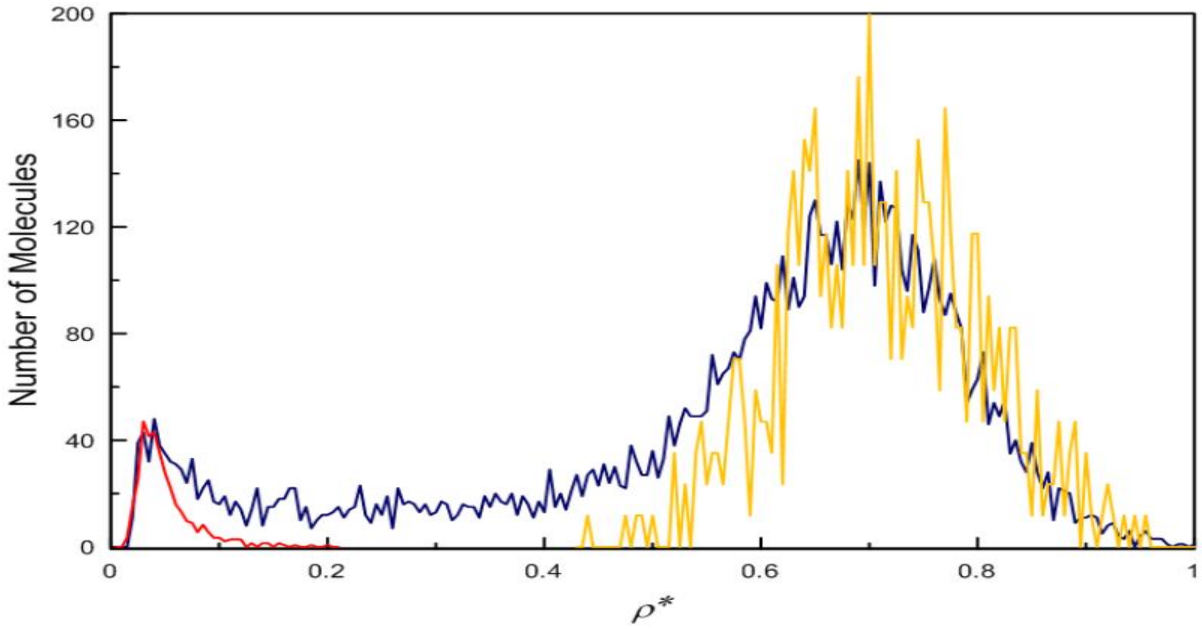

Figure 3-2: Molecular density distribution of a Lennard-Jones fluid for two-phase simulations with number of molecules, NM=8000; reduced temperature, T^*=1.0; interaction potential cutoff, rcutoff*=6.0 (—) and for one-phase simulations with number of molecules, NM=512 (— for vapor and — for liquid)

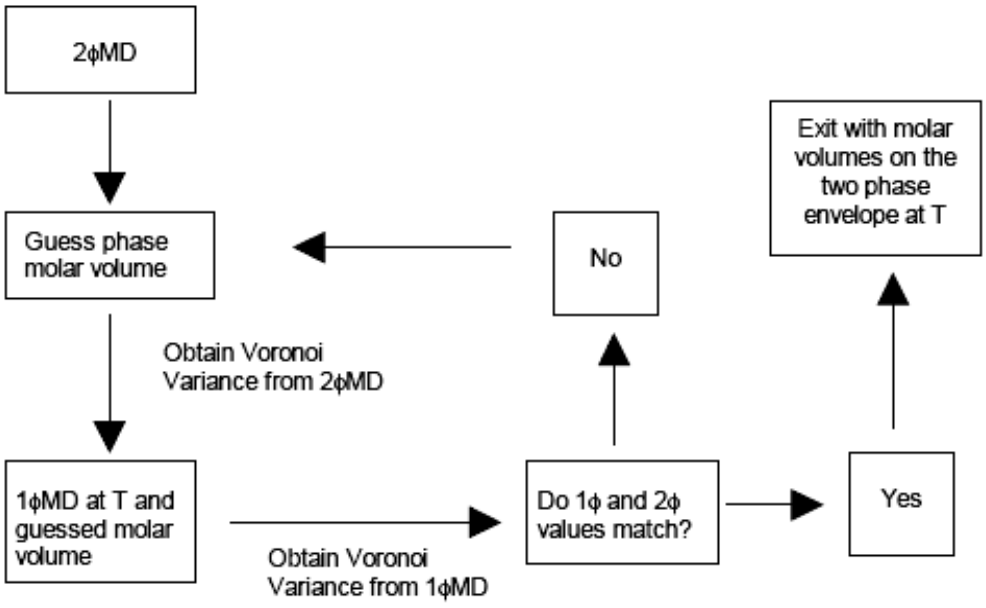

Figure 3-3: Flow sheet describing the procedure to determine the molar volumes of the vapor and liquid phases at each temperature[17]

the vapor peak distribution to include all densities less than the initial mean, up to a cutoff density that produces a mean for the vapor-peak distribution equal to the guessed vapor density. The variances of the two peaks defined by these cutoff values are then calculated. A short 1φ MD simulation with fewer particles is then run at the mean liquid density (and same temperature as the 2φ simulation), and the variance of the resultant 1φ density histogram is compared to the variance of the liquid peak from the 2φ simulation. If the two variances match, then the correct mean density was guessed. If the two variances don't match, then a new guessed mean liquid density value is selected and the 2φ liquid peak is again defined from the highest density to a cutoff value that yields the guessed density. Again a short, small 1φ liquid simulation is run to compare the variances of the 1φ and 2φ liquid peaks at the same mean density. Each iteration involves running just the small 1φ simulations; no new 2φ simulations are performed. The same iterative procedure defines the 2φ vapor density peak, iterating with short 1φ vapor simulations at each of the guessed densities until the mean and variance of the one- and two-phase simulations match. Typically, only four to six 1φ simulations need be performed to refine the coexisting phase densities to the statistical accuracy of the method.

3.4 Critical properties determination

Once the coexisting densities are determined using the above iterative process, the critical temperature and critical density were determined by fitting the liquid and vapor densities in the sub-critical region simultaneously to the density scaling law[6],

$$\rho_{liq} - \rho_{vap} = B(T - T_C)^{\beta} \tag{3-2}$$

and the law of rectilinear diameters[6],

$$\frac{1}{2}(\rho_{liq} + \rho_{vap}) = \rho_C + A(T - T_C) \tag{3-3}$$

where A and B are adjustable parameters, and β is the critical exponent for the order parameter, which is ρ_{liq} - ρ_{vap} for the vapor-liquid coexistence curve. According to a review by Pelissetto and Vicari[66], experimentally derived values of β reported in the past decade range from approximately 0.315 to 0.34 with a possibly best theoretical value of 0.326. We have used a value of β = 0.32 in our application of Eq. (3-2) and (3-3) to obtain T_c and ρ_c from the simulated coexistence data.

The vapor pressures were determined from the virial using the 1φ vapor simulations. The critical pressure, P_c, was then obtained by fitting the vapor pressure data to the Riedel vapor pressure equation,

$$\ln\ (P^*) = A + B + C ln\ (T) + DT^2 \qquad (3\text{-}4)$$

3.5 Conclusions

A method for determining the bulk vapor and liquid densities using the MD simulations along with the MC sampling method was developed. The critical points were then determined by fitting the coexisting densities to the density scaling law and law of rectilinear diameters. In the next three chapters, the simulation results obtained for different molecules used in this work using the abovementioned MD simulations along with MC sampling method are presented. All the details regarding the potential model used, simulation details, and simulations results are mentioned in their individual chapters.

4 2ΦMD SIMULATIONS OF THE PHASE DOME FOR A LENNARD-JONES FLUID AND PROPANE

4.1 Introduction

In this chapter, the Monte Carlo sampling method in conjunction with 2φ MD simulations is validated by reproducing the phase dome obtained by Fern et al.[17] for a simple Lennard-Jones (LJ) fluid. The methodology is then extended to a force field model for a structured molecule (propane), and its coexisting densities and critical point are determined. The results are compared for flexible (bond vibrations and angle bending) and rigid models. A comparison of the results provides an indication of the degree to which internal degrees of freedom may affect the phase behavior and critical point of model fluids. Our flexible model phase-dome results are also compared with the GEMC results of Martin and Siepmann[8] performed with the same intermolecular force field model. The simulation method and the results for the LJ fluid are discussed first and then the results obtained for propane are presented.

4.2 Lennard-jones (LJ) simulations

To benchmark the simulation code, the 2φ procedures were implemented in a comparative study of the Lennard-Jones (LJ) liquid-vapor coexistence curve and critical point. To compare directly with the 2φ results obtained by Fern et al.,[17] similar simulation methods have been employed. The 2φ simulations were performed with 8000 particles with pairwise LJ

interactions truncated at 6σ, where σ is the LJ size parameter. The 1φ simulations were performed with only 512 LJ particles.

An in-house Fortran code for standard NVT MD simulations with periodic boundary conditions was used to perform the simulations using a time step of 1.11 fs. Simulations for a Lennard-Jones fluid were run using dimensionless quantities. Dimensionless quantities are found using the following relations:

$$T^* = \frac{kT}{\varepsilon}, \tag{4-1}$$

$$\rho^* = \rho\sigma^3 N_0, \tag{4-2}$$

$$t^* = t\left(\varepsilon / m\sigma^2\right)^{1/2}, \tag{4-3}$$

$$r_c^* = r_c / \sigma, \tag{4-4}$$

Where T is temperature, ρ is molar density, t is time, r_c is the interaction potential cutoff distance, k is Boltzmann's constant, N_0 is Avogadro's number, m is a molecule's mass, ε is the LJ well-depth parameter, σ is the LJ size parameter. The initial dimensionless starting density ($\rho^* = \rho\sigma^3 = N\sigma^3/V$) was fixed at 0.3, chosen to be in the 2φ region to yield substantial numbers of particles in both phases. Throughout this section an asterisk superscript indicates variables made dimensionless using the Lennard-Jones parameters σ and ε. N and V are the number of particles and simulation box volume, respectively. A neighborhood list with a 2 Å buffer distance and automatic neighbor updates was used to improve simulation efficiency.

4.2.1 Molecular model

The total potential of the fluid, *U*, is represented as the sum of the pair-potential energies between molecule *i* and molecule *j*, u_{ij}.

$$U = \sum \sum_{i<j} u_{ij} \ , \tag{4-5}$$

where the double sum is taken over all $i < j$ to avoid counting each pair of molecules twice. The interaction potential between molecules *i* and molecule *j* is represented by the LJ potential model which is given in the terms of dimensionless potential, $u^* = u/\varepsilon$, and dimensionless intermolecular separation, $r^* = r/\sigma$, as

$$u^*\left(r^*\right) = 4\left(r^{*-12} - r^{*-6}\right). \tag{4-6}$$

4.2.2 Results and discussion

Two issues were explored to optimize the efficiency of the volume sampling technique: the size of the grid point array N_{MC} and the number of independent configurations to save from the MD simulation on which to perform the volume sampling. Functionally, the size of the grid array determines the smoothness of the distribution. A comparison of the density histograms obtained for 64 million, 216 million, and 512 million grid points is shown in Figure 4-1. As can be seen, 64 million grid points are adequate to perform the MC sampling of the volume and assign densities. Noise in the distribution is due to the bin size. However, the level of noise observed in these histograms does not adversely affect determination of the equilibrium phase densities which is done by matching the mean and variance of the 1φ and 2φ density distributions.

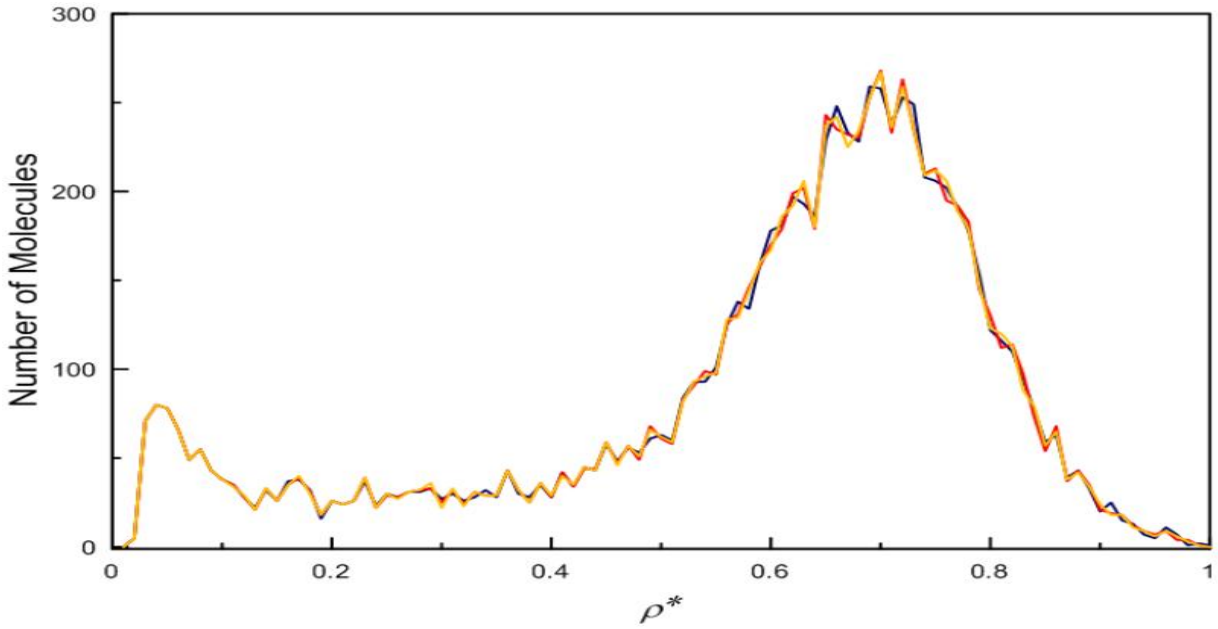

Figure 4-1: Molecular density distribution for two-phase simulations obtained using 64M (—), 216M (—), and 512M (—) MC sample points at T^* = 1.0 for 8,000 LJ particles

The effect of the number of configurations to use in the histogram of densities was examined by comparing the distributions obtained by averaging various numbers of configurations, N_{conf}. As shown in Figure 4-2, N_{conf} values of 1, 5 and 25 produce the same density distribution with no perceptible or statistical change in the distributions. The larger spacing between the volume-sampling grids points (smaller value of N_{MC}) used in this parametric study accounts for the larger noise level exhibited by the liquid phase in Figure 4-2 compared to Figure 4-1. These configurations were generated with 8,000 LJ particles using a cutoff distance of 6σ, T^* = 1.0, and N_{MC} = 5 million. Configurations were generated over 500,000 time steps in all three cases. The separation between the generated configurations was 100,000 time steps for N_{conf} = 5 and 20,000 time steps for N_{conf} = 25. While it is essential to run the simulation for sufficient time to get an equilibrium configuration, the use of multiple configurations does not aid in the analysis of the 2φ distribution. To verify this conclusion even very near the critical

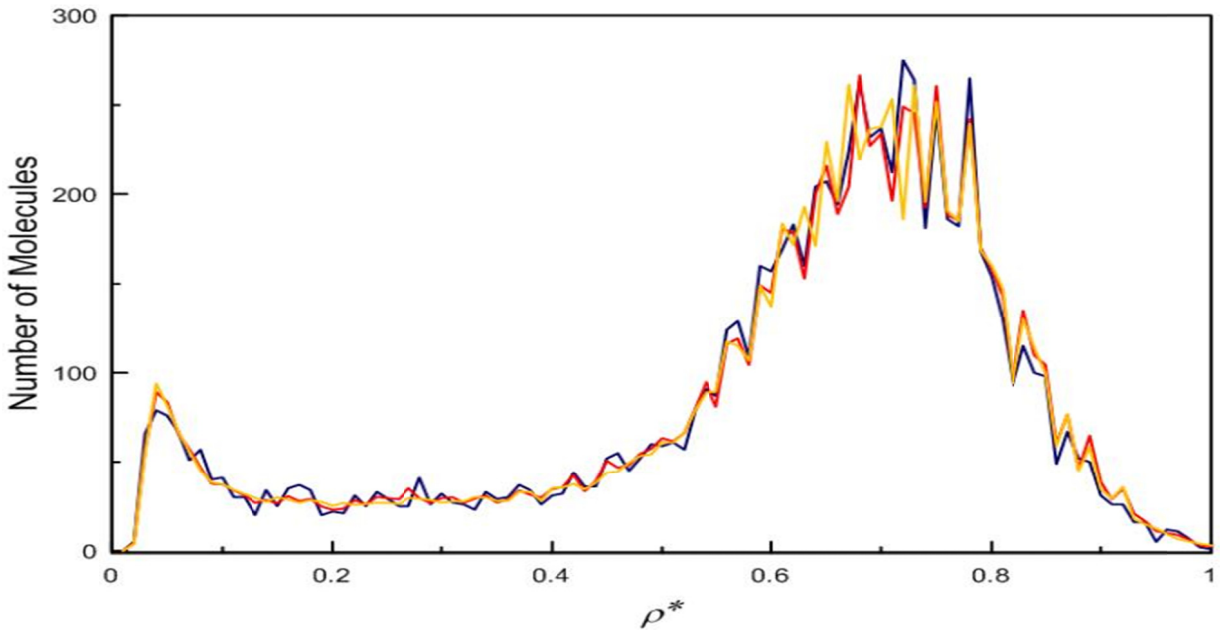

Figure 4-2: Molecular density distributions obtained from 1 configuration (—), from an average of 5 configurations (—), and from an average of 25 configurations (—) at T^* = 1.0 for 8,000 LJ particles

point, we generated and compared the density distributions at $T^* = 1.28$ ($T_c^* = 1.293$)[17] for N_{conf} values of 1 and 5 shown in Figure 4-3. Again the density distribution for $N_{conf} = 5$ was indistinguishable from that of a single configuration, similar to Figure 4-2. Based on these results, the standard volume mapping chosen for the production simulations was N_{MC} = 64 million and $N_{conf} = 1$.

The 2φ simulations were performed for the LJ fluid at reduced temperatures of $T^* = 1.0$ and 1.2 to benchmark our implementation of the method by direct comparison to the results obtained by Fern et al.,[17] who used the Voronoi tessellation (VT). The results obtained are shown in Table 4-1. Also shown in the table are the bulk densities at which the simulations were performed and the equilibration time in nanoseconds at which the final configuration was obtained. To within the statistical uncertainty of the calculations, the equilibrium phase densities obtained are identical to those previously reported by Fern et al.[17]

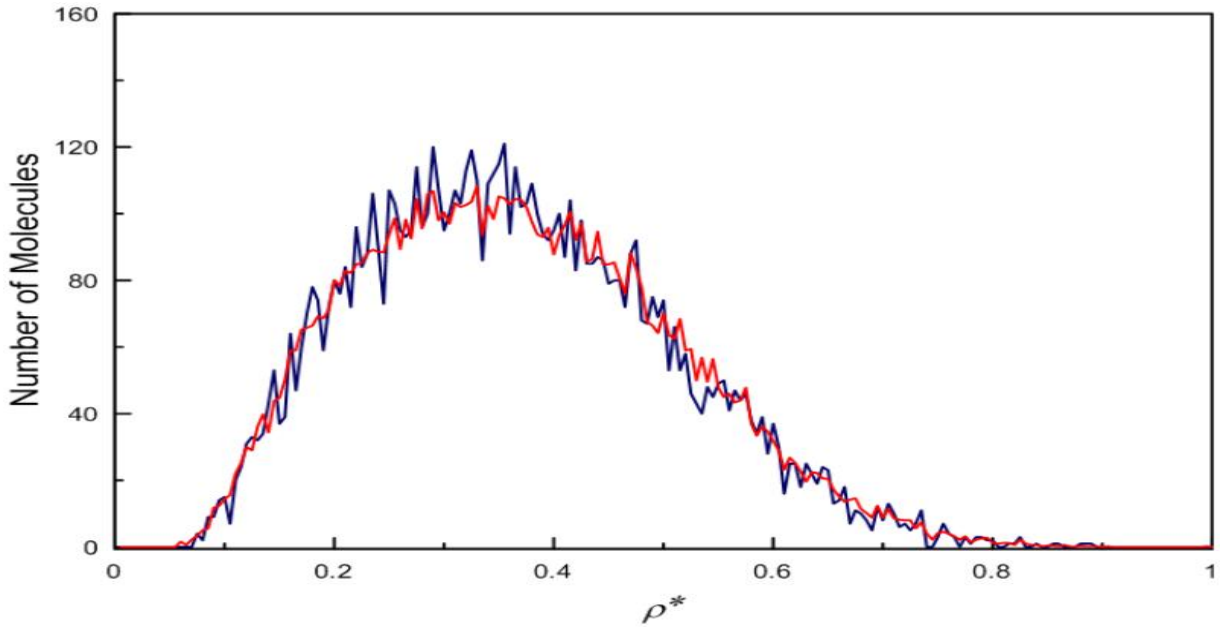

Figure 4-3: Molecular density distributions obtained from 1 configuration (—), from an average of 5 configurations (—), at T^* = 1.28 for 8,000 LJ particles

Table 4-1: Coexisting equilibrium densities for a LJ fluid determined by 2φ simulations using VT[17] and MC sampling

T^*	ρ^* (bulk)	Equilib.	Vapor		Liquid	
			ρ_V^* (MC)	ρ_V^* (VT)	ρ_L^* (MC)	ρ_L^* (VT)
1.0	0.3	1.1 ns	0.034	0.032	0.694	0.694
1.2	0.3	1.65 ns	0.121	0.121	0.548	0.550

The progression of the density histogram distributions with time obtained from the two-phase simulations are shown in Figure 4-4 below. These configurations were generated with 8,000 LJ particles using a cutoff distance of 6σ, T^* = 1.0, and N_{MC} = 5 million at 100,000 time step, 300,000 time step and 500,000 time step after the equilibration is done. As mentioned before the larger noise level exhibited by the liquid phase is due to the larger spacing between the volume-sampling grid points (smaller value of N_{MC} = 5 million) used in this parametric study. Once the simulation has been run for sufficiently long time thereby allowing the system to equilibrate (i.e. free of its initial configuration), the location of the peaks and valleys in the

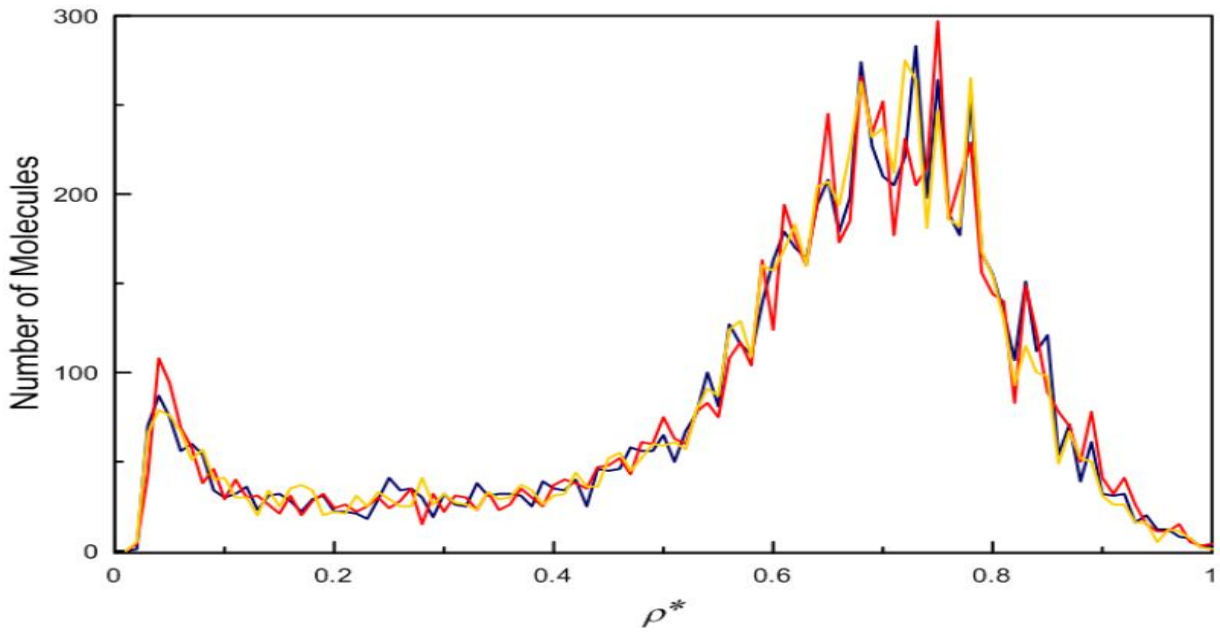

Figure 4-4: Molecular density distributions obtained for 100,000 time step (—), for 300,000 time step (—), and for 500,000 time step (—) after equilibration at T^* = 1.0 & bin size = 0.01 for 8,000 LJ particles

density space does not change much with progression of time as seen from the figure. One good test to determine if the system has reached equilibrium would be to generate the two phase density distributions after some interval of time and compare their structure of densities fluctuations. In the figure density fluctuations with progression of time seems to have persistent structure (peaks and valley at the same locations in the density space) in the density fluctuations because the simulations were performed at the same initial starting densities. Two phase density distributions obtained using two different simulations with different initial starting densities will give different locations of the peaks and valleys in the density space even though the resultant average liquid and vapor densities from the two simulations obtained will be the same.

4.3 Propane simulations

The MC-volume-sampling method is directly applicable to multi-site molecular potential models. In this section, the simulation details and results for propane are presented.

4.3.1 Molecular model

Interaction sites can be located at the centers of all atomic species, as in all-atom potential models, or only at the location of the heavy nuclei (non-hydrogen atoms), as in united-atom models. The united-atom representation is used for propane as shown in Figure 4-5.

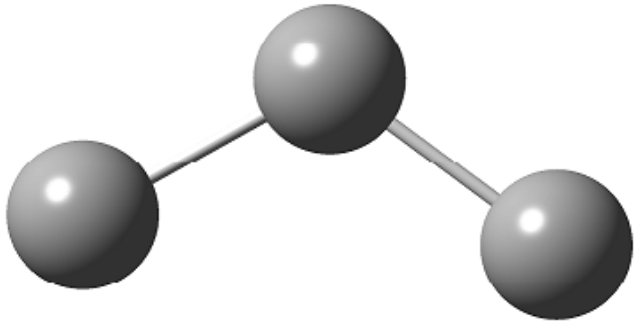

Figure 4-5: United-atom model of propane

The potential energy, u, between two molecules is obtained for these models from the sum of the potential energies between all pairs of interacting sites i,j on the two molecules. In the case where the site-site interactions are modeled with the LJ potential,

$$u = 4\sum_{i=1}^{ns}\sum_{j=1}^{ns}\varepsilon_{ij}\left[\left(\frac{\sigma_{ij}}{r_{ij}}\right)^{12} - \left(\frac{\sigma_{ij}}{r_{ij}}\right)^{6}\right], \tag{4-7}$$

where r_{ij} is the distance between site i on molecule 1 and site j on molecule 2, ns is the number of interaction sites on the molecule, and σ_{ij} and ε_{ij} are the LJ size and energy parameters, respectively, that model the i-j site-site interactions. As was done with the LJ fluid, the post-

processor overlays a grid of N_{MC} points upon the configuration generated by the MD simulation code. Each of the N_{MC} grid points is assigned to the closest interaction site, and the fraction of grid points assigned to any one site represents the fractional box volume that it occupies. The molecular density histograms are then generated from the inverse of the molecular volume, which is the sum of the interaction site volumes for that molecule, using Eq. (3-1).

The liquid-vapor coexistence curve and the critical point of model propane molecules were examined using this method. The basic intermolecular force-field model used was TraPPE-UA[8] developed by Martin and Siepmann. This is a three-site, united-atom model in which the LJ cross interactions [$i \neq j$ in Eq. (4-7] are related to the like interactions through the Lorentz-Berthelot combining rules,

$$\varepsilon_{ij} = \sqrt{\varepsilon_{ii}\varepsilon_{jj}} \qquad \sigma_{ij} = \frac{\sigma_{ii} + \sigma_{jj}}{2}, \tag{4-8}$$

In addition to the LJ site-site interactions of Eq. (4-7), the model also includes a harmonic potential to govern angle bending,

$$u_{angle} = \frac{k_\theta}{2}(\theta - \theta_0)^2, \tag{4-9}$$

where k_θ is the force constant, θ is the bond angle, and θ_0 is the equilibrium angle. Bond distances are fixed at the equilibrium bond distance. A summary of the model parameters used in the simulations is given in Table 4-2. Bond vibrations were also included in our base propane model, which we label *flexible*-TraPPE-UA. The bond vibrations were governed by

$$u_{vibr} = k_v(d_{C-C} - d_{C-C,0})^2, \tag{4-10}$$

where k_v = 96,500 K/Å^2, $d_{C\text{-}C}$ is the distance between any pair of bonded carbon atoms, and $d_{C\text{-}C,0}$ is the equilibrium carbon-carbon bond distance given in Table 4-2.

Table 4-2: TraPPE-UA model parameters used for propane

Parameter	CH_3-CH_3	CH_2-CH_2	CH_3-CH_2	C-C-C
ε/k_B	98 K	46 K	67.14 K	
σ	0.375 nm	0.395 nm	0.385 nm	
$d_{C\text{-}C}$			0.154 nm	
θ_0				114°
k_θ/k_B				62500 K/rad^2

4.3.2 Simulation details

The propane MD simulations were run at four different temperatures, 281 K, 312 K, 330 K, and 344 K, using 2744 molecules (each with three sites) and a step size of 1.34 fs. The temperature of the system was controlled by applying the Gaussian thermostat to the center-of-mass velocities with velocity re-scaling as needed to correct for drift. Specific details for the overall densities, lengths of equilibration time before configurational sampling (t_{eq}), and potential cutoff distances are given in Table 4-3. In all cases, 64 million MC grid points were used to determine the volumes associated with each site and therefore the molecular density used in the density histogram. The LJ potentials were truncated at the values shown in Table 4-3. Because of

Table 4-3: Simulation specifics and results for the 2φMD simulations of propane

T/K	r_c / Å	ρ_m/g·cm^{-3}	t_{eq}/ns	$\rho_{m,vap}$/g·cm^{-3}	$\rho_{m,liq}$/g·cm^{-3}
281	25	0.250	1.27	0.0108	0.5253
312	29	0.130	2.81	0.0321	0.4805
330	29	0.130	2.41	0.0431	0.4131
344	29	0.180	2.35	0.0715	0.4006

the density inhomogeneities in 2φ simulations, the usual cutoff corrections, which assume unity for the radial distribution function at long lengths, cannot be applied directly. We chose instead to use sufficiently large potential cutoff distances to eliminate the need for long-range

corrections. The 1φ simulations were performed with 216 propane molecules. The final values obtained for the simulated equilibrium liquid and vapor mass densities (ρ_m) are given in Table 4-3.

4.3.3 Results and discussion

The vapor-liquid coexistence curve obtained for the *flexible*-TraPPE-UA model for propane is shown in Figure 4-6. Also shown in the plot are the GEMC results obtained by Martin and Siepmann.[8] The new coexistence curve generated from the 2φ simulations agrees within the statistical uncertainty of the simulated points with the GEMC results. The critical temperature and critical density were determined by fitting the liquid and vapor densities in the sub-critical

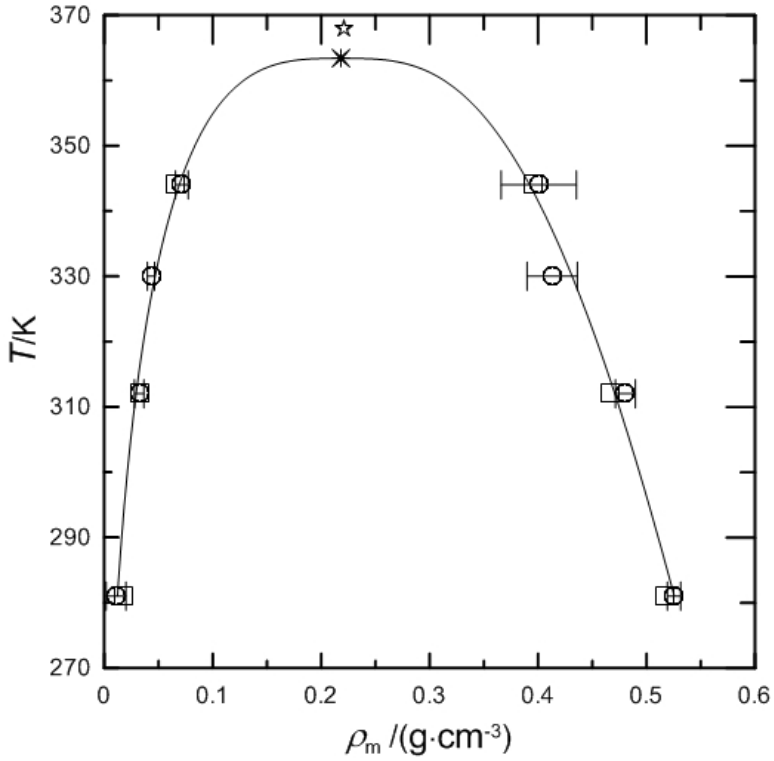

Figure 4-6: Equilibrium coexisting densities obtained for the fully-flexible TraPPE-UA model of propane using 2φMD simulations (○, solid line, error bars) compared to Gibbs-ensemble results (□). Also shown is the resultant critical point for the 2φMD (asterisk) and the Gibbs-ensemble (star) simulations

region simultaneously to the density scaling law Eq. (3-2), and the law of rectilinear diameters Eq. (3-3). We have used a value of $\beta = 0.32$ in our application of Eqs. (3-2) and (3-3) to obtain T_c and ρ_c from the simulated coexistence data which is consistent with the value used by Martin and Siepmann[8]. Table 4-4 shows the resultant critical properties for the models.

The agreement of *flexible*-TraPPE-UA model's coexistence curve and critical point with the GEMC results is interesting because the original TraPPE-UA model does not include the bond vibration potential given by Eq. (4-10). We see only two differences in the implementation of the TraPPE-UA model in this study from the previous GEMC work. One is system size, where we have used 8,000 molecules to both ensure a reasonable number of molecules in both phases and enable the use of a large cutoff distance within the constraints of periodic boundary conditions. The second difference is in the cutoff itself. The GEMC work used a cutoff of 14 Å with analytical cutoff corrections for energy and pressure while we have used cutoffs of at least 25 Å without correction terms.

Table 4-4: Critical properties for the propane model fluids

Method	Model	T_c /K	$\rho_{m,c}$ /(g·cm^{-3})
GEMC[8]	TraPPE-UA	368	0.221
2φMD	*flexible*-TraPPE-UA	363 ± 5	0.219 ± 0.02
2φMD	TraPPE-UA	348 ± 2	0.216 ± 0.02
2φMD	*rigid*-TraPPE-UA	349 ± 3	0.225 ± 0.02
Expt.[67]	-	370	0.217

* The uncertainties shown in the table are calculated by propagating the maximum error

Because others have noted effects on the equilibrium phase dome and critical point for both too short of a cutoff[16] and for intra-molecular degrees of freedom, we have performed additional simulations on models with different potential cutoffs and different degrees of internal flexibility. Such effects upon the critical point are of particular interest to us because of our intent to use 2φMD simulations to estimate critical temperatures and densities for fluids consisting of larger molecules that decompose below the experimental critical temperature. For large molecules, the computational efficiency of simulating rigid molecules (without the flexibility of bond vibrations and angle bending) with shorter cutoff potentials would result in substantial time saving.

Four modifications of the base potential model for propane (*flexible*-TraPPE-UA) described by Eqs. (4-9) and (4-10) were chosen. We label the first modification *rigid*-TraPPE-UA as it fixes the bond angle and distances at their equilibrium values of θ_0 and $d_{C\text{-}C,0}$. This was done in code using the method of Gaussian constraints.[68] The second modification is simply labeled TraPPE-UA as it is equivalent to the original TraPPE-UA used in the GEMC work with fixed bond lengths but flexible bond angles governed by Eq. (4-9). The third modification, labeled *14*-TraPPE-UA, uses the same interaction model as TraPPE-UA, but with a cutoff distance of 14 Å instead of 25 Å. Our fourth modification, *40*-TraPPE-UA, is the TraPPE-UA m model with a cutoff distance of 40 Å. The results obtained for the coexistence curves for these modified models are shown in Figure 4-7 and the corresponding critical points obtained are given in Table 4-4. Experimental critical values[67] are also reported in Table 4-4 for comparison purposes.

Because simulations with a longer potential cutoff run more slowly, the *40*-TraPPE-UA model was only run at a temperature of T = 344 K, so no critical values are reported for it in

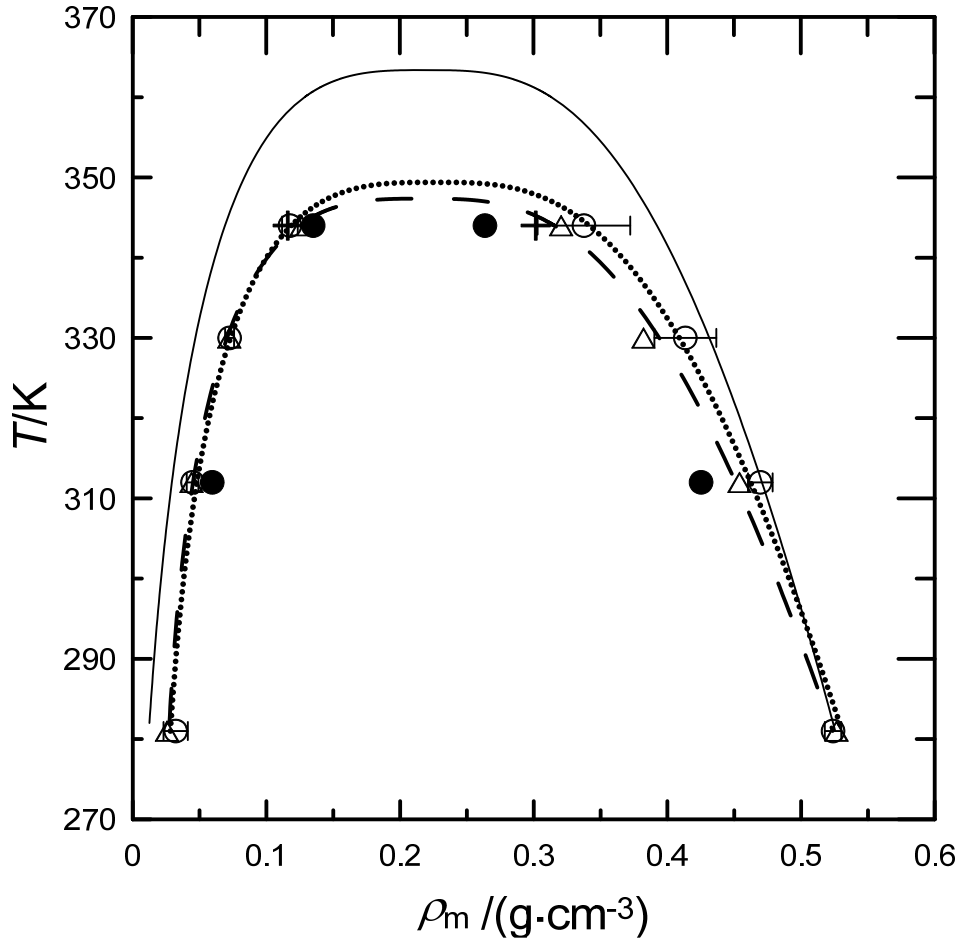

Figure 4-7: Equilibrium coexisting densities obtained from 2φMD propane simulations for the *flexible*-TraPPE-UA model (solid line), the *rigid*-TraPPE-UA model (○ with error bars, dotted line), the TraPPE-UA model (Δ, dashed line), the *14*-TraPPE-UA model (●),and the *40*-TraPPE-UA model (+)

Table 4-4. However, the equilibrium densities at 344 K for this model are compared to the bimodal curves of the other models in Figure 4-7. The coexisting densities obtained for the *40*-TraPPE-UA model at 344 K show no statistical difference from those obtained with the TraPPE-UA model using a 29 Å cutoff, but the bimodal curve for the 14 Å cutoff (without corrections) is narrower than the other models. The excellent consistency between the models with 29 Å and 40 Å supports the view that the cutoff distances shown in Table 4-3 are sufficiently long.

There does not appear to be a significant difference in the coexistence curves and critical properties of the *rigid*-TraPPE-UA and TraPPE-UA models, suggesting that the increased flexibility due to angle bending does not greatly impact the coexistence curve. However, fixed bond lengths tend to narrow the coexistence curve relative to the flexible model and decreases T_c. One explanation for this effect is that the potential for molecular contraction (compression of bond lengths from their equilibrium values) in the condensed phase is eliminated by bond rigidity. However, when we analyzed the bond and angle distributions of the liquid-phase molecules, only a small bond compression, below the level of statistical significance, was observed.

It should be explicitly mentioned that the observed model effects are primarily in the near-critical region. Liquid and vapor saturation densities are fairly independent of the degree of internal molecular flexibility at temperatures below about 300 K for propane. It is because of our focus on the near-critical region with the intent of using near-critical saturation data to determine the critical point that we observe model internal flexibility effects upon the equilibrium phase dome.

Vapor pressures, P^*, were also obtained from the virial using the 1φ vapor simulations. Values obtained for the various models and the resultant regressed vapor pressure curves for the models are shown in Figure 4-8 in comparison to the DIPPR® 801[19] correlation of experimental data. Also shown in the plot are the vapor pressure values obtained by Martin and Siepmann[8] GEMC method. The vapor pressure curves for the *rigid*- and TraPPE-UA are nearly identical (for clarity the *rigid*-TraPPE-UA line is not shown in the figure) and over predict P^*; the vapor pressure curve predicted by the *flexible*-TraPPE-UA model is in excellent agreement with the experimental curve and it agrees well with the GEMC results within the error of uncertainties.

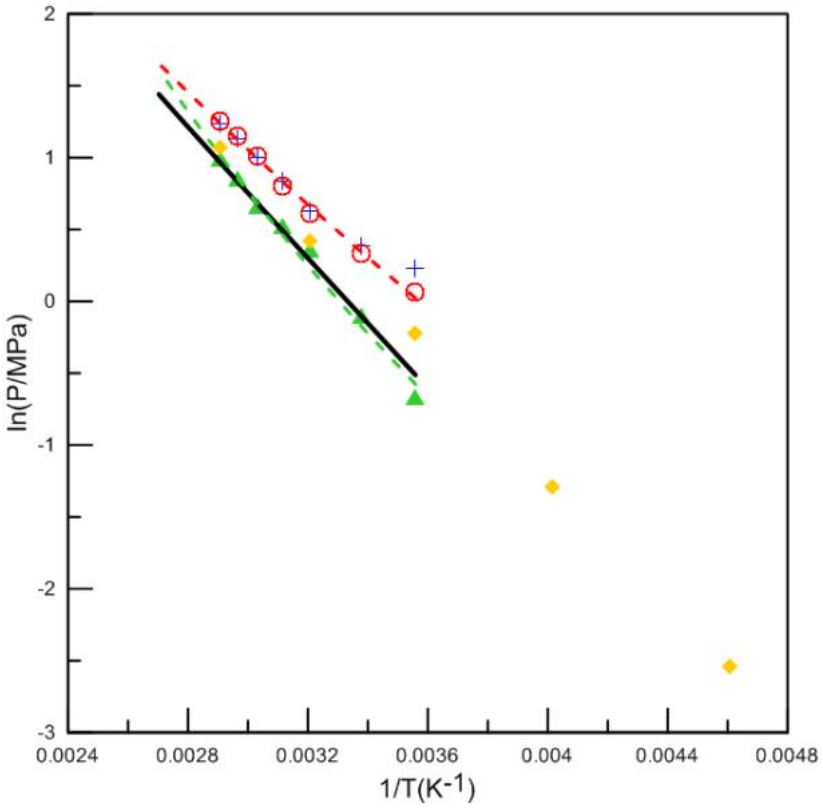

Figure 4-8: Vapor pressure of propane for the *flexible*-TraPPE-UA model (▲, -----), the *rigid*-TraPPE-UA model (+), and the TraPPE-UA model (○, -----) compared to the DIPPR® 801 correlation of experimental data (—) and Gibbs-ensemble results (♦)

The vapor pressure of a particular fluid does not depend on the internal modes of the molecule. As mentioned earlier, the vapor pressure values were obtained by performing the 1φ simulations at the bulk vapor densities obtained at a particular temperature. The different results for vapor pressure for different models at a particular temperature are due to the difference in the values of bulk vapor densities used to perform the simulations. Figure 4-8 shows that the vapor pressure at a particular temperature is very sensitive to the bulk densities values at which the 1φ simulations were performed. Also, inaccuracies in the potential model will affect the coexisting densities and hence the vapor pressure results. These vapor pressure data were used to obtain the critical pressure, P_c, by fitting them to the Riedel vapor pressure equation (Eq. (3- 4)). When compared to the GEMC results, extrapolation of the P^* correlation, Eq. (7), to T_c yields P_c = 4.3 MPa, 3.6

MPa, and 3.7 MPa for the *flexible*-TraPPE-UA, the *rigid*-TraPPE-UA, and the TraPPE-UA models, respectively, or errors of 0.0 %, -16 %, and -14 %, respectively, from the experimental value[19] of 4.3 MPa.

4.4 Conclusions

The 2φMD simulation method using Voronoi tessellations introduced by Fern et al. [17, 18] is a convenient method for determining coexisting liquid and vapor densities near the critical point. Our intention is to develop this method so that in future work it can be used to obtain reliable estimates for the critical properties of fluids that cannot be experimentally determined because of decomposition problems. The 2φMD method of Fern et al. appears well suited for this task as it can be used to determine the coexisting densities of the liquid and vapor phases from the volumes associated with individual molecules in the equilibrated 2φ fluid without the requirement of an interface or complete phase separation.

In anticipation of applying this method to larger more complex molecules, we have modified the post-processing of the 2φMD configurations to use a MC volume sampling method rather than Voronoi tessellations. The new method for determination of the 2φ density distributions is easily programmed and works without additional difficulties for complex, multisite molecules. We have benchmarked the volume sampling methods against the LJ results reported by Fern et al. and have used it to study the coexistence curve of united-atom models for propane. The 2φMD coexisting liquid and vapor densities obtained for the *flexible*-TraPPE-UA model agreed well with those reported using GEMC simulations and the TraPPE-UA model.

We have also examined the effect of model intramolecular flexibility on the resultant phase dome and critical point. While intramolecular flexibility had no noticeable effect upon the binodal curve of propane at temperatures more than 40 K below the critical point, the near

critical region is affected by the internal flexibility of the model. A freezing of either bond vibrations or angle-bending lowers the critical point by approximately 20 K. As was found by previous studies, the phase dome is narrowed by too small of a cutoff in the potential, but the potential cutoff does not affect the coexistence curve if kept to values above about 20 Å.

5 SIMULATIONS OF METHANOL AND 1-PROPANOL

5.1 Introduction

The critical point and vapor-liquid coexisting phase properties produced by a 2φMD simulation for a particular force-field model is a strong test of the efficacy of the model. The sensitivity of these properties, particularly the critical point, to the force field may also offer insights into model improvement. The sensitivity of these properties has led to force field models that have been tuned to experimental vapor pressures and/or vapor-liquid equilibria. For example, the parameters in the OPLS[69] (Optimized Potentials for Liquid Simulations) models were optimized from liquid density and heats of vaporization data. The TraPPE[56] force-field models have also been tuned from specific properties. For example, methanol and ethanol vapor-liquid equilibrium data were used to tune interaction parameters for use in determining phase equilibrium properties of alcohols.[70] When models are tuned with experimental data, the parameters can compensate for model inadequacies, such as three-body effects or oversimplification in model form.

Rowley et al.[20, 21] developed an all-atom, site-site pair potential model for alcohols solely from *ab initio* pair interactions. The resultant energy landscape was fitted to a sum of site-site interactions each modeled with a modified Morse potential. An equivalent fit of the energy landscape was obtained using either the site-site Morse potential to represent all of the interactions or separating out the Coulombic portion by assigning point charges at the nuclear

centers and using the Morse potential to model only the repulsion plus dispersion interactions. Rowley et al. argued that point charges are not required to obtain the correct energy landscape and are not physical in that molecular interactions are created from the distributed charge density, not from a charge at a single point in space. The long-range effect of Coulomb's law for point charges is dampened or shielded by the summation of all of the point charge interactions. One purpose of this work is to test this hypothesis, to ascertain if there is a difference between the equilibrium vapor and liquid densities or the critical points of the two models.

Energies obtained from *ab initio*, isolated dimer potential energy surfaces are true pair potentials; they do not include multi-body interactions. As mentioned, simulation of phase vapor-liquid equilibria with model potentials has proven to be challenging, generally requiring model potentials to be parameterized from phase equilibrium data. Recently these *ab initio* models for alcohols were used to calculate virial coefficients of up to fourth order,[71] but to our knowledge they have not been used to determine the vapor-liquid equilibrium properties of alcohols. Generation of the vapor-liquid coexistence curve and the associated critical points should therefore be an interesting test for these models that contain no adjustable parameters. This is particularly true for these models of methanol and 1-propanol where hydrogen bonding dominates the molecular attractions. The second objective of this work is therefore to probe the sensitivity of the equilibrium densities and critical point to multi-body effects as deviations from experimental values should be predominately due to the lack of multi-body interactions.

Two-phase molecular Dynamics (MD) simulations employing the new Monte Carlo (MC) volume sampling method have been performed using an *ab initio* based force-field model parameterized to reproduce quantum-mechanical dimer energies for methanol and 1-propanol at temperatures approaching the critical. The intermolecular potential models were used to obtain

the bimodal vapor-liquid phase dome at temperatures to within about 10 K of the critical temperature. The efficacy of two all-atom, site-site pair potential models, developed solely from the energy landscape obtained from high-level *ab initio* pair interactions, was tested for the first time. The first model was regressed from the *ab initio* landscape without point charges using a modified Morse potential to model the complete interactions; the second model included point charges to separate Coulombic and dispersion interactions. Both models produced equivalent phase domes and critical loci. The model results for the critical temperature, density, and pressure, in addition to the sub-critical equilibrium vapor and liquid densities and vapor pressures, are compared to experimental data.

5.2 Molecular model

The molecular models used for methanol and 1-propanol are the all-atom, site-site pair potentials regressed from *ab initio* energy landscapes calculated for isolated rigid dimer pairs using MP2/6-311+G(2*df*,2*pd*) by Rowley et al. [20, 21] The molecular potential energy surfaces obtained from *ab initio* calculations are modeled as the pairwise summation of site-site interactions,

$$u = \sum_{i=1}^{ns} \sum_{j=1}^{ns} u_{ij}(r_{ij}), \tag{5-1}$$

where u is the potential energy, ns is the number of sites on each monomer, and u_{ij} is the pair potential between site i on molecule 1 and site j on molecule 2. Interaction sites are located at the centers of all atomic species. A modified Morse model,

$$u_{ij} = -\varepsilon_{ij}(1 - \{1 - \exp[-A_{ij}(r_{ij} - r_{ij}^{*})]\}^{2}), \tag{5-2}$$

is used to represent the interatomic interactions. Here, the three adjustable parameters ε, A, and r^* represent the dispersion well depth, well shape factor, and the location of the minimum in the potential well, respectively. In this model, no point charges are used, but the complete energy landscape is well represented by the sum of the Morse site-site potentials.[20, 21]

In addition to nuclear sites, a satellite site, X, is used to represent the off-center high electron density of the electron pairs on the O atom as shown in Figure 5-1. The satellite site is placed on the vector bisecting the C_α–O–H_α angle of the alcohol, (C_α and H_α refer to the C and H attached to the O atom respectively) but on the side of the O opposite the C_α–O and O–H_α bonds. All interactions with the satellite site are assumed zero except for H_α–X and X–X. The H_α–X are modeled using Eq. (5-2), whereas the X–X interaction is represented by a purely repulsive interaction,

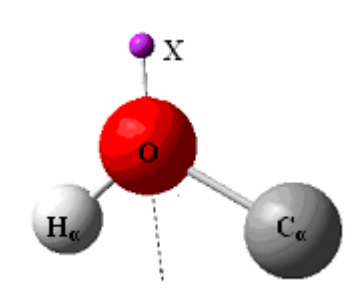

Figure 5-1: Placement of satellite site X

$$u_{XX} = B_{XX} \exp(-C_{XX} r_{XX}), \tag{5-3}$$

where the values of the parameters B_{XX}, C_{XX}, and the O–X distance are regressed from the *ab initio* potential landscapes simultaneously with the site-site parameters of Eq. (5-2). The structure of the optimized methanol and 1-propanol molecules are shown in Figure 5-2 and the values of the force field constants for the modified Morse potentials are given in Table 5-1.

The dihedral or torsional potentials for sites separated by three or more bonds are also required for the MD simulations. These were obtained by calculating individual energies for 18 conformations in 20° increments between -180° and 180° for each dihedral, while holding the other dihedrals fixed using Gaussian 09[72] with MP2/6-311+G(2*df*,2*pd*). These conformational

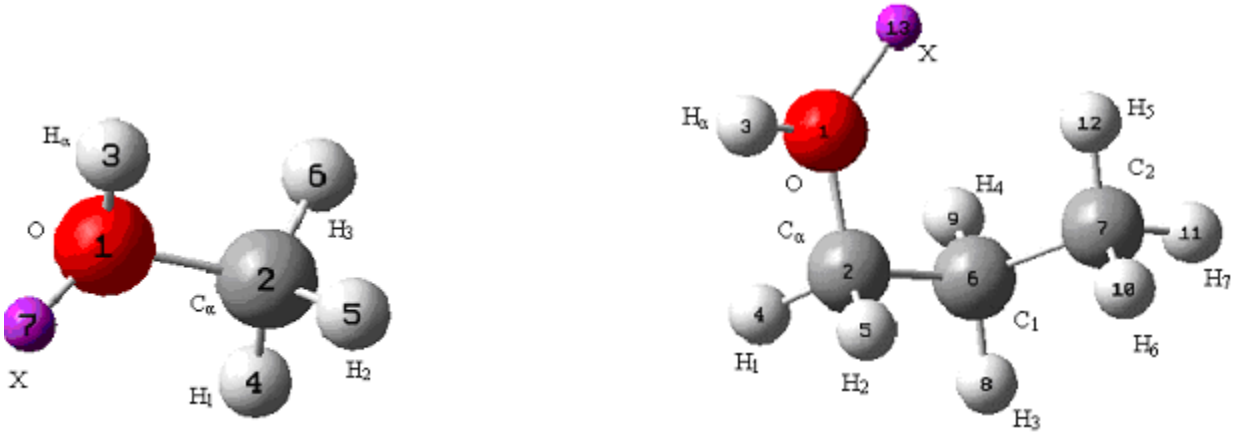

Bond	Length (nm)	Bond	Length (nm)	Angle	Angle (deg)
O–C_α	0.1420	O–C_α	0.1425	O–C_α–C_1	107.77
O–H_α	0.0959	O–H_α	0.0960	C_α–C_1–H_2	112.42
C_α–H_1	0.1085	C_α–C_1	0.1512	H_α–O–C_α	108.39
C_α–H_2	0.1091	C_α–H_1	0.1093	O–C_α–H_1	110.54
		C_α–H_2	0.1095	O–C_α–H_2	110.49
Angle	**Angle (deg)**	C_2–C_1	0.1522	C_α–C_1–H_3	108.21
H_α–O–C_α	108.049	C_1–H_3	0.1091	C_α–C_1–H_4	108.36
O–C_α–H_1	106.69	C_1–H_4	0.1091	C_1–C_2–H_5	110.58
O–C_α–H_2	111.99	C_2–H_5	0.1087	C_1–C_2–H_6	110.72
		C_2–H_6	0.1090	C_1–C_2–H_7	111.26
		C_2–H_7	0.1088		

Figure 5-2: Optimized geometries for methanol (left) and 1-propanol (right)

energies were then modeled with the Ryckaert–Bellemans potential[73],

$$\frac{U(\phi)}{k} = \sum_{k=0}^{5} a_k \cos^k \phi \,, \tag{5-4}$$

where U is the torsional potential energy and ϕ is the torsional angle. The torsional parameters obtained are listed in Table 5-2.

A second model was also developed by Rowley et al.[20] from the same *ab initio* landscape. In this model, Coulombic interactions were split out from the repulsion and dispersion

Table 5-1: Force field constants for methanol and 1-propanol without point charges. Values are given in the order ε (kcal/mol), A (nm^{-1}) and r^* (nm), respectively, for Eq. (5-2) and B (kcal/mol), C (nm^{-1}), and r_{OX} (nm) for Eq. (5-3)

Interaction	Methanol	1-Propanol	Interaction	Methanol	1-Propanol
O–O	0.5624	0.0270	H–H	0.0105	0.0105
	11.815	15.530		12.607	12.607
	0.3743	0.4363		0.3975	0.3975
$O–C_\alpha$	0.1452	3.2564	X–X	14.6338	4.8975
	9.309	17.524		7.147	6.639
	0.4161	0.2720		0.0961	0.1321
$O–H_\alpha$	12.4639	14.1998	$H_\alpha–X$	0.8665	0.4693
	16.272	15.935		5.354	7.504
	0.1506	0.1337		0.1634	0.1946
O–H	0.5296	0.0026	C–H		0.3556
	12.850	9.290			21.117
	0.2948	0.6285			0.2602
$C_\alpha–C_\alpha$	0.2711	9.43×10^{-11}	C–C		0.0513
	31.838	83.522			14.599
	0.3213	0.3493			0.4341
$C_\alpha–H_\alpha$	6.4902	6.1637	O–C		3.8188
	122.482	128.060			16.371
	0.0346	0.0540			0.2815
$C_\alpha–H$	0.4277	6.8580	$C_\alpha–C$		0.3873
	47.775	94.497			23.939
	0.0500	0.0600			0.3713
$H_\alpha–H_\alpha$	1.34×10^{-5}	5.20×10^{-5}	$C–H_\alpha$		0.01640
	7.152	7.174			54.852
	1.1277	1.027			0.0098
$H_\alpha–H$	6.78×10^{-5}	8.95×10^{-7}			
	3.808	26.442			
	1.4702	0.4360			

Table 5-2: Torsional potential parameters (in K) used for methanol and 1-propanol in Eq. (5-4)

Molecule	Dihedral	a_0	a_1	a_2	a_3	a_4	a_5
methanol	H_α-O-C_α-H_1	702.25	-256.71	-277.48	719.48	48.85	11.75
1-propanol	H_α-O-C_α-C_1	834.08	25.50	-160.94	730.90	124.92	43.05
	O-C_α-C_1-H_3	1312.45	-3717.49	99.43	4795.77	-405.02	-93.80
	C_α-C_1-C_2-H_7	766.38	-2310.85	2.39	3090.24	-4.76	-2.12

interactions by assigning point charges at each nuclear site and using Coulomb's law

$$u_{ij,coul} = \frac{q_i q_j}{r_{ij}}, \tag{5-5}$$

to find the interaction energy between the charges[20, 21]. The total molecular pair potential in this model is again given by Eq. (5-1) where now the site-site contribution is given by the sum of Eqs. (5-2) and (5-5) (or (5-3) and (5-5) as the case may be) using a different set of parameters in Eq.(5-2). The point charges (Mülliken) for this model are given in Table 5-3 and the site-site parameters for use in Eqs. (5-2) and (5-3) are listed in Table 5-4.

Table 5-3: Point charges used for the second model of methanol and 1-propanol to be used in Eq. (5-5)

Site	methanol	1-propanol
O	-0.6423	-0.6264
C_α	0.2551	0.2255
H_α	0.3873	0.4009
C	------	0
H	0	0

Table 5-4: Force field constants for methanol and 1-propanol with point charges. Values are given in the order ε (kcal/mol), A (nm^{-1}) and r^* (nm), respectively, for Eq. (5-2) and B (kcal/mol), C (nm^{-1}), and r_{OX} (nm) for Eq. (5-3)

Interaction	Methanol	1-Propanol	Interaction	Methanol	1-Propanol
O–O	0.2813	8.4955	H–H	0.0105	0.0105
	20.117	9.2558		12.607	12.607
	0.3149	0.0634		0.3975	0.3975
$O–C_\alpha$	0.0005	3.22×10^{-5}	X–X	0.2846	1.0100
	28.797	7.7014		67.946	42.413
	0.3990	0.2606		0.0093	0.0448
$O–H_\alpha$	0.0095	3.6250	$H_\alpha–X$	0.0316	0.0009
	23.928	18.637		18.153	6.7026
	0.0966	0.1936		0.2981	0.7775
O–H	4.79×10^{-6}	5.25×10^{-5}	C–H		0.3556
	14.464	9.468			21.117
	0.6755	0.8350			0.2602
$C_\alpha–C_\alpha$	0.5343	4.9560	C–C		0.0513
	54.287	13.002			14.599
	0.0547	0.2919			0.4341
$C_\alpha–H_\alpha$	1.2029	1.7491	O–C		7.1651
	14.856	28.277			14.606
	0.2410	0.2390			0.2566
$C_\alpha–H$	0.3065	5.7208	$C_\alpha–C$		0.0099
	18.009	48.478			3.2723
	0.2674	0.0597			1.0863
$H_\alpha–H_\alpha$	0.0030	5.70×10^{-11}	$C–H_\alpha$		0.0642
	15.943	9.655			100.15
	0.3812	1.531			0.0057
$H_\alpha–H$	9.08×10^{-5}	0.6860			
	1.8342	46.264			
	0.1384	0.00002			

5.3 Simulation details

The simulations were performed using the in-house Fortran code for standard NVT (constant number, volume and temperature) MD simulations with periodic boundary conditions. Time steps between 0.2 - 0.6 fs were employed in the simulations with the longer time step used at lower densities. A total of 1331 molecules (each with 7 sites) and 729 molecules (each with 13 sites) were used for the methanol and 1-propanol simulations, respectively. The 1φ simulations were performed with only 125 molecules. A sufficiently large potential cutoff distance was chosen to be used to eliminate the need for long-range corrections. In this study, we employed a cut off of 27 Å for the methanol simulations and a cut off of 30 Å for the 1-propanol simulations. Due to the large value of the interaction cut off, no long range corrections were included in the simulations. Equilibration runs consisted of at least 10^6 steps with longer equilibration times at higher temperatures.

Results of the parametric study to find optima in the number of Monte Carlo grid points, N_{MC}, and the number of sampling times or configurations, N_{conf}, discussed in Chapter 3 were used here. For the Lennard-Jones fluid $N_{MC} = 64 \times 10^6$ and $N_{conf} = 1$ appeared to be optimal for a combination of efficiency and accuracy, and these values were used in all the simulations reported in this chapter. The critical temperature and critical density were determined by fitting the liquid and vapor densities in the sub-critical region simultaneously to the density scaling law Eq. (3-2), and the law of rectilinear diameters Eq. (3-3). The value of β was fixed to the classical value of 0.32.

5.4 Results and discussion

Table 5-5 and Table 5-6 contain the results of the 2φ simulations for the *ab initio* models for methanol and 1-propanol, respectively, using the Morse potential model without point charges. Shown in the tables are the starting bulk mass densities, ρ_m, the equilibration times, t_{eq}, prior to sampling the configuration to generate the density histogram, and the equilibrium vapor and liquid mass densities, $\rho_{m,vap}$ and $\rho_{m,liq}$. Figure 5-3 and Figure 5-4 show these results

Table 5-5: Simulation specifics and results for the 2φMD simulations of methanol

T (K)	ρ_m(g cm^{-3})	t_{eq} (ns)	$\rho_{m,\mathrm{vap}}$(g cm^{-3})	$\rho_{m,liq}$(g cm^{-3})
375	0.150	0.78	0.0054	0.8606
425	0.150	0.73	0.0118	0.7778
475	0.180	0.70	0.0290	0.7418
500	0.200	0.84	0.0378	0.7236
550	0.250	0.80	0.0533	0.6154
600	0.280	0.80	0.1183	0.5233
630	0.280	0.75	0.1860	0.4314

Table 5-6: Simulation specifics and results for the 2φMD simulations of 1-propanol

T (K)	ρ_m(g cm^{-3})	t_{eq} (ns)	$\rho_{m,\mathrm{vap}}$(g cm^{-3})	$\rho_{m,liq}$(g cm^{-3})
200	0.150	2.86	0.0280	0.8968
250	0.150	2.56	0.0333	0.8450
300	0.150	2.34	0.0644	0.8133
400	0.200	2.03	0.0856	0.6592
415	0.250	2.06	0.1452	0.6062
435	0.250	2.83	0.1977	0.5698
450	0.250	3.27	0.1980	0.4602

graphically as well as the smoothed coexistence curves obtained from regression of the data using Eqs. (3-2) and (3-3). The experimental phase domes are also shown in these figures. These curves were obtained using the recommended values for T_c and V_c in the DIPPR® 801 database,[19] the correlations for the saturated liquid densities of methanol and 1-propanol from the same source, and saturated vapor densities calculated using the Soave equation of state at the indicated

temperature and at the corresponding vapor pressure. The latter was obtained from the vapor pressure correlation in the DIPPR® 801 database.

The *ab initio* potential model obtained from the energy landscape of dimer pairs significantly over predicts the saturated liquid density of methanol at the sub-critical temperatures studied although the vapor densities are in relatively good agreement. Interestingly,

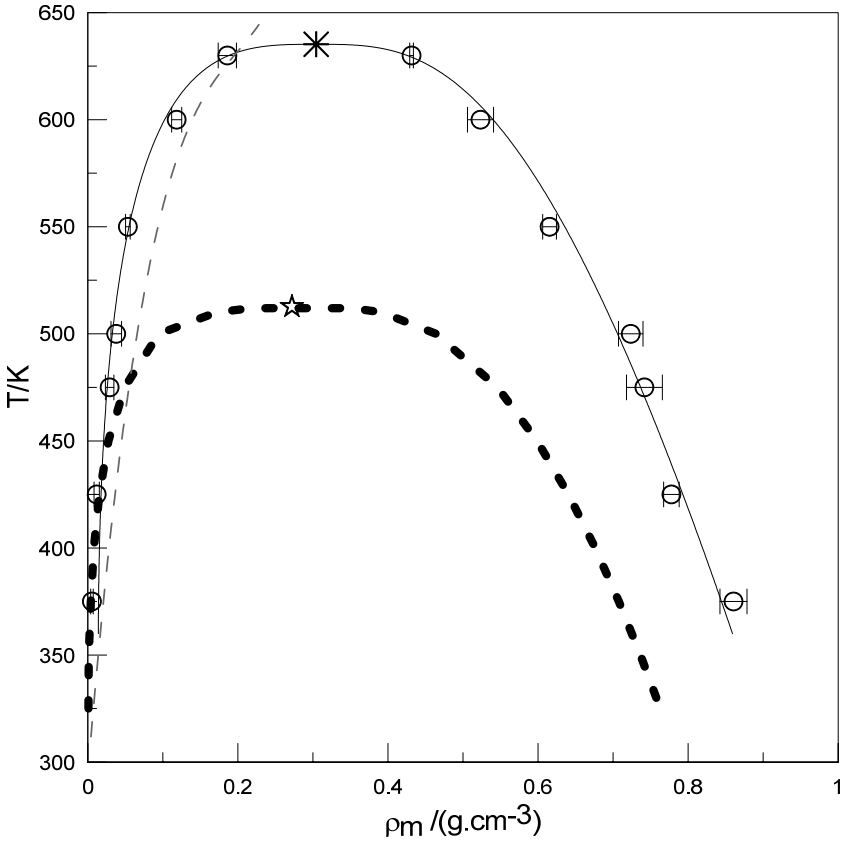

Figure 5-3: Vapor-liquid phase diagram for the ab initio pair-potential model for methanol without point charges (○, solid line, error bars) compared to saturated liquid densities from the DIPPR® 801 database and saturated vapor densities from the Soave equation of state (dashed line). Also, shown are the model (asterisk) and experimental (star) and the vapor spinodal line (gray dashed line) obtained by Shaul et al.[71] from a fourth-order virial equation of state

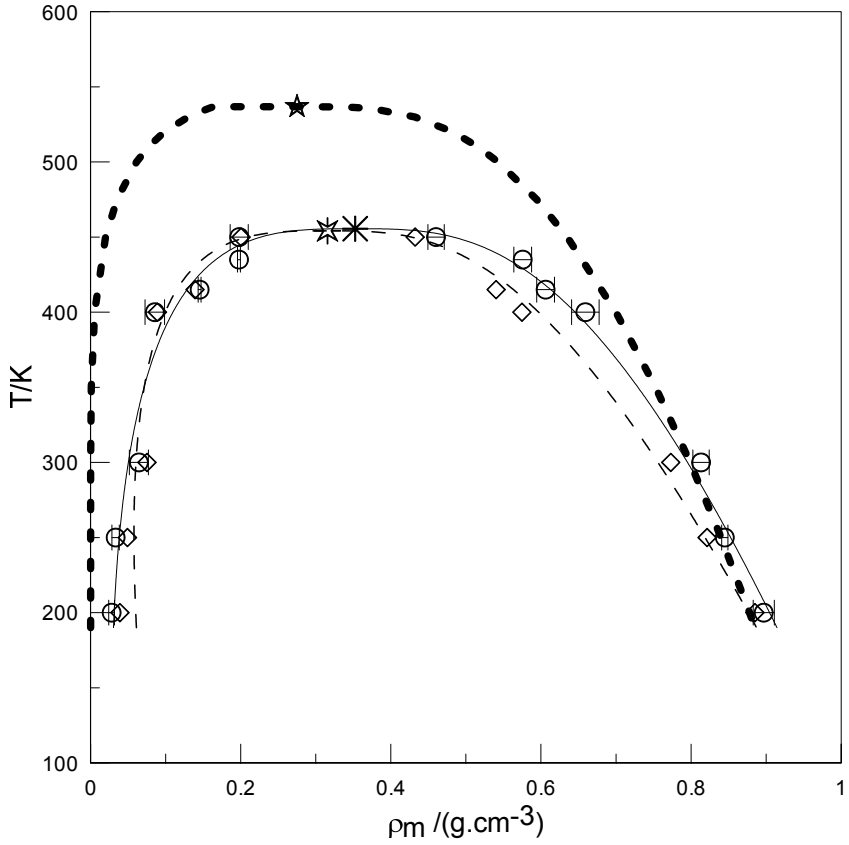

Figure 5-4: Vapor-liquid phase diagram 1-propanol from the *ab initio* pair-potential model without charges (○, solid line, error bars) and with charges (◊, thin dashed line) in comparison to the saturated liquid densities from the DIPPR® 801 database and saturated vapor densities from the Soave equation of state (dashed line). Also, shown are the model without charges (asterisk), model with charges (asterisk-star), and experimental (star) critical points

the *ab initio* potential model for 1-propanol produces saturated liquid densities that are in good agreement with the experimental values while the saturated vapor densities are higher than those calculated from the Soave equation of state. While the model's phase dome for methanol is quite poor, the model's predictions of coexistence curve for 1-propanol is actually not too bad considering that the *ab initio* model was developed from isolated rigid dimer pairs with no adjustable parameters. Force field models that provide better accuracy of the phase dome generally have multiple site-site parameters regressed from experimental data, often vapor-liquid coexistence data, and therefore implicitly contain multi-body effects.

The critical properties obtained from simulations for the two alcohol models without charges are compared with the corresponding experimental values in Table 5-7. One-phase vapor simulations were performed at temperatures below the critical point at saturated vapor densities obtained from the solution of Eqs. (3-2) and (3-3). These points were also fitted to Eq. (3-4) to obtain the values P_c given in Table 5-7. The errors in T_c, $\rho_{m,c}$, and P_c for methanol are 23.9 %, 11.9 %, and 39.8%, respectively. For 1-propanol these errors are -17.8 %, 28.2 %, and -42.3 %.

Table 5-7: Critical properties of methanol and 1-propanol

Molecule	Method	T_c (K)	$\rho_{m,c}$ (g·cm^{-3})	P_c (MPa)
Methanol	2ϕMD	635 ± 1	0.30 ± 0.01	11.3
	experiment	512.64	0.272	8.09
1-propanol	2ϕMD	456 ± 1	0.35 ± 0.01	2.9
	experiment	536.78	0.275	5.17

Shaul et al.[71] calculated virial coefficients for methanol using the same *ab initio* potential model examined in this study (shown in Figure 5-5). They found that the second virial coefficient B_2 values generally matched experimental correlation and the available experimental data, reproducing experimental data well at temperatures below 400 K with a negative deviation at higher temperatures. They compared these results to those for the TraPPE model (also shown in Figure 5-5) with parameters adjusted to experimental phase coexistence data and found that the TraPPE B_2 results agreed well with experimental data at temperatures above 600 K but gave significantly lower values at lower temperatures. These deviations at the higher temperature may be due to inadequate representation of the entire *ab initio* landscape by the analytical pair potential model, and improvements in the analytical representation could improve the B_2 results and the coexistence curve obtained in our study. The TraPPE model produced third virial

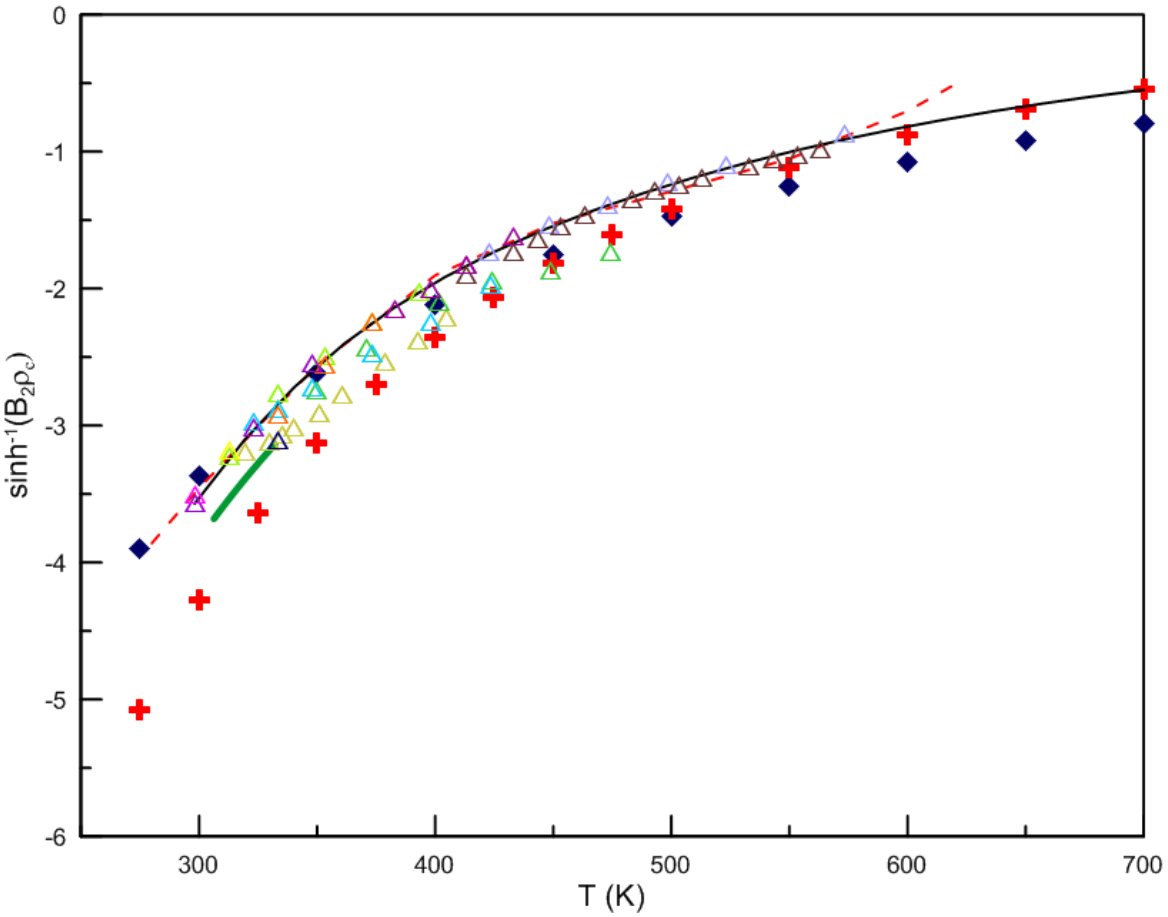

Figure 5-5: Temperature dependence of B_2 for the *ab initio* pair-potential model without charges (◆) and the TraPPE-UA model (✚) (Values taken from Shaul et al. [71]) for Methanol. Also, shown are the experimental correlation of Tsonopoulos and Dymond[74] (--- line), the DIPPR® 801 correlation of experimental data (— line), the experimental correlation data from Loras et al.[75] (— line). Open triangles are experimental data[76-89]

coefficient (B_3) values that were in excellent agreement with the majority of the available experimental data while the B_3 values from the *ab initio* model only agreed with the data of Shakhverdiev et al.[90] but gave significantly more positive values than the preponderance of the available experimental data at lower temperatures. Larger positive deviations between the TraPPE model with regressed parameters and the *ab initio* potential were observed for fourth order virial coefficient (B_4) values though there are no experimental data for comparison. These observations are consistent with the fact that B_2 depends only on the integral over a single pair

potential while B_3 and higher virial coefficients depend upon multiple pair potentials in three-body and higher clusters.

Shaul et al.[71] used their calculated virial coefficients up through B_4 and used the virial equation of state (VEOS) truncated both after the third and fourth terms to obtain the vapor spinodal curve. The third- and fourth-order VEOS spinodal curves were very similar at lower temperatures, but the fourth order spinodal curve at temperatures approaching the critical was substantially lower than the third order. For comparison, the vapor spinodal obtained by Shaul et al. for the fourth order VEOS is displayed with our binodal curve in Figure 5-3. The vapor spinodal is consistent with the coexistence curve from our MD simulations except very near the critical point where higher order terms in the VEOS are likely needed. Nevertheless, the critical temperature from the VEOS is remarkably close even though the critical density predicted by the VEOS is somewhat lower than that obtained from the simulation.

The substantially better coexistence curve obtained for 1-propanol than for methanol is interesting. It seems likely that the model's predicted liquid densities would be strongly dependent upon the extent of hydrogen bonding that takes place in the liquid phase as the oxygen-hydrogen interactions dominate the much weaker dispersion attractions. However, the oxygen-hydrogen interactions between the isolated dimer pairs are surprisingly similar for the two alcohols, in light of the differences in the simulated phase domes. This can be seen in Figure 5-6 where the *ab initio* energies for two of the routes that emphasize O-H interactions are shown for each of the two molecules. The energy profiles shown are for a fixed relative orientation of the two monomers as the molecules are moved apart along the line shown connecting them in the dimer configurations given at the bottom of the figure. The purple sphere shows the midpoint of this O-H distance and identifies the path along which the monomers are

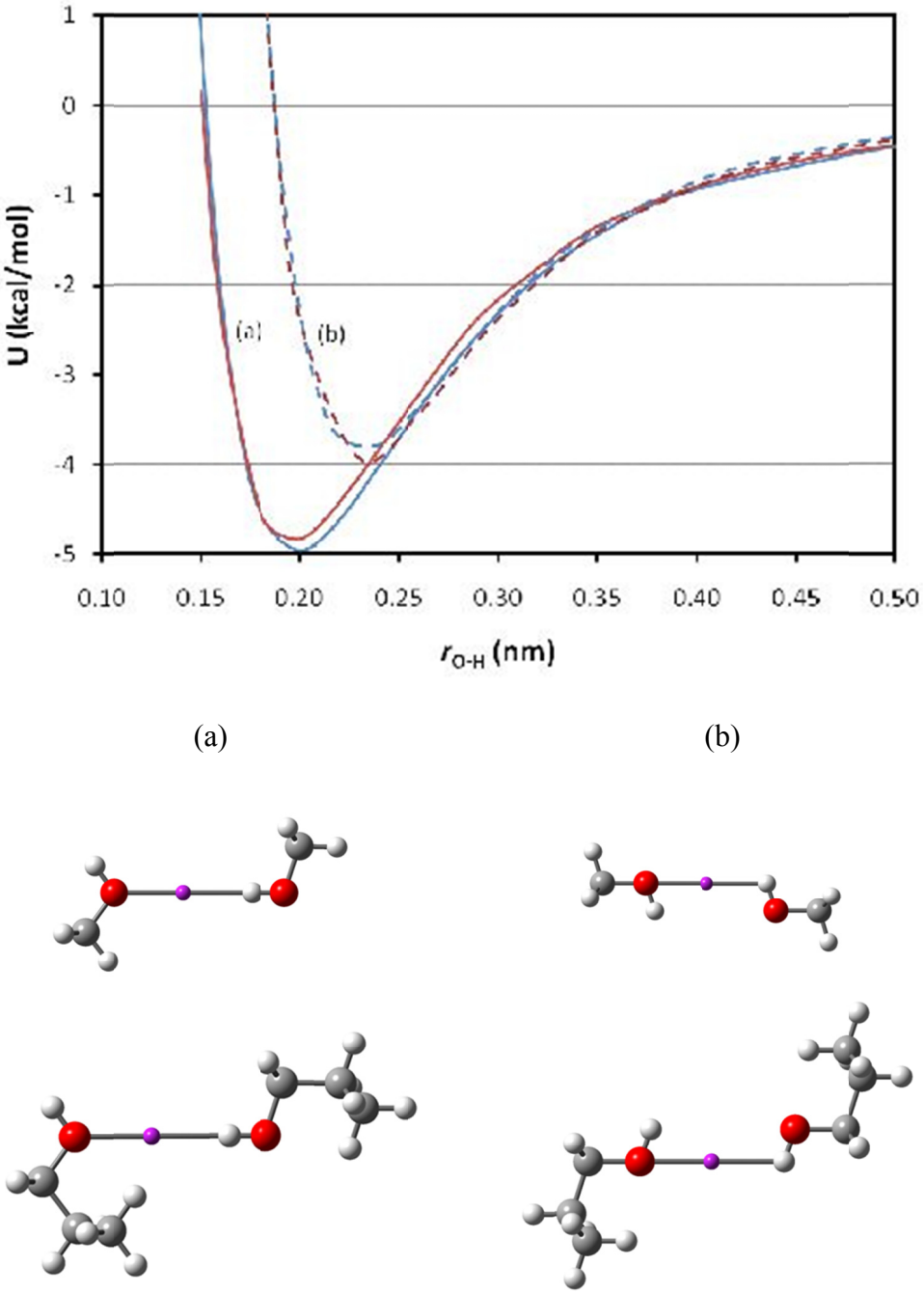

Figure 5-6: MP2/6-311+G(2*df*,2*pd*) dimer pair energies for (a) direct H----O approach and (b) OH-------HO approach of the two methanol (red lines) or 1-propanol (blue lines) monomers. The approach orientation is shown at the bottom with the purple sphere representing the center of the drawn in approach line between the O and H atoms

moved. Case (a) in the figure is a route that brings the O and H atoms toward each other unshielded by other atoms. As can be seen in the figure, the attractive wells for methanol and 1-propanol along this path are nearly indistinguishable. Case (b) is meant to focus on bringing the molecules together with the opportunity for both the H and O on one monomer to interact with the O and H, respectively, on the other monomer. Again the energy profiles for methanol and 1-propanol are nearly indistinguishable for the similar routes.

As it is common practice in developing potential models to attempt to separate out Coulombic interactions from dispersion as in Eq. (5-5), it is of interest to see the effect upon the phase dome and the corresponding critical locus when the energy landscape is represented in this manner. We therefore performed similar 2φ simulations using the 1-propanol model including point charges. The results obtained for this model are also included in Figure 5-4. Interestingly, the results are very similar; approximately the same within the combined uncertainties of the simulated densities, to those obtained using the model with no point charges. A few coexistence points were also obtained for methanol using the model with point charges. These also agree with the values previously determined from the model without point charges, though not shown in Figure 5-3. The evidence suggests that at least for these pure fluids, the long-range nature of the potential shown in Eq. (5-5), which arises from the treatment of charge-charge interactions as though between two point charges, need not be employed as long as the pair potentials accurately reproduce the true energy landscape. As can be seen from Figure 5-6, the true intermolecular pair potentials dampen faster than individual point charge interactions.

The disparity between the experimental and simulated phase domes must arise from differences in the actual condensed-phase interactions and the isolated pair interactions obtained from the *ab initio* energy landscapes. Moreover, the effect is different for the two alcohols since

the liquid densities for methanol are over predicted while those for 1-propanol are in good agreement with experiment. Multi-body effects in the condensed phase, which can also be thought of in terms of polarizability of the potential model, are the most likely explanation. These would likely diminish the hydrogen-oxygen interaction energy per pair as neighboring molecules distort the electron-rich environment around the oxygen atom. Multiple neighbors competing for hydrogen bonding are expected to weaken the individual hydrogen bonds. Use of the pair-potential which omits polarizability or multi-body effects in the condensed phase would therefore likely produce higher densities. Smaller molecules are more easily polarized, and therefore methanol would be expected to be more prone to the error associated with omission of these effects from the model. Non-conformality of the smallest member within a chemical family is a familiar manifestation of this concept that causes difficulties for group-contribution and corresponding states methods that assume uniform contributions per unit or group regardless of the potential for polarization or longer range effects. Shaul et al.[71] suggest that the more repulsive nature of the observed B_3 and B_4 virial coefficients for methanol relative to experiment and the TraPPE model could be due to inaccuracies in the analytical fit of the *ab initio* energies. Indeed the fit of some of the *ab initio* attractive wells for O–O routes reported by Rowley et al.[20, 21] could be improved. Other possible contributing factors not addressed here are the accuracy of the *ab initio* calculations themselves, including inaccuracies in the energies obtained due to incomplete level of theory and basis set size as well as other quantum and computational issues. These issues would likely have some impact on the absolute accuracy of the virial coefficients, but they would not likely explain the disparity observed here between the simulated methanol and 1-propanol coexistence curves.

One-phase vapor simulations were performed at temperatures below the critical point at saturated vapor densities to obtain the vapor pressures. The resultant vapor pressure curves obtained are shown in Figure 5-7. In Figure 4-8 it was shown that the vapor pressure curves are very sensitive to the value of saturated vapor densities used to perform one-phase vapor simulations. Given the errors associated with the coexisting densities for methanol and 1-propanol, it is not too surprising that the model vapor pressure curves are shifted from the experimental values, down for methanol and up for 1-propanol. Although the slopes of the

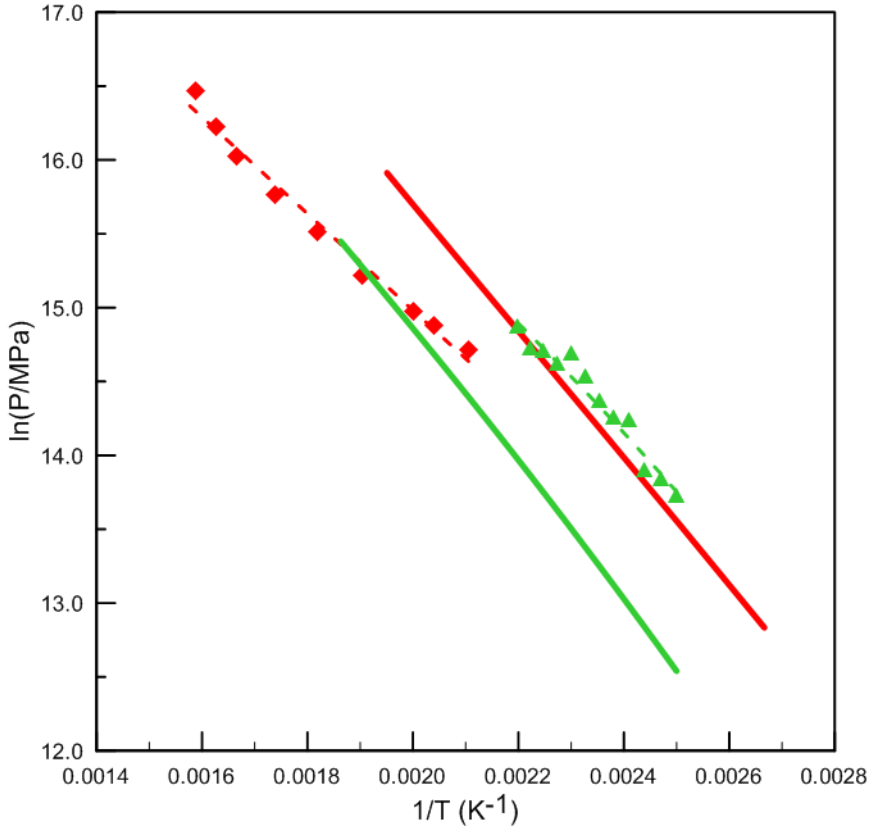

Figure 5-7: Vapor pressures of methanol and 1-propanol. Points were obtained from 1φ simulations using the potential model (without charges) for methanol (♦, -----) and 1-propanol (▲, -----). Solid lines of same color are from the recommended correlation in the DIPPR® 801 databases for the respective alcohols

experimental and simulated vapor pressure curves are in reasonable agreement, indicating that the model heats of vaporization are consistent with real fluid properties, the model pressures are significantly in error due to the inaccurate vapor densities produced by the model for a given temperature. Experimentally, the critical point of methanol is lower than the critical point of 1-propanol indicating methanol is more volatile than 1-propanol, i.e. the vapor pressure of methanol is greater than that of 1-propanol at a particular temperature. Since in this work the simulated critical temperature for methanol is higher than that for 1-propanol, it would be consistent for the simulation to give a lower vapor pressure curve for methanol than 1-propanol. This is what we see in Figure 5-7. In Table 5-8, the vapor pressure (P^*) values for methanol and 1-propanol were compared at two different temperatures, showing the vapor pressure of methanol to be less than that of 1-propanol. So, even though the vapor pressure data for methanol and 1-propanol deviate from their experimental values, due to the uncertainties in the vapor densities, the vapor pressure curve obtained from our simulations are in this qualitative way consistent with the phase dome calculations.

Table 5-8: Comparison of vapor pressure values at two temperatures for methanol and 1-propanol

T (K)	Molecule	P^* (MPa)
425	Methanol	1.50
	1-propanol	1.72
450	Methanol	1.86
	1-propanol	2.45

5.5 Conclusions

Ab initio energy landscapes have been generated from isolated, rigid dimer energy calculations for a number of different types of molecules. Some of these potential energy hyper-dimensional surfaces have been used to regress analytical pair potential models. Though available for use in simulations, such potentials have not been used in molecular simulation work. Effective pair potentials, which implicitly include some multi-body and polarization effects in the parameters regressed from experimental data, are of course expected to provide better results for most properties. Simulation of the coexistence curve and critical properties is a very rigorous test of the efficacy of a purely predictive model and provides insights into the model's limitations and directions that can be taken to improve the model. The objectives of this study were to test for the first time the use of *ab initio* derived pair potentials for phase equilibrium and critical property predictions, to identify the effect of multi-body interactions on these properties, and to compare results obtained from pair potential models that represent the total potential energy landscape without the use of point charges to the more traditional representation that includes point charges.

While the coexistence curve obtained for methanol is in poor agreement with experiment, the results for the 1-propanol model are considerably better, though the model produced results for neither produced that are quantitatively satisfactory. The liquid saturated densities are over predicted for methanol which produces a broader phase dome and a higher critical temperature than is observed for the real fluid. The properties of methanol, the smallest molecule in the 1-alcohol family, will be more affected by polarization in the liquid phase by surrounding molecules. These multi-body effects in the actual fluid are not included in the pair-potential model and would be expected to decrease the liquid density from that predicted by rigid,

nonpolarizable pair potentials due to competition for the hydrogen bonding between the neighbors. We have shown that the O-H interactions between pairs are nearly identical for methanol and 1-propanol, but the decrease in effective pair potential due to neighbors in the condensed phase would be expected to be less for the molecule with the larger alkyl group as there is less effective competition for the hydrogen bond sites.

The traditional use of point charges to model the interaction between the charge distributions within the actual molecule introduces an artificial long-range Coulombic interaction between the point charge loci that is not observed between the two complete molecules in the dimer potential obtained from *ab initio* calculations. At least for the pure fluids studied here, the computationally less expensive potential model regressed from the energy landscape without point charges provides an equivalent phase dome and critical properties to that obtained when point charges are used.

The development of intermolecular potentials from *ab initio* calculations has considerable future promise. Cluster potential energies for example might be used in the future to produce energy landscapes more appropriate for condensed-phase simulations. Alternatively, corrections for higher-body interactions can be developed by looking at three-, four- and five-body effects on the *ab initio* potential energy landscapes. These effects will need to be included before critical properties and phase behavior can be accurately predicted directly from *ab initio* calculated potentials.

6 SIMULATIONS OF 1-PENTANOL

6.1 Introduction

Development of a full force-field model for each chemical of industrial application would be an enormous, likely impossible, task. Instead, the approach taken by most researchers to obtain force fields for use in molecular simulations of various properties and phenomena of industrial relevance is to assume the full molecular force field can be represented as a sum of site-site or atom-atom interactions as in Eq. (4-5). This allows force fields to be constructed from the individual atom-atom interaction pieces. The atom-atom terms are parameterized from small molecules and the assumption is made that the individual atom-atom contributions to the molecular force-field is independent of the molecule, or, in other words is, transferable. This principle of transferability thus assumes that intermolecular potentials can be developed and successfully applied to the prediction of large molecules composed of the same site-site interactions. If transferability of a model is not satisfied, then time consuming parameter calibration would be required to investigate any new molecule for which the potential has not been developed. If transferability of a potential is poor, then the extrapolation capability of the site-site model to new molecules will also be poor. For all homologous series, fewer experimental data are available for higher molecular weight compounds. As a fully optimized set of transferable potential parameters becomes available, the MD simulations can be used for prediction of phase coexistence properties and critical points where experimental data are not

available because of high temperature and pressure, or because the compound undergoes thermal decomposition.

In Chapter 5, the *ab initio* based force-field model parameterized to reproduce quantum-mechanical dimer energies, developed by Rowley et al. [20, 21] was used to determine the coexistence densities and critical points for methanol and 1-propanol. In their work, they also obtained generalized Morse parameters for their model from a composite regression of the energy landscapes for methanol, ethanol, propanol, isopropanol, *t*-butanol, and *sec*-butanol. The quality of fit for all these energy landscapes using these generalized parameters suggested a fairly good level of transferability to other alcohol molecules for the site-site interactions. But Rowley et al. never tested these generalized parameters in larger alcohols.

In the present work, the transferability of the *ab initio* based potential model developed by Rowley et al.[20, 21] is tested by applying it to a molecule other than one of those used to develop the potential. Specifically, the generalized set of Morse parameters obtained from a composite regression using the energy landscape data of all small alcohols containing up to four carbon atoms is used to determine coexisting liquid and vapor densities of 1-pentanol as a function of temperature. This test of the transferability of the site-site interaction parameters will help in examining the extent to which the model parameters can be taken as independent of the alcohol dimers from which they were regressed and thereby in determining the possible use of these parameters for use in predicting other alcohol dimer potential.

In this chapter, the *ab-initio* potential models using the generalized parameters are used in 2φMD simulations to determine coexisting liquid and vapor densities of 1-pentanol as a function of temperature. The MC sampling method is then used to extract the bulk vapor and liquid densities from the 2φMD simulations and the critical point is determined from the resultant

equilibrium densities in conjunction with the law of rectilinear diameters and the known critical exponent for the liquid-vapor density difference. Results obtained for the critical temperature, the critical density, and bulk vapor and liquid densities for the model are compared to experimental data. Errors due to transferability of the potential model are separated from errors due to the use of a true-pair potential by calculating counterpoise (CP)-corrected dimer energies at the MP2/6-311 + G(2df,2pd) level for 1-pentanol at various distances for three different relative orientations of the two 1-pentanol molecules and comparing the results to values obtained from the generalized site-site model using the transferability assumption. The calculated dimer energies were sampled at thirteen to sixteen separation distances along each route or relative orientation of the rigid monomers.

6.2 Molecular model

The potential model used for 1-pentanol is similar to that used for methanol and 1-propanol; i.e., the total potential energy is modeled as the pairwise summation of molecular interactions each of which is itself modeled as the sum of site-site interactions given by Eq. (5-1). The interaction sites are located at each atomic center. The individual atom-atom pair interactions are represented by the modified Morse potential,

$$u_{ij} = -\varepsilon_{ij}(1-\{1-\exp[-A_{ij}(r_{ij}-r_{ij}^{*})]\}^{2}), \tag{6-1}$$

where ε, A, and r^{*} are adjustable parameters representing the dispersion well depth, well shape factor, and the location of the minimum in the potential well, respectively. As in the model for methanol and 1-propanol, a satellite site X was placed on the vector bisecting the C_α–O–H_α angle of the alcohol, (C_α and H_α refer to the C and H attached to the O atom respectively) but on the side of the O opposite the C_α–O and O–H_α bonds, to represent the off-center high electron

density of the electron pairs on the O atom. All interactions with the satellite site are assumed zero except for H_α–X and X–X. The H_α –X interactions are modeled using the modified Morse potential Eq. (6-1), but the X-X interactions are modeled using a purely repulsive interaction,

$$u_{XX} = B_{XX} \exp(-C_{XX} r_{XX}) . \tag{6-2}$$

The adjustable parameters B_{XX}, C_{XX}, and the O–X distance, along with the site-site parameters ε, A, and r^*, are obtained from regression of the energy landscapes of all the small alcohols containing up to four carbon atoms.

The geometry of the isolated monomers of 1-pentanol, optimized with MP2/6-311+G (2*df*, 2*pd*) using Gaussian 09[72], is shown in Figure 6-1. As discussed in chapter 5, two models were used for the methanol and 1-propanol simulations, one with point charges and one without point charges. In their work, Rowley et al.[20, 21] regressed the two models separately to ascertain the most transferable generalized model parameters. They found that the model with point charges did not produce transferable site-site interaction parameters; i.e., no set of model parameters for the model with point charges was capable of representing the potential energy surfaces of all the alcohols up to four carbon atoms. However, the site-site model without point charges produced a generalized set of parameters that represented all of the alcohol energy surfaces quite well. The results for 1-propanol in chapter 5 showed that potential model regressed from the energy landscape without point charges provides an equivalent phase dome and critical properties to that obtained when point charges are used. Therefore in this study of the transferability of the site-site models for predicting the phase dome and critical point of 1-pentanol no point charges were used. The values of the generalized force field constants for the modified Morse potentials are given in Table 6-1.

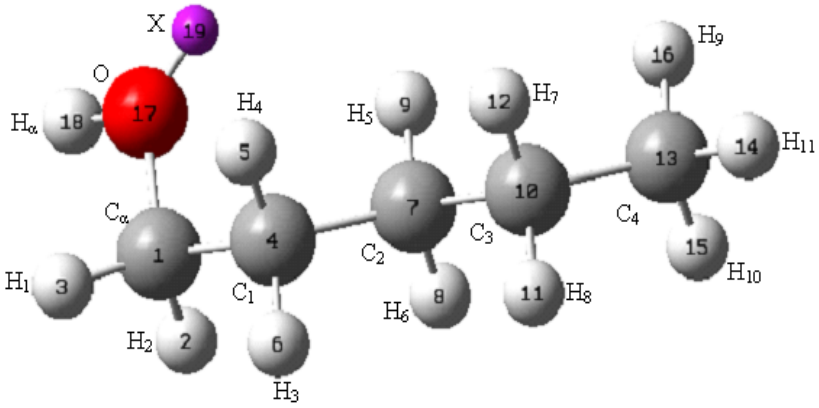

Bond	Length (nm)	Angle	Angle (deg)	Dihedral	Dihedral (deg)
$O–C_\alpha$	0.1426	$H_\alpha–O–C_\alpha$	108.35	$H_\alpha–O–C_\alpha–H_1$	-59.48
$O–H_\alpha$	0.0960	$O–C_\alpha–H_1$	110.52	$H_\alpha–O–C_\alpha–H_2$	60.21
$C_\alpha–C_1$	0.1512	$O–C_\alpha–H_2$	110.50	$H_\alpha–O–C_\alpha–C_1$	-179.88
$C_\alpha–H_1$	0.1093	$O–C_\alpha–C_1$	107.78	$O–C_\alpha–C_1–C_2$	-63.43
$C_\alpha–H_2$	0.1094	$C_\alpha–C_1–C_2$	113.04	$O–C_\alpha–C_1–H_3$	174.56
$C_2–C_1$	0.1521	$C_\alpha–C_1–H_3$	108.44	$O–C_\alpha–C_1–H_4$	58.64
$C_1–H_3$	0.1093	$C_\alpha–C_1–H_4$	108.50	$C_\alpha–C_1–C_2–H_6$	-58.95
$C_1–H_4$	0.1092	$C_1–C_2–H_6$	109.23	$C_\alpha–C_1–C_2–C_3$	179.35
$C_2–H_5$	0.1091	$C_1–C_2–C_3$	112.79	$C_\alpha–C_1–C_2–H_5$	57.19
$C_2–H_6$	0.1094	$C_1–C_2–H_5$	109.17	$C_1–C_2–C_3–H_8$	57.62
$C_3–C_2$	0.1522	$C_2–C_3–H_8$	109.36	$C_1–C_2–C_3–C_4$	179.78
$C_3–H_7$	0.1092	$C_2–C_3–C_4$	112.43	$C_1–C_2–C_3–H_7$	-58.28
$C_3–H_8$	0.1093	$C_2–C_3–H_7$	109.08	$C_2–C_3–C_4–H_{10}$	-59.80
$C_4–C_3$	0.1522	$C_3–C_4–H_{10}$	110.80	$C_2–C_3–C_4–H_{11}$	179.85
$C_4–H_9$	0.1090	$C_3–C_4–H_{11}$	111.79	$C_2–C_3–C_4–H_9$	59.50
$C_4–H_{10}$	0.1090	$C_3–C_4–H_9$	110.73		
$C_4–H_{11}$	0.1089				

Figure 6-1: Optimized geometry for 1-pentanol

For sites separated by three or more bonds, the dihedral or torsional potentials are used to restrict the dihedral rotation around bonds. These were obtained by calculating individual energies for 18 conformations in 20° increments between -180° and 180° for each dihedral, while holding the other dihedrals fixed, using Gaussian 09[72] with MP2/6-311+G(2*df*,2*pd*).

Table 6-1: Force field constants for 1-pentanol without point charges. Values are given in the order ε (kcal/mol), A (nm^{-1}) and r^* (nm), respectively, for Eq. (6-1)) and B (kcal/mol), C (nm^{-1}), and r_{OX} (nm) for Eq. (6-2)

Interaction	Methanol	Interaction	Methanol	Interaction	Methanol
O–O	0.0955 13.069 0.4240	C_α–C_α	0.2711 31.838 0.3213	H–H	0.0105s 12.607 0.3975
O–C_α	0.1235 14.341 0.3848	C_α–H_α	6.4902 122.482 0.0346	X–X	14.1931 7.646 0.0901
O–H_α	13.371 15.146 0.1470	C_α–H	4.8732 136.439 1.39×10^{-7}	H_α–X	0.7119 6.0378 0.1525
O–H	0.3475 14.570 0.2820	H_α–H_α	0.0020 6.2605 0.8650	C–H	0.3556 21.117 0.2602
C_α–C	0.0981 16.693 0.3953	H_α–H	8.36×10^{-7} 7.7778 1.0945	C–C	0.0513 14.599 0.4341
C–H_α	1.8110 16.622 0.1669	O–C	0.0002 18.435 0.5304		

The Ryckaert–Bellemans potential form[73] was used to model these conformational energies,

$$\frac{U(\phi)}{k} = \sum_{k=0}^{5} a_k \cos^k \phi \,, \tag{6-3}$$

where U is the torsional potential energy and ϕ is the torsional angle. The torsional parameters obtained are listed in Table 6-2.

Table 6-2: Torsional potential parameters (in K) used for 1-pentanol in Eq. (6-3).

Dihedral	a_0	a_1	a_2	a_3	a_4	a_5
H_α-O-C_α-C_1	856.66	-43.87	-398.42	536.37	305.71	278.83
O-C_α-C_1-H_3	1141.91	-2677.01	-661.54	3801.11	409.12	-139.42
C_α-C_1-C_2-C_3	956.74	127.04	4980.18	4745.62	-3275.84	-2193.05
C_1-C_2-C_3-C_4	989.29	-2250.33	82.25	3101.40	861.77	1130.30
C_2-C_3-C_4-H_{11}	836.38	-2473.01	-32.44	3315.83	25.95	-2.96

6.3 Simulation details

The simulations were performed using the in-house Fortran code for standard NVT (constant number, volume and temperature) MD simulations with periodic boundary conditions, and with 729 molecules (each with 19 sites) of 1-pentanol. The 1ϕ simulations were performed with only 125 molecules. Time steps between 0.13 - 0.60 fs were employed in the simulations with the longer time step used at lower densities. In this study, a cut off was employed beyond 30 Å. Due to the large value of the interaction cut off, no long-range corrections were included in the simulations. Equilibration runs consisted of at least three million steps with longer equilibration times at higher temperatures.

Based on the parametric study for Lennard-Jones fluid (in chapter 3) to find optima in the number of Monte Carlo grid points, N_{MC}, and the number of sampling times or configurations, N_{conf}, to use in obtaining accurate density distributions from the 2ϕ simulations, $N_{MC} = 64 \times 10^6$ and $N_{conf} = 1$ values were used in all the simulations reported in this chapter. The critical properties were estimated by fitting the coexisting densities data to the density scaling law Eq. (3-2), and the law of rectilinear diameters Eq. (3-3) with the value of β fixed to the classical

value of 0.32. The critical pressure was determined by fitting the simulated vapor pressure to the Riedel vapor pressure equation Eq. (3- 4).

6.4 Results and discussion

The starting bulk mass densities, ρ_m, the equilibration times, t_{eq}, prior to sampling the configuration to generate the density histogram used in all the simulations are reported in Table 6-3. Also, shown in the tables are the equilibrium vapor and liquid mass densities, $\rho_{m,vap}$ and $\rho_{m,liq}$ obtained from the simulations. These results for the coexisting data and the smoothed

Table 6-3: Simulation specifics and results for the 2ϕMD simulations of 1-pentanol

T (K)	ρ_m(g cm^{-3})	t_{eq} (ns)	$\rho_{m,\text{vap}}$(g cm^{-3})	$\rho_{m,liq}$(g cm^{-3})
200	0.150	2.86	0.0420	0.8602
250	0.150	2.90	0.0411	0.8116
300	0.150	2.90	0.0459	0.7693
350	0.200	2.90	0.0905	0.6643
400	0.200	2.90	0.1210	0.6187
450	0.250	3.00	0.1876	0.4969
475	0.250	3.10	0.2263	0.4207

curves obtained from regression of the data using Eqs. (3-2) and (3-3) are shown in Figure 6-2. The experimental phase dome also shown in this figure was obtained using the recommended values for T_c and V_c in the DIPPR® 801 database,[19] the correlations for the saturated liquid densities of 1-pentanol from the same source, and saturated vapor densities calculated using the Soave equation of state at the indicated temperature and at the corresponding vapor pressure. The latter was obtained from the vapor pressure correlation in the DIPPR® 801 databases. The results in Figure 6-2 show that the saturated vapor densities are higher than those calculated from the Soave equation of state and the saturated liquid densities are lower than the experimental values. There are two things at work here that might lead to errors or these deviations of the simulations

results from the experimental values: 1) transferability of the generalized parameters for the potential model and 2) inaccuracies in the potential model itself. The later could be due to inadequate representations of the entire *ab initio* energy landscapes by the analytical pair potential model or inaccuracies of the *ab initio* calculations themselves or inaccuracies of the energies obtained due to inadequate level of theory and basis set size as well as other quantum and computational issues.

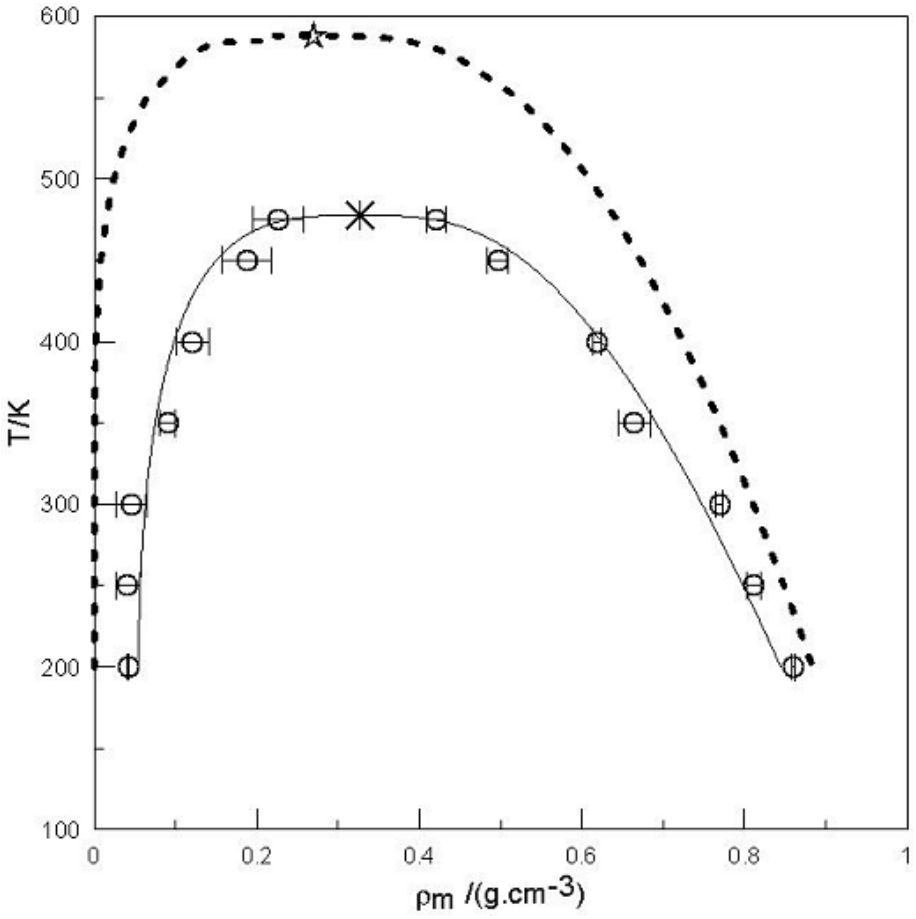

Figure 6-2: Vapor-liquid phase diagram 1-pentanol from the *ab initio* pair-potential model without charges (○, solid line, error bars) in comparison to the saturated liquid densities from the DIPPR® 801 database and saturated vapor densities from the Soave equation of state (dashed line). Also, shown are the model without charges (asterisk), and experimental (star) critical points

To identify the errors due to transferability of the potential, the two probable sources of errors must be separated from each other. To spot check the efficacy of the transferable potential model, the actual dimer energies for 1-pentanol were calculated at the MP2/6-311 + G (2df, 2pd) level for varying distances along three approach routes. All potential energies of the dimer pair were counterpoise (CP) corrected to minimize basis set superposition error (BSSE). Potential energy scans were performed for the dimers along routes of fixed relative monomer orientations. The energy landscape was sampled at thirteen to sixteen dimer separation distances for three different routes or relative orientations of the rigid monomers shown in Figure 6-3.

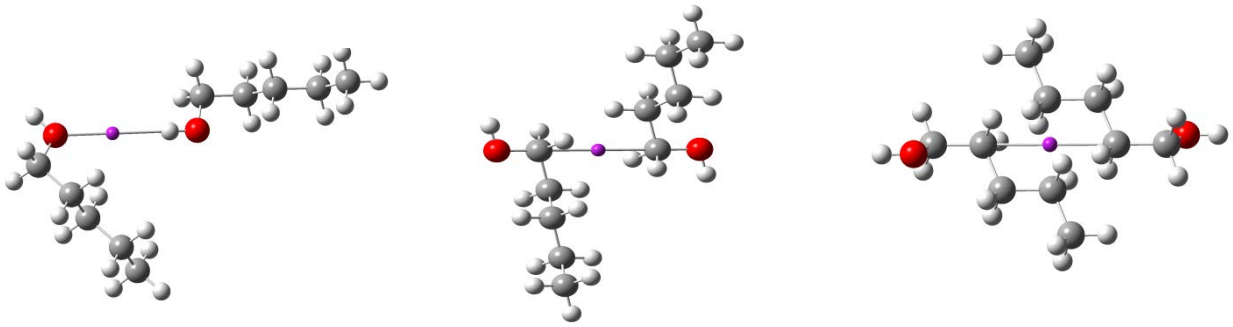

Route 1: O-H_α route Route 2: C_α-C_α route Route 3: C_1 -C_1 route

Figure 6-3: The approach orientation of the three routes: Route 1 (O-H_α route); Route 2 (C_α - C_α route); Route 3 (C_1 –C_1 route)

Admittedly this is a very small sampling of the overall landscape, but the dimer approach routes were chosen to sample what are expected to be the deepest attractive wells where hydrogen bonding can occur. The routes were defined in terms of an approach axis along which the distance between the two monomers was varied. The central site in these routes, represented by the purple sphere in the figure, is a dummy site used in the scan to vary *r*, the distance between the positions of the two C_α nuclei. The *ab initio* dimer potential energies obtained for each of the

routes are shown in Figure 6-4. Also, shown are the potential energies calculated using the site-site potential model with the generalized Morse potential parameters for comparison. Route 1, which brings the O and H_α atoms together for the hydrogen bonding, is the dominant attractive route. It exhibits a very deep attractive well (-5.5 kcal/mol). As shown in the figure, the site-site model gets the maximum in the well depth and location of the well depth very well for this route.

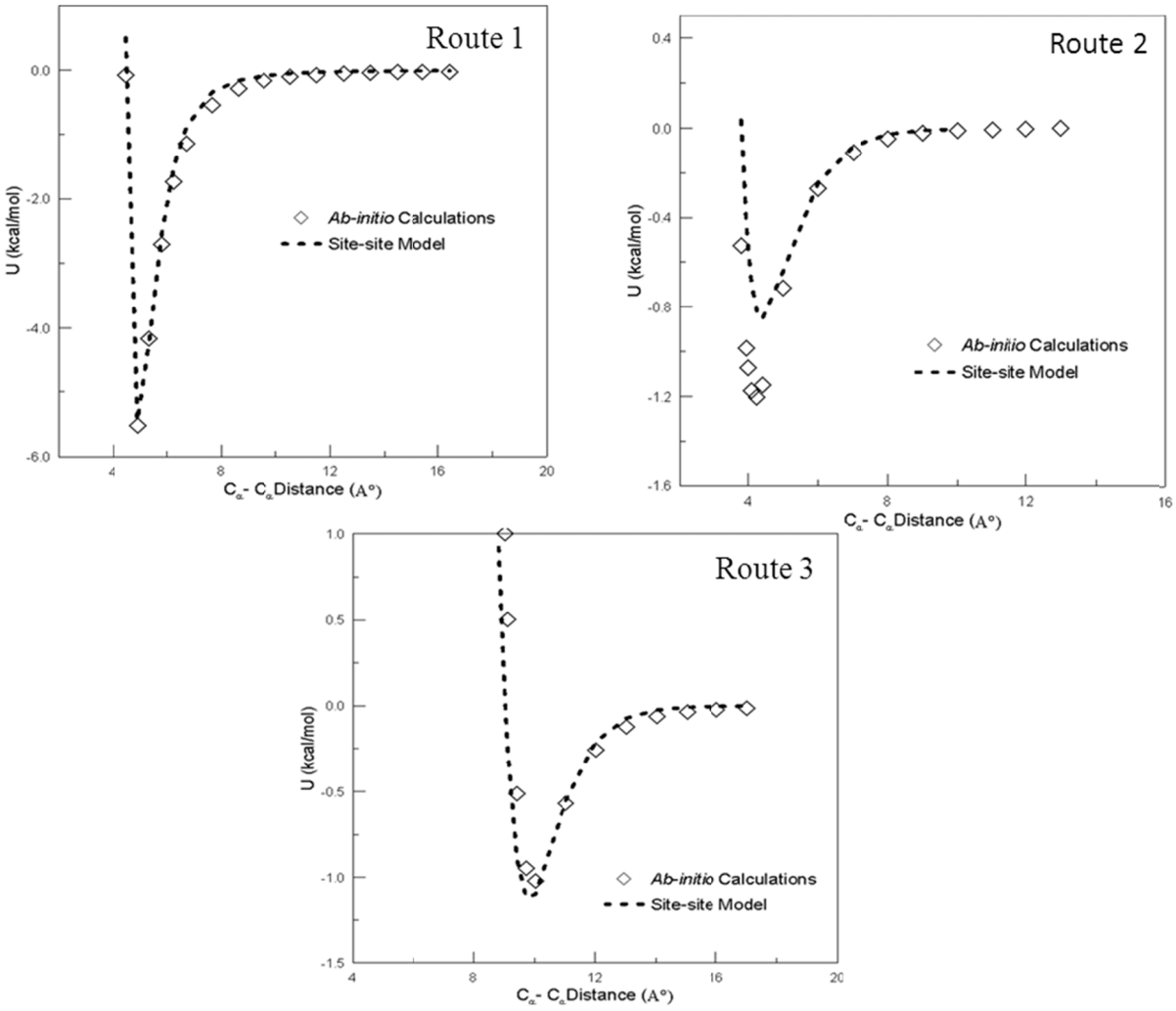

Figure 6-4: MP2/6-311+G(2*df*,2*pd*) dimer pair energies (◊) and the potential energies from the site-site model (dotted lines) for Route 1 (O-H_α route); Route 2 (C_α - C_α route); Route 3 (C_1 –C_1 route)

Route 2 (C_α- C_α route) and Route 3 (C_1-C_1 route) exhibit modest attractive wells with -1.1 kcal/mol and -1.0 kcal/mol well depths respectively. The O and H atoms are at opposite ends of the dimer and play only a minor role in the interactions. For Route 2, though the site-site model correctly reproduces the shapes of the attractive wells and the location of the well minimum, it underestimates the well depth. Pairs of molecules in the model are not as attractive in this orientation as they should be. The site-site model reproduces the behavior of Route 3 very well. The resultant coexistence curve and the critical points obtained from a pair potential model depends on the accuracy of the analytical site-site model used to represent the actual *ab initio* energy landscapes. As shown in Figure 6-2, the coexistence curve obtained using the site-site model is lower than the experimental values. The less attractive site-site model for the C_α- C_α route (Route 2) than the actual pair interactions might be one of the contributing factors. If model molecules are less attractive in the liquid then the actual fluid, it would raise the vapor pressure and thereby lower the critical point and coexistence curve which is consistent with the results obtained in our work.

Regression of the generalized parameters in the original work by Rowley et al.[20, 21] did not produce a perfect description of the energy landscape obtained from their extensive sampling over many, many relative dimer orientations and distances. While the difference in the attractive well depth for Route 2 is larger than most of the differences seen in their fit of the *ab initio* dimer energy data, the agreement between the true dimer energies and the site-site model is generally similar to their regressed fits for the smaller alcohols and is of the same quality that would be expected by transferable parameters. The generalized set of parameters used in this study reproduces quite well the potential energy landscapes for the three routes of 1-pentanol dimers suggesting fairly good level of transferability for the generalized parameters. This left us with the

conclusion that the deviation of the coexisting densities obtained using the generalized Morse potential parameter from the experimental values are not due to the transferability of the potential parameter but are likely due to the inaccuracies in the potential model such as missing higher-order interaction terms (i.e, three-body effects), etc.

The critical temperature (T_c) and critical densities ($\rho_{m,c}$) values for 1-pentanol obtained using the simulations are 477.66 K and 0.327 g/cm^3; the experimental reported values are 588.10 K and 0.270 g/cm^3, respectively. The errors in T_c, $\rho_{m,c}$ are 21.0 % and -18.78 % respectively. The vapor pressure curve obtained by performing one-phase vapor simulations at different temperatures below the critical temperature using saturated vapor phase densities are reported in Figure 6-5. As mentioned in Chapters 4 and 5, the vapor pressure curves are very sensitive to the

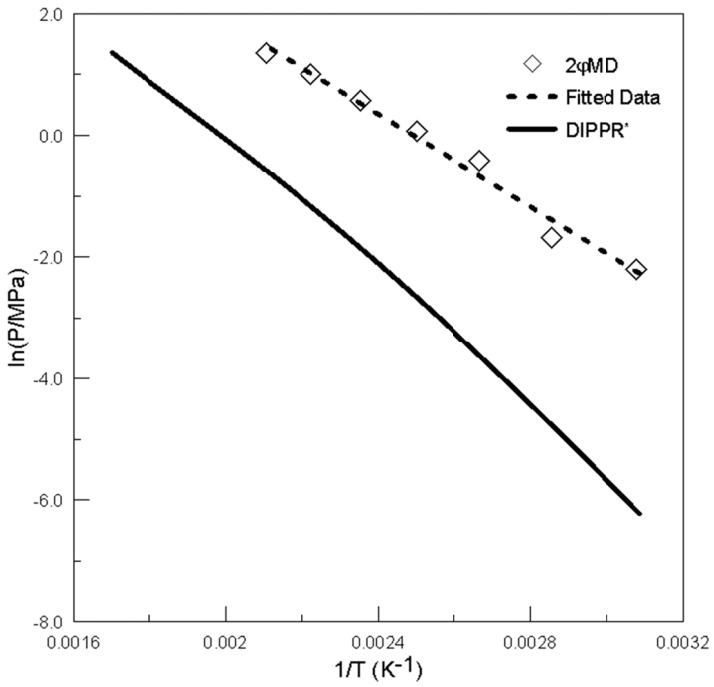

Figure 6-5: Vapor pressures of 1-pentanol (□, dashed line). The solid line styles are from the recommended correlation in the DIPPR® 801 database for 1-pentanol

saturated vapor densities used to perform one-phase simulation to obtain the vapor pressure value. As can be seen from Figure 5-7, the vapor pressure data does not match well with the

experimental values, which is not surprising given the errors associated with the coexisting densities values. Factors like inaccuracies in the potential model, and transferability of the model affect the results for densities and hence the vapor pressure. The critical pressure, P_c, was obtained by fitting the vapor pressure data to the Riedel vapor pressure equation (Equation (3-4)). The critical pressure value obtained was 4.56 MPa, and the experimental reported values are 3.89 MPa giving an error of 17.1 % for critical pressure. The error in the critical pressure is due to the error associated with the vapor pressure values obtained using simulations in this work.

6.5 Conclusions

The transferability of the generalized Morse potential parameters for alcohols obtained by Rowley et al.[20, 21] from the composite regression of the potential energy landscapes of the small alcohols up to four carbon atoms was tested by determining equilibrium vapor and liquid densities and the critical point of 1-pentanol. When compared to the experimental phase dome, the coexistence curve obtained from the potential model over predicts vapor densities and under predicts liquid densities giving a lower or narrower phase-dome for 1-pentanol. The vapor pressure data and hence the critical pressure values are very sensitive to the bulk vapor densities used to simulate them. Therefore any uncertainties in the vapor densities value will contribute to the error in the vapor pressure data and hence the critical pressure. The discrepancies in the results for coexisting densities obtained from our simulation with that from experimental values might be either due to the error associated with the transferability of the generalized potential parameter or due to the inaccuracies in the potential model. In an attempt to separate the source of errors, the *ab initio* molecular pair potential was calculated for three dimer approach routes. The transferable site-site model provided a good representation of the very attractive *ab initio* hydrogen bond potential wells (Route 1) and also for the potential energy landscapes for the C_1-

C_1 route (Route 3). One of the routes (Route 2) was observed to be more attractive than the results predicted by the site-site model which is consistent with a higher critical point as experimentally observed. In general the results obtained here for 1-pentanol were similar in quality to their regressed fit for smaller alcohols obtained by Rowely et al.[20, 21] and are as good as it could be expected from a transferable parameter. All this suggests the deviation of the coexisting densities and the critical points results from the experimental values are not due to the transferability of the generalized potential parameter. To improve the results obtained for the coexisting densities and the critical points using an *ab initio* based potential model, the multi-body effects will need to be implemented in the potential model. There are several ways to proceed. In one way, *ab inito* derived molecular pair potential models can be scaled and supplemented with polarizability to take into account multibody effects and better represent experimental results.[91] Alternatively, multibody effects calculated from clusters of molecules could be incorporated into more sophisticated models if needed. Also, corrections for higher-body interactions can be developed by looking at three-, four- and five-body effects on the *ab initio* potential energy landscapes and adding the corrections to the pair potentials.[92] But to know which inaccuracies in the potential model cause the errors we need to also consider the following questions: 1) Do the level of theory and basis set size used in the original work to obtain the *ab initio* potential model by Rowley et al.[20, 21] accurately give the true pair potential? 2) How much of the effect is due to the reduction in fidelity of the *ab initio* landscapes by the regression to a simple Morse potential model?

7 CONCLUSIONS AND RECOMMENDATIONS

7.1 Conclusions

The use of molecular simulation to study VLE (Vapor Liquid Equilibrium) has been evolving since the seminal work of Panagiotopoulos[22] and will continue to evolve in the future. Fern et al.[17,18] introduced one such simulation technique based on 2φMD with Voronoi tessellations (VT) that can be used to determine equilibrium vapor and liquid densities even near the critical point without requiring an interface or complete phase separation. In this MD+VT method, one can unambiguously determine the bulk liquid and vapor phases in the two-phase simulations utilizing simple statistical parameters such as, mean and variance, from both two-phase and one-phase simulations. The bulk phase densities are determined using local properties and without requiring any prior knowledge of phase densities. The later advantage is very useful for the investigation of unknown compounds. The only problem associated with the VT method is its complexity in implementing in the code. Also, this method needed further modifications to apply it to multisite molecules. An objective of this work was to extend the method developed by Fern et al. in such a way that it can be easily applied to complex molecules, i.e., molecules with intermolecular potential models represented with multiple interaction sites involving both van der Waals and Coulombic potentials. The extension developed in this study uses a Monte Carlo sampling technique in conjunction with 2φMD simulations to provide a usable, efficient simulation method for prediction of bulk vapor and liquid densities and the critical temperature

and density for the model fluid. Accuracy of the predicted values of course depends upon the efficacy of the model itself.

The new MD + MC sampling technique was tested and benchmarked by performing simulations for the equilibrium vapor and liquid densities for a simple Lennard-Jones (LJ) fluid. The results were in excellent agreement with those reported by Fern et al.[17,18]. The new MC sampling technique replacing the Voronoi volume determinations made extension of the method to multisite molecules straightforward. Two-phase simulations were then performed for a model potential for propane. The results showed this new method to be as reliable and accurate as previously favored MC methods to study VLE without the disadvantage of required particle insertions near the critical point where MC methods become inefficient and even untenable without complex biasing techniques.

Different models for propane were studied to determine the sensitivity of the critical density and temperature to various intramolecular features of the potential model. The results obtained using the flexible model (with flexible bond distance and bond angle) for propane matched very well with the results reported for the GEMC method. The effect of intramolecular flexibility suggested that the resultant phase dome and critical point are more affected by internal flexibility near the critical region then far from the critical point. Also, the phase dome is affected if too small of an interaction potential cutoff is used in the simulation. The phase dome is narrowed by a smaller cutoff in the potential, but the potential cutoff does not affect the coexistence curve for cutoff values larger than about 20 Å.

A second objective of this work has been to evaluate for the first time the efficacy of the *ab initio* based potential model for alcohols developed by Rowley et al. [20, 21] by determining the critical properties of methanol and 1-propanol. Though the potential model yields an unrealistic

coexistence curve and densities for methanol but more reasonable results, for 1-propanol qualitatively considering it is a true pair potential with no adjustable parameter regressed using experimental data. Polarization effects may affect the smaller molecule, methanol, more than 1-propanol. The intention here was also to identify the effect of multi-body interactions on the equilibrium vapor and liquid densities and critical properties as deviations of the simulated results from the experimental values are expected to be due mainly to the lack of multi-body interactions in these true pair potential models. The effect of using the potential model with and without including point charges on the phase dome and critical properties was also investigated. For 1-propanol, modeling the potential with or without point charges does not seem to affect the coexistence curve and critical properties results. The later representation is computationally less expensive because it avoids difficulties associated with long-range effects of a point-charge type model. This is not to say that charge distributions don't impact the phase dome. Rather the results show that the actual charge distribution interactions can be accurately represented by empirical pair potentials parameterized to give the dimer energy landscape without resorting to the use of point charges to represent the actual charge distribution within the molecule. True pair Coulombic interactions are thus of shorter range than explicitly implied by the point charge interactions.

Lastly, the transferability of the *ab initio* based potential model was investigated by applying the potential model to 1-pentanol, a molecule which was not used to develop the potential. Due to the limitations of the computational time needed to perform the simulations, molecules bigger than 1-pentanol couldn't be used in our simulations. The coexisting densities and the critical properties results obtained were very similar to those for 1-propanol. An attempt to identify errors due to transferability separate from the errors due to the use of a true pair

potential was made by comparing energy profiles for some relative dimer orientations produced from new *ab initio* calculations made in this study with the profiles obtained using the site-site potential model and the generalized Morse parameters obtained from smaller alcohol parameterizations by Rowley et al. [20, 21] The results suggested a good level of transferability for the site-site model. The lack of multi-body effects appears to be dominant weakness in using the generalized *ab inito* potential model for determination of the phase dome and critical properties of larger alcohols. Also, inaccuracies in the potential model itself, either due to the inaccuracies in the *ab initio* calculations due to inadequate level of theory and basis set as well as other quantum and computation issues or inaccuracies in the analytical fit of the *ab initio* energies, might also contribute to the deviations of the simulated results from experimental values.

7.2 Recommendations

The first recommendation is to further improve the efficiency of the code used for MD simulations and for the MC sampling technique. Even though the codes employed in this work are very effective, the computational time can be further reduced by parallelizing the code. These MD and MC sampling codes should be very amenable to parallelization and thereby substantial time saving could be achieved. This will also assist in simulating very large molecules which are not possible right now due to limitations of computational time.

The new technique developed in this work using MD simulations coupled with the MC sampling technique could be used to explore other fascinating areas of research. It would be interesting to study multi-component multi-phase systems using this method. In these studies, one would need to calculate and then separate the volume associated with each component. The phases could then be determined using the same iterative process. Other phase equilibrium points could also be investigated using this MD+MC method. For example the triple point of a system

where three phases are in equilibrium can be studied. In that case, modifications will have to be made to the convergence procedure used to determine the phases. The MD+ MC method could be used in the future to study different families of hydrocarbons. One could study the effect of branching or the effect of chain length on critical properties for different families using this method. As the chain length becomes larger and larger, the experimental data become more scarce either due to infeasible experimental conditions or due to thermal instability. It would be helpful to have this simulation technique available for predicting the critical properties for such compounds. Furthermore, MD simulations allow for the investigation of interfacial properties such as diffusion of molecules through an interface, thickness of the interface, surface tension at the molecular level, molecular orientation at the interface etc. The dynamics of interface formation and destruction can also be observed using MD simulations.

In the method used here, the bulk vapor and liquid phase densities were determined by matching two statistical properties of the molecular distribution curves obtained using two-phase and one-phase simulations: the mean and the variance. However, the shape of the distribution can be different. The assumption here is that the distributions are characterized adequately by mean and variance only and all other higher order moments of the distributions are ignored. This is true for a Gaussian distribution but in cases where the single phase distributions are more skewed or have kurtosis (non-Gaussian) it might be necessary to use higher order moments in the statistical analysis of the phases. The agreement in the shape of distributions between the two-phase and one-phase simulations worsens as the temperature increases because the distribution becomes increasingly skewed. The molecular distributions obtained from the single-phase simulations are skewed, especially in the vapor phase at high temperature. In systems with hydrogen bonding, the single-phase distributions become highly skewed as temperature

approaches the critical temperature. Ignoring the higher order of moments for highly skewed systems might compromise the results. To address this issue, one could implement a new convergence scheme that included the higher-order moments of the volume distributions. Also, if a theory that predicts the shape of the volume distributions can be developed, it could help match the shape of the distributions and thereby predict more accurate results for systems where the distributions are skewed.

At lower temperatures, the system has two distinguished peaks in the molecular distributions corresponding to the liquid and vapor densities in equilibrium with each other. As the temperature increases, the vapor peak shifts to higher densities and the liquid peak shifts toward lower densities and both peaks broaden. At the highest temperature, i.e. close to the critical point, there is significant overlap between the two peaks. Sometimes due to this significant overlap, it is very difficult to distinguish between the phases especially very close to the critical point. Just by looking at the distributions, it is very difficult to know if we are above or below the critical point. There may not be a good solution to this problem, but one way around this problem is to fit more points far from the critical point or in other words to perform more simulations at lower temperatures and to include those points when determining critical properties by fitting the coexisting data to the law of rectilinear diameter and to the density scaling law.

There are still many avenues for new and interesting research in the development of intermolecular potential from *ab initio* calculations. To predict critical properties accurately and phase behavior directly from *ab initio* derived potentials, the potential may need multi-body corrections and polarization effects. Multi-body corrections can be developed by looking at three-, four- and five-body effects on the *ab initio* potential energy landscapes. Cluster potential

energies for example might be used in the future to produce energy landscapes more appropriate for condensed-phase simulations. Improvements in the analytical pair potential model used to represent the entire *ab inito* landscape could improve the results for the coexistence curve and hence the critical properties. The energies obtained using the *ab initio* method and hence the quality of the analytical fit could be further improved by using even higher levels of theory and larger basis sets.

At this point, a method has been developed for the determination of coexistence densities and critical properties and it can be reliably applied to a simple or polyatomic molecules. As always, the accuracy of the results is dependent upon the accuracy of the interaction potential model to represent the interactions of the real system. There are still many avenues for new and interesting research using the MD + MC method developed here. The potential also exists for further improving the *ab initio* potential model used in this work.

APPENDIX A. CODE FOR VOLUME DETERMINATION USING MC SAMPLING METHOD

The following algorithm to determine the volume associated with each molecule using the Monte Carlo (MC) sampling method was written in the computer program named *volconfig.cpp*. The entire code is given here.

```
/This code is used to calculate the volume of individual molecules
#include <iostream>
#include <cmath>
#include <cstdlib>
#include <ctime>
#include <fstream>
#include <math.h>
#include <vector>
#include <cstdio>
#include <iomanip>
#include <set>
#include <sstream>
#include <time.h>
#include <string>

using namespace std;
int NM;
int NM1;
int NS;
int NPT;
int ninb;
int ncfig;
double CUBE;

double volume(int *num, double *vol)
{ cout<<"NM="<<NM<<endl;
  double sum= 0.0;
  double totvol = CUBE * CUBE * CUBE;
  cout<<"totvol="<<totvol<<endl;
  for(int i = 0; i < NM; ++i)
  {
    vol[i] = (num[i] * totvol)/double(NPT);
    //cout<<"i="<<i<<"\t"<<vol[i]<<endl;
    sum += vol[i];
  }
  return sum;
  //cout<<"Volume check. Total volume ="<<sum<<endl;
}

void gethist(double *volmol,  int *ihist)
```

```
{
    int irbin;
    double rhoi, dvn, dvni;
    double binsize = 0.01;
/*This is the conversion factor to convert from ang^3 to gm/cm^3 for Methanol. Need to
change this for the particular molecule you are simulating */
    double conv = 53.1992;
     for(int i = 0; i < NM1; ++i)
   {
      rhoi = conv/volmol[i];
      irbin = floor((rhoi/binsize));
      //cout<<"irbin="<<irbin<<endl;
      ihist[irbin] += 1;
    }
  /*  for(int i = 0; i < ninb; ++i)
   {
       cout<<"i="<<i<<"\t"<<ihist[i]<<endl;
    }*/
 //  return dvn;
}

int main()
{
    time_t start, end;
    //time_t start1, end1;
    time (&start);
    string line;
    string filename1, filename2, filename3,filename4,filename5;
    istringstream iss;
    ifstream indata1, indata2;
    ofstream outdata,outdata1,outdata2;
    string runid="01";

     //filename1 = 'input.txt';
     //indata1.open(filename1.c_str());
     /*VORDAT2 is the input file for configuration (X,Y,Z positions in dimensional
unit)*/

     filename2 = "VORDAT2";
     indata2.open(filename2.c_str());

     filename3 = "out";
     filename3 += "_" ;
     filename3 += runid;
     filename3 += ".txt";
     //cout<<filename1<<endl;
     outdata.open(filename3.c_str(), ios::app);

     filename4 = "outavg";
     filename4 += "_" ;
     filename4 += runid;
     filename4 += ".txt";
   //cout<<filename2<<endl;
    outdata1.open(filename4.c_str(), ios::app);

     filename5 = "ix";
     filename5 += "_" ;
     filename5 += runid;
     filename5 += ".txt";
   //cout<<filename2<<endl;
    outdata2.open(filename5.c_str(), ios::app);

  /* Change number of molecules, NM1 and number of sites, NS, Length of box, CUBE
```

```
   according to the particular system */
  NM1=1331; NS=6; NM = NM1*NS; NPT = 64000000; ncfig = 1;
  CUBE = 77.8666; ninb = 150;

  int istep, nlin, SITE;
  int num[NM],ihist[ninb];
  double SP,SP2,XI,YI,ZI,RS,MIN;
  double rg[NM][3],X[3],dis[3],dist[3],vol[NM],volmol[NM1];
  //double ucell[3][3],tranm[3][3],tranmi[3][3];
  double props[ninb][2];

  nlin = int(pow((double(NPT)+0.1), (1.0/3.0)));
  cout<<"nlin="<<nlin<<endl;
  SP = CUBE/double(nlin);
  SP2 = SP/2.0;
  //Position of the first point
  XI = SP2; YI = SP2; ZI = SP2;
  cout<<"spacing distance="<<SP<<"\tsp2="<<SP2<<endl;

  for(int i = 0; i < ninb; ++i)
   {
      for(int j = 0; j <2; ++j)
     {
         props[i][j] = 0;
     }
   }

//Start calculation for each configurations
for(int ic = 0; ic < ncfig; ++ic)
{
  //Initialization
   for(int i = 0; i < NM; ++i)
   {
      for(int j = 0; j <3; ++j)
     {
         rg[i][j] = 0.0;
     }
   }
   for(int i = 0; i < NM; ++i)
   {
     num[i] = 0;
   }
   for(int i = 0; i < NM; ++i)
   {
     vol[i] = 0.0;
   }
   for(int i = 0; i < NM1; ++i)
   {
     volmol[i] = 0.0;
   }
   /* for(int i = 0; i < 3; ++i)
   {
      for(int j = 0; j <3; ++j)
     {
         ucell[i][j] = 0.0;
         tranmi[i][j] = 0.0;
         tranm[i][j] = 0.0;
     }
   }*/
    for(int i = 0; i <ninb; ++i)
   {
      ihist[i] = 0;
   }
```

```
  //Reading the positions from file
  indata2>>istep;
  cout<<"istep="<<istep<<endl;
  for(int i = 0; i < NM; ++i)
  {
     for(int j = 0; j <3; ++j)
    {
        indata2>>rg[i][j];
    }
  }
   outdata<<"**********Configuration starts *****************"<<endl;
   for(int i = 0; i < NM; ++i)
   {  // cout<<"i="<<i<<endl;
     for(int j = 0; j <3; ++j)
    {
       outdata<<rg[i][j]<<"\t";
      // cout<<rg[i][j]<<"\t";
    }
    outdata<<endl;
    //cout<<endl;
  }
 outdata<<"**********Configuration ends *****************"<<endl;
  //Defining unit cell
 /* for(int i = 0; i < 3; ++i)
  {
     for(int j = 0; j <3; ++j)
    {
         if(i == j)
            ucell[i][j] = 1.0;
    }
  }*/
  //Calculate the box dimension based upon the total volume
// get_tranm(ucell, tranm, tranmi);
 outdata<<" ***********Site volumes starts***********"<<endl;
 for(int ix = 0; ix < nlin; ++ix)
 {
   outdata2<<"ix="<<ix<<endl;
   //time (&start1);
  for(int iy = 0; iy < nlin; ++iy)
  {
   for(int iz = 0; iz < nlin; ++iz)
   {
      X[0] = XI + SP * ix;
      X[1] = YI + SP * iy;
      X[2] = ZI + SP * iz;
      //cout<<ix<<"\t"<<iy<<"\t"<<iz<<"\t"<<X[0]<<"\t"<<X[1]<<"\t"<<X[2]<<endl;
      MIN = 100000.0;
      SITE = 0;
      for(int iatm = 0; iatm < NM; ++iatm)
      {
       for(int id = 0; id < 3; ++id)
       {
           dis[id]=0.0;
          // dist[id] =0.0;
       }
       for(int id = 0; id < 3; ++id)
       {
           dis[id] = X[id] - rg[iatm][id];
       }
       //This is one way to do minimum image convention
      // cout<<"iatm"<<iatm<<"\t"<<dis[0]<<"\t"<<dis[1]<<"\t"<<dis[2]<<endl;
      /* for(int k = 0; k <3; ++k)
      {
```

```
             dist[k] = tranm[k][0] * dis[0] + tranm[k][1] * dis[1] + tranm[k][2] *
dis[2];
          //cout<<dist[k]<<endl;
          //Minimum image convention......
          if( dist[k] > 0.5)
          { // cout<<"hello1..."<<endl;
             dist[k] = dist[k] - 1.0;
          }
          if( dist[k] < -0.5)
          { //cout<<"hello2...."<<endl;
            dist[k] = dist[k] + 1.0;
          }
         // cout<<dist[k]<<endl;
         // cout<<rg[iatm][k]<<"\t"<<rg[jn][k]<<"\t"<<dis[k]<<endl;
        }
        for(int k = 0; k <3; ++k)
        {
          dis[k] = tranmi[k][0] * dist[0] + tranmi[k][1] * dist[1] + tranmi[k][2] *
dist[2];
          //cout<<dis[k]<<endl;
        }*/
         //cout<<"iatm"<<iatm<<"\t"<<dis[0]<<"\t"<<dis[1]<<"\t"<<dis[2]<<endl;
          //This is another way to implement minimum image convention
          for(int id = 0; id < 3; ++id)
          {
            dis[id] = dis[id] - (CUBE * round(dis[id]/CUBE));
          }
         // cout<<"iatm"<<iatm<<"\t"<<dis[0]<<"\t"<<dis[1]<<"\t"<<dis[2]<<endl;
          RS = dis[0]*dis[0] + dis[1]*dis[1] + dis[2]*dis[2];
          //cout<<"RS="<<RS<<endl;
          if (RS < MIN)
          {
            MIN = RS;
            SITE = iatm;
          }
         // cout<<"iatm="<<iatm<<"\tSITE="<<SITE<<endl;
         } //iatm loop ends
         // cout<<"SITE="<<SITE<<endl;
         num[SITE] += 1;

      }//iz loop ends
    }//iy loop ends
   //time (&end1);
   //double diff1 = difftime(end1, start1);
   //cout<<"Time difference in mins for loop ="<<(diff1/60.0)<<endl;
   } //ix loop ends
  /* for(int i = 0; i < NM; ++i)
   {
     cout<<"i="<<i<<"\t"<<num[i]<<endl;
   }*/
   double sum =volume(num, vol);
   for(int i = 0; i <NM; ++i)
  {
     outdata<<"i="<<i<<"\t"<<vol[i]<<endl;
  }
  outdata<<" ***********Site volumes ends***********"<<endl;
  outdata<<"Volume check. Total volume ="<<sum<<endl;

  outdata<<" ***********Molecular volumes starts***********"<<endl;
  int j =0;
  for(int i = 0; i <NM1; ++i)
  {
    for(int k = 0; k <NS; ++k)
```

```
    {
       volmol[i]+= vol[j+k];
    }
    j = j + NS;
  }
  for(int i = 0; i <NM1; ++i)
  {
     outdata<<"i="<<i<<"\t"<<volmol[i]<<endl;
  }
  outdata<<" ***********Molecular volumes ends********** "<<endl;
  gethist(volmol, ihist);
  /* for(int i = 0; i < ninb; ++i)
   {
        props[i][0] = (ihist[i]);
    }*/
    //standard save for remaining props
     for(int i = 0; i < ninb; ++i)
     {
        props[i][0] += ihist[i];
      //props[i][2] += props[i][0] * props[i][0];
     }
    } //configuration loop ends here

   for(int i = 0; i < ninb; ++i)
   {
     props[i][1] = props[i][0] / double(ncfig);
    // props[i][4] = (props[i][2] / double(ncfig)) - (props[i][3] * props[i][3]);
     /*if( props[i][4] > 0.0)
     {
        props[i][5] = pow(props[i][4], 0.5);
     }*/
  }//Configuation loop ends
  outdata1<<"Report results "<<endl;
  outdata1<<endl;
  for(int i = 0; i < ninb; ++i)
  {
     outdata1<<i<<"\t"<<props[i][1]<<endl;
  }
   /*for(int i = 0; i < ninb; ++i)
   {
     cout<<i<<"\t"<<ihist[i]<<endl;
   }*/

   time (&end);
   double diff = difftime(end, start);
   outdata<<"Time difference in mins ="<<(diff/60.0)<<endl;
   cout<<"Time difference in mins ="<<(diff/60.0)<<endl;
   //indata1.close();
   indata2.close();
   outdata.close();
   outdata1.close();
   //outdata1.close();
   return 0;
}
```

REFERENCES

[1] Nikitin, E. D.; Pavlov, P. A.; Skripov, P. V.; "Measurement of the critical properties of Thermally Unstable Substances and Mixtures by the Pulse-Heating method."; *J. Chem. Thermodynamics*; **25**; 869; 1993.

[2] VonNiederhausern, D. M; Wilson, G.M.; Giles, N. F.; "Critical-Point and Vapor Pressure Measurements at High Temperatures by Means of a New Apparatus with Ultralow Residence Times."; *J. Chem. Engg. Data*.; **45**; 157; 2000.

[3] Reid, R.C, Prausnitz, J. M., Poling, B. E., "The Properties of Gases and Liquids", Fourth edition, McGraw-Hill, New York, 1987 (Chapter 2).

[4] Wescott, J. T.; Kung, P.; Nath, S. K.; " Vapour-lqiuid coexistence properties and critical points of two branched alkanes series."; *Fluid Phase Equil.*; **208**; 123; 2003.

[5] Panagiotopoulos, A.Z.; " Monte Carlo Methods for Phase Equilibria of Fluids.";*J. Phys. Condens. Matter*; **12**; R25; 2000.

[6] Frenkel, D.; Smit, B.; "Understanding Molecular Simulation From Algorithms to Applications."; **2nd ed**., Academic Press: San Diego, Ca, 2002.

[7] Siepmann, J. I.; Karaborni, S.; Smit, B.; "Simulating the critical behaviour of complex fluids."; *Nature*; **365**; 330; 1993.

[8] Martin, M. G.; Siepmann, J. I.; "Transferable Potentials for Phase Equilibria: 1. United-Atom Description of n-Alkanes."; *J. Phys. Chem. B*; **102**; 2569; 1998.

[9] Lofti, A.; Vrabec, J.; Fischer, J.; " Vapoour liquid equilibria of the Lennard-Jones fluid from the NpT plus test particle method."; *J. Mol. Phys.*; **76**; 1319; 1992.

[10] Vrabec, J.; Hasse, H.; "Grand Equilibrium: vapour-liquid equilibria by a new molecular simulation method."; *Mol. Phys.*; 100; 3375; 2002.

[11] Vrabec, J.; Kedia, G. K.; Fuchs, G. ; Hasse, H.; "Vapour-liquid coexistence of the truncated and shifted Lennard-Jones fluid."; *Mol. Phys.*; 104; 1509; 2006.

[12] Chapela, G. A.; Saville, G.; Thompson, S. M.; Rowlinson, J. S.; "Computer simulation of a gas-liquid surface. Part 1."; *Faraday Trans.*; **73**; 1133; 1977.

[13] Duque, D.; Vega, L.F.; "Some issues on the calculation of interfacial properties by molecular simulation." ; *J. Chem. Phys.*; **121**; 8611; 2004.

[14] Holcomb, C. D.; Clancy, P.; Thompson, S. M.; Zollweg, J. A.; "A critical study of the simulation of the liquid-vapour interface of a Lennard-Jones fluid."; *Fluid Phase Equil.*; ***75***, 185; 1992.

[15] Gelb, L. D.; Müller, E. A.; "Location of phase equilibria by temperature-quench molecular dynamics simulations. "; *Fluid Phase Equil.*; **203**; 1; 2002.

[16] Pamies, J. C.; McCabe, C.; Cummings, P. T.; Vega, L. F.; "Coexistence Densities of Methane and Propane by Canonical Molecular Dynamics and Gibbs Ensemble Monte Carlo Simulations."; *Molecular Simulation*; **29**; 463; 2003.

[17] Fern, J.T.; Keffer, D.J.; Steele, W.V.; " Measuring Coexisting Densities from a Two-phase Molecular Dynamics Simulation by Voronoi Tessellations."; *J. Phys. Chem. BI*; **111**; 3469; 2007.

[18] Fern, J.T.; Keffer, D.J.; Steele, W.V.; "Vapor-Liquid Equilibrium of Ethanol by Molecular Dynamics Simulation and Voronoi Tessellation."; *J. Phys. Chem. B*; **111**; 13278; 2007.

[19]R.L. Rowley, W.V. Wilding, J.L. Oscarson, Y.Yang, N.F.Giles, *DIPPR® Data Compilation of Pure Chemical Properties*, Design Institute for Physical Properites, AIChE, New York, NY (2009).

[20] Rowley, R.L. ; Christopher, M.T. ; Pakkanen, T.A. ; "Potential energy surfaces for small alcohol dimers I: Methanol and ethanol."; *J. Chem. Phys.*; **125**; 154302; 2006.

[21] Rowley, R.L.; Tracy, C.M.; Pakkanen, T.A.; "Potential energy surfaces for small alcohol dimers. II. Propanol, isopropanol, *t*-butanol, and *sec*-butanol."; *J. Chem. Phys.*; **127**; 025101; 2007.

[22] Panagiotopoulos, A. Z.; "Direct determination of phase coexistence properties of fluids by Monte Carlo simulation in a new ensemble." ; *Mol. Phys.;* **61**; 813; 1987.

[23] Ladd, A. J. C.; Woodcock, L. V.; "Interfacial and co-existence properties of the Lennard-Jones system at the triple point."; *Molec. Phys.*; 36; 611; 1978.

[24] Panagiotopoulos, A. Z.; Stapleton, M.; "The gibbs method for molecular-based computer simulations of phase equilibria."; *Fluid Phase Equil.*; **53**; 133; 1989.

[25] Laso, M.; De Pablo, J. J.; Suter, U. W.; "Simulation of phase equilibria for chain molecules."; *J. Chem. Phys.;* **97(4)**; 2817; 1992.

[26] Siepmann, J. I.; Karaborni, S.; Smit, B.;"Vapor-Liquid Equilibria of Model Alkanes."; *J. Am. Chem. Soc* ;**115**; 6454; 1993.

[27] Jorgensen, W.L.; Madura, J. D.; Swenson, C. J.; "Optimized Intermolecular Potential Functions for Liquid Hydrocarbons."; *J. Am. Chem. Soc.*; **106**; 6638; 1984.

[28] Anselme, M. J.; Gude, M.; Teja, A. S.; " The critical temperatures and densities of the n-alkanes from pentane to octadecane."; *Fluid Phase Equil.*; **57**; 317; 1990.

[29] Alejandre, J.; Tildesley, D. J.; Chapela, G. A.; " Fluid phase equilibria using molecular dynamics: the surface tension of chlorine and hexane. "; *Molec. Phys.*; **85(3)**; 651; 1995.

[30] Cui, S. T.; Cummings, P. T.; Cochran, H. D.; "Configurational bias Gibbs ensemble Monte Carlo simulation of vapor-liquid equilibria of linear and short-branched alkanes."; *Fluid Phase. Equil.*; **141**; 45; 1997.

[31] Siepmann, J. I.; Martin, M. G.; Mundy, C. J.; Klein, M. L.; "Intermolecular potentials for branched alkanes and the vapour-liquid phase equilibria of n-heptane, 2-methylhexane, and 3-ethylpentane."; *Molec. Phys.*; **90(5)**; 687; 1997.

[32] Vlugt, T. J. H.; Martin, M. G.; Smit, B.; Siepmann, J. I.; Krishna, R.; "Improving the efficiency of the configurational-bias Monte Carlo algorithm."; *Molec. Phys.*; **94(4)**; 727; 1998.

[33] Trokhymchuk, A.; Alejandre J.; "Computer simulations of liquid/vapor interface in Lennard-Jones fluids: Some questions and answers. "; *J. Chem. Phys.*; **111(18)**; 8510; 1999.

[34] Martínez-Veracoechea, F.; Müller, E. A.; "Temperature-quench Molecular Dynamics Simulations for Fluid Phase Equilibria. "; *Molec. Simul.*; **31(1)**; 33; 2005.

[35] Supple, S.; Quirke, N.; "Short range united atom potentials for alkanes: decane and nonane"; *Molec. Simul.*; **29**; 77; 2003.

[36] De Pablo, J. J.; Bonnin, M.; Prausnitz, J. M.; "Vapor-liquid equilibria for polyatomic fluids from site-site computer simulations: pure hydrocarbons and binary mixtures containing methane."; *Fluid Phase Equil.*; **73**; 187; 1992.

[37] De Pablo, J. J.; Laso, M.; Suter, U. W.; "Estimation of the chemical potential of chain molecules by simulation."; *J. Chem. Phys.;* **96**; 6157; 1992.

[38] Ferrenberg, A.M.; Swendsen, A.M.; " New Monte Carlo technique for studying phase transitions."; *Phys. Rev. Lett.*; **61**; 2635; 1988.

[39] Möller, D.; Fischer, J.; " Vapour Liquid Equilibrium of a Pure Fluid from Test Particle Method in Combination with NpT Molecular Dynamics Simulations."; *Molec. Phys.*; **69**; 463; 1990.

[40] Harris, J. G., "Liquid-Vapor Interfaces of Alkane Oligomers. Structure and Thermodynamics from Molecular Dynamics Simulations of Chemically Realistic Models."; *J. Phys. Chem.*; **96**; 5077; 1992.

[41] Smit, B.; Karaboni, S.; Siepmann, J. I.; "Computer simulations of vapor-liquid phase equilibria of n-alkanes."; *J. Chem. Phys.*; **102**; 2126; 1995.

[42] Rodger, P. M.; Stone, A. J.; Tildesley, D. J.; "Anisotropic Site-Site Potential in Molecular Dynamics."; *J. Molec. Simul.*; **8**; 145; 1992.

[43] Toxvaerd, S.; " Molecular dynamic calculation of the equation of state of alkanes."; *J. Chem. Phys.*; **93**; 4290; 1990.

[44] Ahunbay, M. G.; Kranias, S.; Lachet, V.; Ungerer, P.; "Prediction of thermodynamics properties of heavy hydrocarbons of Monte Carlo simulation."; *Fluid Phase Equil.*; **228**; 311; 2005.

[45] Jorgensen, W.L.; " Optimized Intermolecular Potential Functions for Liquid Alcohols. "; *J. Phys. Chem. B*; **90**; 1276; 1986.

[46] Mooji, G.C.A.M; Frenkel, D.; Smit, B.; "Direct simulation of phase equilibria of chain molecules." ; *J. Phys. Condensed Matter*; **4**; L255; 1992.

[47] Van Leeuwen, M. E.; "Prediction of the vapour-liquid coexistence curve of alkanols by molecular simulation. "; *Molec. Phys.*; **87(1)**; 87; 1996.

[48] Jorgensen, W.L.; Maxwell, D. S.; Tirado-Rives, J.; "Development and Testing of the OPLS All-Atom Force Field on Conformational Energetics and Properties of Organic Liquids. "; *J. Am. Chem. Soc.*; **118**; 11225; 1996.

[49] Chen, B.; Martin, M. G.; Siepmann, J. I.; "Thermodynamic Properties of the Williams, OPLS-AA, and MMFF94 All-Atom Force Fields for Normal Alkanes."; *J. Phys. Chem. B*; **102**; 2578; 1998.

[50] Nath, S. K.; Escobedo, F. A.; De Pablo, J. J.; "On the simulation of vapor-liquid equilibria for alkanes."; *J. Chem. Phys.*; **108(23)**; 9905; 1998.

[51] Chen, B.; Martin, M. G.; Siepmann, J. I.; "Transferable Potentials for Phase Equilibria. 3. Explicit-Hydrogen Description of Normal Alkanes."; *J. Phys. Chem. B*; **103**; 5370; 1999.

[52] Errington, J. R.; Panagiotopoulos, A.Z.; " A New Intermolecular Potential Model for the n-Alkane Homologous series."; *J. Phys. Chem. B*; **103**; 6314; 1999.

[53] Nath, S. K.; De Pablo, J. J.; "Simulation of vapour-liquid equilibria for branched alkanes."; *Molec. Phys.*; **98**; 231; 2000.

[54] Ungerer, P.; Beauvais, C.; Delhommelle, J.; Boutin, A.; Rousseau, B.; Fuchs, A. H.; "Optimization of the anisotropic united atoms intermolecular potential; for n-alkanes."; *J. Chem. Phys.*; **112**; 5499; 2000.

[55] Kettler, M.; Vörtler, H. L.; Nezbeda, I.; Strnad, M.; " Coexistence properties of higher n-alkanes modeled as Kihara fluids: Givvs ensemble simulations."; *Fluid Phase Equil.*; **181**, 83; 2001.

[56] Chen, B.; Potoff, J. J.; Siepmann, J. I.; " Monte Carlo Calculations for Alcohols and Their Mixtures with Alkanes. Transferable Potentials for Phase Equilibria. 5. United-Atom Description of Primary, Secondary, and Tertiary Alcohols. "; *J. Phys. Chem. B*; **105**; 3093; 2001.

[57] Bourasseau, E.; Ungerer, P.; Boutin, A.; Fuchs, A. H.; " Monte Carlo simulation of branched alkanes and long chain n-alkanes with anisotropic united atoms intermolecular potential."; *Molec. Simul.*; **28(4)**; 317; 2002.

[58] Khare, R.; Sum, A. K.; Nath, S. K.; De Pablo, J. J.; "Simulation of Vapor-Liquid Equilibria of Primary Alcohols and Alcohol-Alkane Mixtures. "; J. Phys. Chem. B; 108; 10071; 2004.

[59] Chang, J. ; Sandler, S. I.; "Interatomic Lennard-Jones potentials of linear and branched alkanes calibrated by Gibbs ensemble simulations for vapor-liquid equilibria."; *J. Chem. Phys.*; **121(15)**; 7474; 2004.

[60] Martin, M. G.; "Comparison of the AMBER, CHARM, COMPASS, GROMOS, OPLS, TraPPE, and UFF force fields for prediction of vapor-liquid coexistence curves and liquid densities. "; *Fluid Phase Equil.*; **248**, 50; 2006.

[61] Pérez-Pellitero, J.; Bourasseau, E.; Demachy, I.; Ridard, J.; Ungerer, P.; Mackie, A. D.; " Anisotropic United-Atoms (AUA) Potential for Alcohols. "; *J. Phys. Chem. B*; **112**; 9853; 2008.

[62] Ferrando, N.; Lachet, V.; Teuler, J.-M.; Boutin, A.; "Transferable Force Field for Alcohols and Polyalcohols. "; *J. Phys. Chem. B*; **113**; 5985; 2009.

[63] Allen, M. P., Tildesley, D. J., *Computer Simulations of Liquids*, Oxford University Press, New York, 1987.

[64] Alejandre, J. ; Tildesley, D.J.; Chapela, G.A.; "Molecular dynamics simulation of orthobaric densities and surface tension of water."; *Chem. Phys.*; **102**; 4574; 1995.

[65] Holcomb, C.D.; Clancy, P.; Thompson, S.M.; Zollweg, J.A.; "A critical study of simulations of the Lennard-jones liquid-vapor interface."; *Fluid Phase Equil.*; **88**; 303; 1993.

[66] Pelissetto, A.; Vicari, E.; "Critical phenomena and renormalization-group theory."; *Phys. Rep.*; **368**; 549; 2002.

[67] Teja, A. S.; Lee, R. J.; Rosenthal, D.; Anselme, M.; "Correlation of the critical properties of alkanes and alkanols."; *Fluid Phase Equilib.*; **56**; 153; 1990.

[68] Edberg, R.; Morriss, G.P.; Evans, D.J.; "Rheology of *n*-alkanes by nonequilibrium molecular dynamics."; *J. Chem. Phys.*; **86**; 4555; 1987.

[69] Jorgensen, W.L.; "Transferable intermolecular potential functions for water alcohols, and ethers: Application to liquid water."; *J. Am. Chem. Soc.*; **103**; 335; 1981.

[70] Boutard, Y.; Ungerer, Ph.; Teuler, J.M.; Ahunbay, M.G.; Sabater, S.F.; Pérez-Pellitero, J.; Mackie, A.D. ; Bourasseau, E.; "Extension of the anisotropic united atoms intermolecular potential to amines, amides and alkanols: Application to the problems of the 2004 Fluid Simulation Challenge."; *Fluid Phase Equil.*; **236**; 25;2005..

[71] Shaul, K.R.S.; Schultz, A.J.; Kofke, D.A. ; "Mayer-sampling Monte Carlo calculations of methanol virial coefficients."; *Molec. Simulation*; **36**; 1282; 2010.

[72] Gaussian 09

[73] Ryckaert, J.P.; Bellemans, A.; "Molecular dynamics of liquid alkanes."; *Discuss. Faraday Soc.*; **66**; 95; 1991.

[74] Tsonopoulos, C.; Dymond, J.H.; "Second virial coefficients of normal alkanes, linear 1-alkanols (and water), alkyl ethers, and their mixtures."; *Fluid Phase Equilibr.*; **133**; 11; 1997.

[75] Loras, S.; Aucejo, A.; Munoz, R.; Wisniak, J.; "Azeotropic Behavior in the System Methanol + Methyl 1,1-Dimethyethyl Ether."; *J Chem Eng Data*; **44**; 203; 1999.

[76] Lambert, J.D.; Roberts, G.A.H.; Rowlinson, J.S.; Wilkinson, V.J.; "Heat Capacities of Methanol Vapors."; *Proc. Roy. Soc. A*; **196**; 113; 1949.

[78] Kretschmer, C.B.; Wiebe, R.; "Pressure-Volume Temperature Relations of Alcohol Vapors."; *J. Amer. Chem. Soc.*; **76**; 2579; 1954.

[79] Fox, O.R.; Morcillo, J.; Mendez, A.; "Compressibilities of the Vapors of Several Alcohols." *An R. Soc. esp Fis. Quim.*; **17B**; 23; 1954.

[80] Bottomley, G.A.; Spurling, T.H.; "Measurement of the Temperature Variation of Virial Coefficients: III. the Second Virial Coefficient of Carbon Disulphide, Methyl Chloride, Acetone, and Methanol, and Certain of their Binary Mixtures."; *Aust. J. Chem.*; **20**; 1789; 1967.

[81] Nagata, I.; Tamura, K.; Miyai, K.; "Isothermal vapor-liquid equilibria of mixtures of (methanol + ethanol + 1-propanol or 2-propanol) at 333.15 K."; *Fluid Phase Equili.*;**170**; 37; 2000.

[82] Kell, G.S.; McLaurin, G.E.; "Virial Coefficients of Methanol from 150 to 300 C and Polymenzation in the Vapor."; *J. Chem. Phys.*; **51**; 4345; 1969.

[83] Zubarev, V.N.; Bagdonas, A.V.; "Saturation curve properties and specific volumes of methanol."; *Thermal Eng.*; **16**; 5; 139; 1969.

[84] Knoebel, D.H.; Edmister, J.C.; "Second Virial Coefficients of Binary Mixtures of Benzene with Methanol, Ethanol, Acetone, and Diethyl Ether."; *J. Chem. Eng. Data*; **13**; 312; 1968.

[85] Kudchadker, A.P.; Eubank, P.T.; "Second Virial Coefficient of Methanol."; *J. Chem. Eng. Data*; **15**; 7; 1970.

[86] Lepori, L.; Matteoli, E.; Bernazzani, L.; Ceccanti, N.; Conti, G.; Gianni, P.; "Isothermal vapour/liquid equilibria of binary mixtures with dibutyl ether at 298.15 K."; *Phys. Chem. Chem. Phys.*; **2**; 4837; 2000.

[87] Olf, G.; Schnitzler, A.; Gaube, J.; "Virial Coefficients of Binary Mixtures Composed of Polar Substances."; *Fluid Phase Equil.*; **49**; 49; 1989.

[88] Goral, M.; Oracz, P.; Warycha, S.; "Vapour-liquid equilibria XI. The quaternary system cyclohexane + hexane + acetone + methanol at 313.15 K."; *Fluid Phase Equilib.*; **135**; 51; 1997.

[89] Cadogan, D.F.; Conder, J.R.; Locke, D.C.; Purnell, J.H.; "Concurrent Solution and Adsorption Phenomena in Chromatography. II. System Alcohols-Squalane."; *J. Phys. Chem.*; **73**; 708; 1969.

[90] Shakhverdiev, A. N.; Naziev, Y. M.; Safarov, D. T.; "Densities of aliphatic alcohol vapors."; *Teplofiz. Vys. Temp.*; **31**; 369; 1993.

[91] Sum, A. K.; Sandler, S. I.; Bukowski, R.; Szalewicz, K.; "Prediction of the phase behavior of acetonitrile and methanol with ab initio pair potentials. I. Pure components."; *J. Chem. Phys.*; **116**; 7627; 2002.

[92] Rowley, R. L.; Pakkanen, T.; "Determination of a methane intermolecular potential model for use in molecular simulations from ab initio calculations."; *J. Chem. Phys.*; **110**; 3368; 1999.